

S16

Instruments and Methods

This chapter on methods for measuring the large-scale circulation and water properties of the ocean, emphasizing instrumentation, is published solely online at <http://booksite.academicpress.com/DPO/>; “S” denotes online supplemental material. Many of the methods for measuring basic properties such as temperature, salinity, and pressure were described briefly in Chapter 3. Some of the satellite observations were described in Chapters 3–5. Many of these techniques are also used for smaller scale phenomena such as waves. Every decade brings new advances and thus the descriptions presented in succeeding editions of this text have been quickly outdated. Nevertheless, it is useful to understand what types of instruments have been available at different points in oceanographic development and their resolution, precision, and accuracy. The information here primarily supports Chapter 6, Data Analysis Concepts and Observational Methods, in the printed textbook.

In Section S16.1 some of the sampling issues for physical oceanography are discussed, augmenting the discussion in Chapter 1. In Section S16.2 platforms for observations are described. In Sections S16.3 through S16.8 instruments for in situ observations (within the water column) are reviewed. Section S16.9 is an overview of satellite remote sensing, and Section S16.10 briefly describes oceanographic archives. A recent review of oceanographic instrumentation by Howe and Chereskin (2007) is also recommended.

S16.1. THE IMPACT OF SPACE AND TIMESCALES ON SAMPLING AND INSTRUMENTATION

The time and space scales of physical oceanographic phenomena were summarized in Chapter 1 (Figure 1.2). Data collection requirements to study motions with so many time and space variations are demanding, calling for a wide variety of sampling methods. As described in Chapter 6, studies at almost every scale require averaging or filtering to remove space and timescales that are not of interest. It is not possible to measure every space and time-scale, however, to form perfect averages and statistics. Therefore observational oceanographers must understand the sources of error and uncertainty, which can be due to instrumental or sampling limitations, or to signals at different frequencies and wavelengths.

For example, traditional *deep oceanographic profiles* (Section S16.4) were and continue to be made from research ships to study the very largest spatial and temporal scales of the ocean circulation and property distributions. These remain the only way to measure the deep ocean with high accuracy, and the only way to make most chemical measurements. A deep oceanographic station can take up to three hours and a cross-section across an ocean can take up to two months, posing limitations to interpretation. The individual, widely separated profiles

cannot be used to study tides, internal waves, or eddies, for instance, but these and other smaller scale motions affect the individual station measurements. There are, however, useful ways to process and analyze the data so that they can be used to study the large space and timescales of interest.

As a second example, *satellite altimeters* (Section S16.9.9) measure the ocean's surface height, passing over each point on the ocean's surface every week or two. Surface height depends on several things: the ocean circulation, surface waves and tides, expansion and contraction due to more or less heat or salt in the water, and the uneven distribution of mass in the solid earth (variations in the geoid). The geoid, which does not vary in time, dominates the altimetric signal. Therefore the time-dependent altimetry measurements have been most useful, providing significant information about the time-dependent "mesoscale" (tens to hundreds of kilometers) and large-scale time dependence in sea-surface height, which is associated with changes in large scale circulation, climate variability such as El Niño, and global sea level rise.

Interpretation of the altimetry measurements in the presence of thermal expansion requires information on the temperature and salinity structure beneath the surface, which a satellite cannot see. Therefore in situ measurements are combined with altimetry. Since the different data sets are mismatched in sampling frequency and location, the combination poses significant data analysis challenges, dealt with most recently through use of data assimilation (Section 6.3.4). And as a third example drawn from altimetry, the many days between satellite passes over a given location means that shorter timescales, due for instance to tides, are measured at different times in their cycles on each satellite pass. This "*aliasing*" produces a false long timescale (Section 6.5.3). Great care is taken in choosing satellite orbital frequency and in interpretation of the data to properly deal with these shorter timescales, to remove

them as much as possible from the longer timescales.

Returning to observing the largest scale circulation from the top to the bottom of the ocean, which is the primary focus of this text, it might appear that employing numerous instruments that measure the currents directly would be the best approach. Indeed, at the onset of the twenty-first century a global program (Argo, described in Section S16.5.2) to continuously monitor velocity within the water column was initiated using relatively inexpensive *subsurface floats* that follow the subsurface currents (mostly at a single depth) and report back to satellites at regular intervals. This program has already revolutionized observing of the ocean interior, primarily because of the temperature and salinity profiles collected on every trip to the surface, which has been standardized at ten-day intervals; the velocity data have been less utilized. A global deployment of *surface drifters* accomplishes the same objective at the sea surface (Section S16.5.1). These ocean-wide Lagrangian sampling methods were not possible prior to the beginning of global satellite communications, and it is still prohibitively expensive to instrument the ocean at all depths. *Current meters*, both mechanical and acoustic, directly measure flow at a given point for several years; they were developed and deployed widely after the 1950s. Current meters give information on the velocity (speed and direction) of the water only close to the location (in time and space) of the instrument itself; experience indicates that large variations in velocity can occur over small distances as well as over small time intervals. Because of these spatial scales and because of the high expense of current meter deployments, it has not proven possible to widely instrument the ocean. Current meters are now used primarily in well-defined currents of no more than several hundred kilometers width, or in specific target areas to sample all of the temporal scales (the full time spectrum) in that area, sometimes for many years. All of the

direct current measurements of subsurface currents have provided just a small proportion of our observed knowledge of the ocean circulation. On the other hand, where they have been used they provide invaluable information; for instance, quantifying the total transport and variations of strong, relatively narrow currents like the Gulf Stream or Kuroshio.

In the absence of sufficient direct measurements of ocean currents, oceanographers studying the circulation use indirect methods. One of the oldest, remaining in very common use, is the geostrophic or dynamic method, which relates the horizontal pressure distribution to horizontal currents (Section 7.6). Most currents with timescales greater than a few days (except at the equator) are in geostrophic balance, which is a balance between the horizontal change (gradient) in pressure and the Coriolis force. The geostrophic velocity is perpendicular to the pressure gradient direction due to Earth's rotation. The pressure distribution depends on sea-surface height and also on the vertical profile of seawater density at a given latitude and longitude. Thus the chief method for mapping ocean circulation has been to measure the temperature and salinity distribution of the ocean. The density distribution is then calculated, from which the horizontal pressure gradient is calculated at every depth, given an assumption of the pressure gradient at one depth (which could be at the surface, due to surface height). The geostrophic currents are then calculated.

The step of estimating the pressure gradient at one depth is nontrivial, given the general lack of distributed velocity observations. (The subsurface float deployments starting in the 1990s were first motivated by providing such a velocity field at one depth.) The traditional approach has been to require mass conservation within ocean regions and then to make educated guesses about the velocity distribution at a given depth, based on mapping property distributions within the ocean. "Inverse methods" (introduced but not developed in Section 6.3.4)

formalize the use of constraints based on mass conservation and on property distributions, which are affected by mixing.

Some water properties also are inherent tracers of time (Sections 3.6 and 4.7). These include tracers that are biologically active and are reset at specific locations. For example, oxygen content is saturated through contact with the atmosphere in the surface layer, and is then consumed by bacteria within the water column, yielding a rough age for a given water parcel. The built-in clock of radioactive decay in *transient tracers* offers more promise, as it is independent of the physical and biological character of the environment. *Anthropogenic tracers* such as chlorofluorocarbons (CFCs) have been injected into the earth system by mankind. If the history of their release into the environment is known, as is the case for CFCs, then they are useful tracers of the paths taken by surface ocean waters as they move into the interior ocean.

S16.2. PLATFORMS

Manned measurement platforms are described here. Autonomous (unmanned) platforms such as floating or moored instruments, or satellites, are described in later sections.

S16.2.1. Ocean Research Vessels

The majority of oceanographic measurements have been made from research ships with auxiliary measurements from merchant ships (ocean temperature and salinity, weather) and from coastal stations (tide gauges, wave staffs, lighthouse temperature and salinity observations, etc.). Today the research vessel continues to be essential for oceanographic research, but rapid improvements in technology, including satellite communications and long-lived mooring capabilities, have introduced new options. These include wider use of commercial vessels as platforms for expendable devices and deployment

FIGURE S16.1 The *R/V Roger Revelle* is a modern research vessel. (Photo courtesy of Katy Hill.)



of autonomous instruments that can profile the ocean while reporting their data via satellite. New options also include drifting and moored platforms as well as a new potential for interactive devices, such as gliders. In addition, the advantages of observing the earth from aircraft and satellites have further motivated the continued development of these measurement technologies. The need to validate and verify satellite surface measurements has given rise in turn to new in situ sampling programs to provide these calibration data.

Research vessels have evolved in the past few decades from rather large all-purpose vessels to smaller, more automated ships that can perform the same large variety of tasks at a lower cost of operation. The need to deploy deep-sea moorings, launch open ocean sampling systems, and make specific process measurements ensures the continued need for ocean research vessels. A good research vessel is reliable, maneuverable, stable at sea, and has comfortable living and working spaces. The *R/V Revelle* (Figure S16.1) is a typical large research vessel

(Scripps Institution of Oceanography, 2009). The *Revelle* was built in 1996. Its overall length is 277 feet and its displacement is 3180 tons. It carries a crew of 23 with room for 38 scientists.

For work in ice-covered regions, icebreakers are required. Most of the icebreakers used for research have dual purposes, including as supply and rescue ships. The U.S. Coast Guard's icebreakers are primarily used for research in the Arctic and Antarctic. The Alfred Wegener Institute's *FS Polarstern*, which began operation in 1982, is a dedicated research ship (Figure S16.2). Icebreakers have double hulls and rounded bows, as seen in this figure. Ice is broken by running the ship up onto the ice.

S16.2.2. Propulsion and Maneuverability

Maneuverability is a critical factor in research vessel operations, which primarily involve working with instruments deployed over the side of the ship into the ocean. Many research operations are improved if the ship can remain at



FIGURE S16.2 The *FS Polarstern* is a modern icebreaking research ship. (Photo courtesy of P. Lemke/Alfred Wegener Institute.)

a geographical location and if the angle between the sea surface and cables deployed over the side remains constant. This level of control is usually achieved by a variety of methods including twin propellers and various types of thrusters.

S16.2.3. Winches, Wires, and Support Systems

The hydrographic winch is an essential piece of equipment on an oceanographic vessel. The winch has a drum holding wire rope on which instruments are lowered into the sea. For water sampling without electronic instruments (which is now rare), or sampling with instruments with internal batteries and data recording, a medium-duty winch with 2000 to 6000 m of 4 mm diameter wire rope and a 7-to 15-kW motor may be used. For heavier work, such as dredging, coring, and so forth, winches with up to 15,000 m of 10-to 20-mm wire and 75 to 150 kW have been used. The wire rope used is multi-strand for flexibility,

and made of galvanized or stainless steel (more expensive) to resist corrosion. (Seawater is one of the most corrosive substances known, given time to act.) The winches must be capable of reeling the wire in or out at speeds up to 100 m/min but must also be controllable in speed so that an instrument can be brought accurately to a position for operation or to where it can be reached for recovery.

For instruments that telemeter their information to the surface, a steel cable incorporating one or more insulated electrical conductors is used. The winch must have “slip rings” to transmit the electrical signals from the wire to the deck instruments while the winch drum is turning. Early versions of these slip rings were simple copper brushes slipping over a rotating steel shaft. More recently the slip rings are mercury baths in which the steel-conducting shaft rotates. Either way the purpose is to transmit electrical signals for a rotating system. Since most electronic profiling instruments transmit multiple observables to the sea surface, these signals are

frequency-multiplexed in the instrument and then transmitted on the same single conductor wire.

Most research ships are designed with open deck workspaces to allow easy access to the water, often in the form of a lowered deck at the rear of the ship or a science deck on one side of the ship. Multiple support systems (cranes, A-frames, etc.) are available to load equipment as well as to lower equipment over the side into the water and back again on to the deck. Winches and cranes are placed in appropriate locations for handling samplers and sensors that go over the side. As an example, a schematic of a portion of the “science deck” of another research ship of the Scripps Institution of Oceanography, the *R/V Melville*, (Figure S16.3) shows the winches, A-frames, and cranes. In addition to these winches and A-frames, this deck has cranes for manipulating equipment and storage vans. Thus, supplies and equipment for particular experiments can be stored in a container van that can then be loaded intact on the ship.

Winches and their support/deployment systems are often part of the ship’s equipment, although individual research groups often provide specialized winches. Many research ships may have a weather-protected winch house, as shown in Figure S16.4, which also shows the “joystick” type of controls (black knobs) used to operate the winch and the associated booms and cranes.

S16.2.4. Workspaces: Dry Labs and Wet Labs

Research vessels have various laboratory spaces. Open or partially enclosed spaces near the winches are used for sampling or servicing instruments. Interior laboratories are divided into “wet labs” and “dry labs.” In the former, water samples can be analyzed, fish samples examined, net tows examined, and so forth. In the latter, samples are examined under a microscope, data

are analyzed, and other computer and instrument hardware might be used or serviced.

The distribution of the different types of labs on the main deck of the *R/V Melville* is shown in Figure S16.5. Here the dry lab is referred to as the “analytical lab” and the main lab serves as the wet lab. Note the double-door access from the main lab to the deck needed to bring large pieces of equipment and oceanographic samples into the lab. This main lab also has good access to the other labs on the ship. Similar lab spaces are found on all research ships.

S16.2.5. Navigation (also Section S16.9.13.2)

Research vessels require accurate and precise navigation as all oceanographic sampling is associated with a time and a location. As discussed in Chapter 1, early oceanographic expeditions had to rely on traditional methods of navigation using sextant and chronometer. While it is surprising how well the early ship captains were able to specify their locations, it is clear that these methods cannot compare in accuracy with modern navigation methods, which are now based mainly on GPS satellites (Section S16.9.13.2). It is important to remember this navigation limitation when analyzing historical data, particularly when they are mixed with more modern data.

S16.2.6. Alternative Sampling Platforms

S16.2.6.1. Aircraft

A rapid sampling alternative to working from a research vessel is to use sensors mounted on aircraft. Many airborne systems sense remotely using radiation either emitted or reflected from the ocean’s surface. Infrared sensors are used to map sea-surface temperature (SST) patterns while visible light sensor channels are used to measure patterns of ocean color related to biological productivity and the

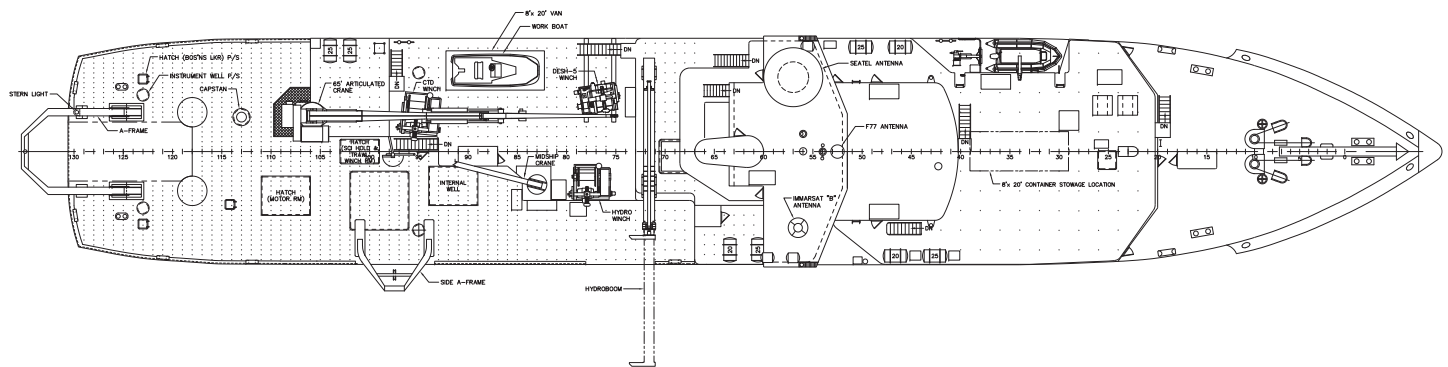


FIGURE S16.4 FS *Polarstern* winch station (foreground) and deck operations. (Photo courtesy of H. Grobe/Alfred Wegener Institute.)



amount of chlorophyll in the surface waters. Multispectral scanners are capable of simultaneously measuring radiation in both the visible and thermal infrared channels. Recently, passive and active microwave sensors have also been flown on aircraft to sense ocean parameters. One of the most useful of these is Synthetic Aperture Radar (SAR), which uses the motion of the aircraft to synthesize a larger antenna than an aircraft could carry, making it possible to greatly improve the ground resolution. Aircraft SAR imagery has been particularly useful in the detailed mapping of sea ice and its motion.

Another important use of aircraft is in the collection of upper layer temperature profile data using expendable profilers, described below in Section S16.4.2.5. Helicopters and aircraft are often used in polar studies to ferry instruments from the ship to and from the ice and may also carry instrumentation over large portions of the ice cover. The limited range of helicopters limits their usefulness in normal oceanographic sampling. When long transects

are required, such as in the Arctic, fuel must be stored on the ice to refuel the helicopter for continued operation. Routine sampling throughout the Arctic is conducted in this manner by Russia, using aircraft to reach sampling sites on the ice.

S16.2.6.2. Ships of Opportunity

As early as the eighteenth century, Matthew Fontaine Maury realized that routine observations from ships operating at sea for other than oceanographic measurement purposes could be useful for a variety of applications. Most of the maps of air–sea heat fluxes in Chapter 5 are based on the routine weather observations made by various ships at sea and not by dedicated research vessels. This sampling concept was extended in the 1970s to include routine deployment of expendable temperature profilers (expendable bathythermograph or XBTs, described in Section S16.4.2.5) from merchant vessels to provide repeat coverage of the upper layer (<700 m) thermal structure. Some the programs also

include expendable conductivity, temperature and depth profilers (XCTDs), which measure both temperature and conductivity, so that salinity profiles are also available. These Ship of Opportunity (SOOP) or Volunteer Observing Ship (VOS) programs started in the North Pacific but quickly spread to other parts of the Pacific and to the Atlantic and Indian Oceans. Today many shipping lines collect XBT and XCTD profiles on a routine basis.

Coastal vessels such as ferries are also used as ships of opportunity. Ferries frequently travel through interesting regions such as river discharges or isolated seas between islands. Instruments can be installed in ferries to continuously monitor near surface temperature and salinity to study the temporal changes associated with the river outflow. For example, a British Columbia ferry was instrumented to study fluctuations of the Fraser River outflow into Georgia Strait in western Canada and the effect this outflow has on local pollution in the Strait. Infrared radiometers can also be installed on such ferries to continuously measure the skin SST. Cruise ships in the Caribbean and Bahamas are also collecting research data relevant to the Gulf Stream system along their regular tracks.

Merchant vessels also collect continuous records while underway (in addition to meteorology). SST observations are relatively common. Several ships are outfitted with research-specific acoustic Doppler current profilers. Others collect underway surface water carbon dioxide ($p\text{CO}_2$) or oxygen measurements.

S16.2.6.3. Special Sampling Platforms: Floating Laboratory Instrument Platform

Some specialized sampling platforms have been developed for oceanographic sampling. The Floating Laboratory Instrument Platform (FLIP) from Scripps Institution of Oceanography is particularly unique. FLIP is not a ship; it is a 355 foot spar buoy with research and living quarters at one end. It is towed in the horizontal position to its operating location.

(This limits its range in comparison with a standard research vessel, which can work very far from home port.) Once on site, part of FLIP is flooded so that its lower half sinks. During FLIP's transition, everything must rotate through 90 degrees. FLIP was developed by Fred Spiess and Fred Fisher and built in 1962; it had a major refit from 1994 to 1996, and continues to operate on a full schedule.

FLIP provides a very stable platform for long-term measurements at sea. Numerous booms and radial supports allow various instruments to be installed and suspended from the platform (Figure S16.6). Instruments can also be mounted on the submerged portion of the hull. Unlike a research vessel, FLIP is designed to remain relatively motionless. It does have a well-characterized mode of vertical oscillation that must be compensated for when analyzing time series data it has collected.

FLIP provides an ideal platform for air–sea interaction studies. It has been equipped with instruments to measure the air–sea fluxes and coincident upper ocean characteristics, and has contributed immensely to knowledge of surface fluxes and associated surface layer processes (mixed layer development, internal wave generation, Langmuir circulation, etc.). One limitation of FLIP is that it is unsafe in high seas, so it is difficult to measure air–sea interaction at high wind speeds and sea states.

S16.3. DEPTH AND PRESSURE MEASUREMENTS

When instruments are lowered or dropped into the ocean, it is necessary to measure their depth. This has not always been easy. Depths for instruments attached to cables were originally estimated using the amount of cable deployed. This is measured using a meter wheel, which counts the number of turns of a pulley over which the cable passes. In calm conditions with negligible winds or currents, this is close



FIGURE S16.6 FLIP on station.
Source: From *Marine Physical Laboratory, Scripps Institution of Oceanography* (2009).

to the actual depth. More often the ship drifts with the wind or surface currents and the wire is neither straight nor vertical, so the actual depth is less than the length of wire paid out.

A much more accurate and modern method of measuring the depth of an instrument is to measure its pressure directly. The pressure is related to depth through the hydrostatic relation (Section 3.2 and Table 3.1). Pressure can be precisely converted to depth using the local value of gravity and the vertical density profile. Oceanographers usually use a non-SI unit for pressure, the decibar, where $1 \text{ dbar} = 10^4 \text{ Pa}$ and the Pascal (Pa) is the SI unit. Efforts on the part of major publishing companies to change this practice failed because the decibar is an intuitive unit: 1 dbar is nearly equal to 1 meter in depth.

Historically, the pressure difference recorded in the mercury columns of paired protected and unprotected reversing thermometers was used to accurately measure the depth of the bottle sample. (See Sections 3.3.1 and S16.4.2 on temperature measurements.)

Pressure is now measured directly on most instruments. Very accurate pressure measurements can be made using a quartz crystal, whose

frequency of oscillation depends on pressure. This technology is used in modern CTDs. Temperature must be accurately measured for the best pressure accuracy. In CTDs, a thermistor is part of the quartz pressure transducer. The accuracy is $\pm 0.01\%$ and precision is $\pm 0.0001\%$ of full-scale values. A bourdon tube arrangement is used to transfer pressure changes to the support of the quartz sensor, and a “tuning fork” is used to sense the change in oscillating frequency due to the pressure changes (Figure S16.7).

Older devices that measured pressure directly, but much less accurately, included the “bourdon tube” with a sliding electrical potentiometer. It may be accurate to $\pm 0.5\text{--}1.0\%$. Another device is the electrical strain-gauge pressure transducer, which uses the change of electrical resistance of metals under mechanical tension. Accuracies to $\pm 0.1\%$ or better of full-scale pressure range are claimed, with resolution of $\pm 0.01\%$ or better. Yet another device is the “Vibratron” pressure gauge, in which the water pressure varies the tension in a stretched wire, which is caused to vibrate electromagnetically. The frequency of vibration depends on the wire tension and hence on the

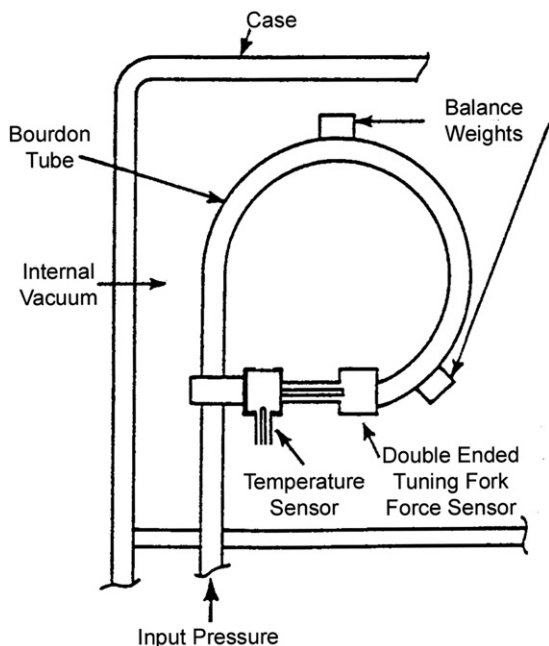


FIGURE S16.7 Quartz pressure sensor, designed for high pressures. The quartz crystal is in the “tuning fork.”
Source: From Paroscientific, Inc. (2009).

depth. The vibration frequency gives a measurement of pressure to about $\pm 0.25\%$ accuracy.

Expendable instruments such as the XBT (Section S16.4.2.5), which measures temperature using a thermistor, do not actually measure depth directly but infer it from the time of a “freely falling” body with an assumed “known” constant fall rate. This is an error source for the XBT’s temperature profile since there are many reasons why an individual probe’s actual fall rate might deviate from a known constant. First, since a spool of copper wire pays out from the probe to achieve “free fall,” the XBT is continually undergoing a change of mass and hence fall rate. This change is offset by the fact that the probe reaches its maximum operating depth well before its wire supply is depleted. At the same time the buoyancy of an individual probe must be dictated by the density structure at the location where the probe is deployed. It is best assumed that fall rate equations yield XBT “depths” that are not

accurate to more than a few meters, which is consistent with the lack of individual XBT thermal calibration, as discussed in Section S16.4.2.5.

Seafloor topography is mapped with acoustic systems that use the round-trip travel time of an acoustic pulse to determine the sea bottom depth below the ship (Section 2.9). Often called “echo sounders” or “depth sounders,” these systems can take the form of less precise instruments often called “fathometers” used for routine bottom mapping from the ship’s bridge. More complex systems are used to precisely map the seafloor. The resolution of topographic features is a function of the acoustic frequency used to sense the bottom. Since acoustic transmission is inversely proportional to sound speed, low frequency sound penetrates deeper with a wider beam and less spatial resolution, while higher frequencies can resolve the detailed bottom structure better but require a much greater input energy to reach significant depths. Acoustic transponders, called *pingers*, are often attached to lowered instruments to ensure that an oceanographic sensor is not accidentally run into the bottom.

S16.4. WATER PROPERTY MEASUREMENTS (TEMPERATURE, SALINITY, DENSITY, AND TRACERS)

S16.4.1. Water-Sampling Bottles

To determine the properties of a seawater sample, we must first obtain the sample. For a “surface” sample, a bucket on a rope sufficed in the past to obtain water for temperature and salinity measurements, and is still sometimes used (Figure S16.8). The older buckets were wooden (Figure S16.8b), which worked well with slowly moving sailing ships. These were replaced with canvas buckets and then with plastic. Since water temperature is often measured from the buckets, the shift from wood to canvas to plastic has had consequences for constructing useful climate records (Folland

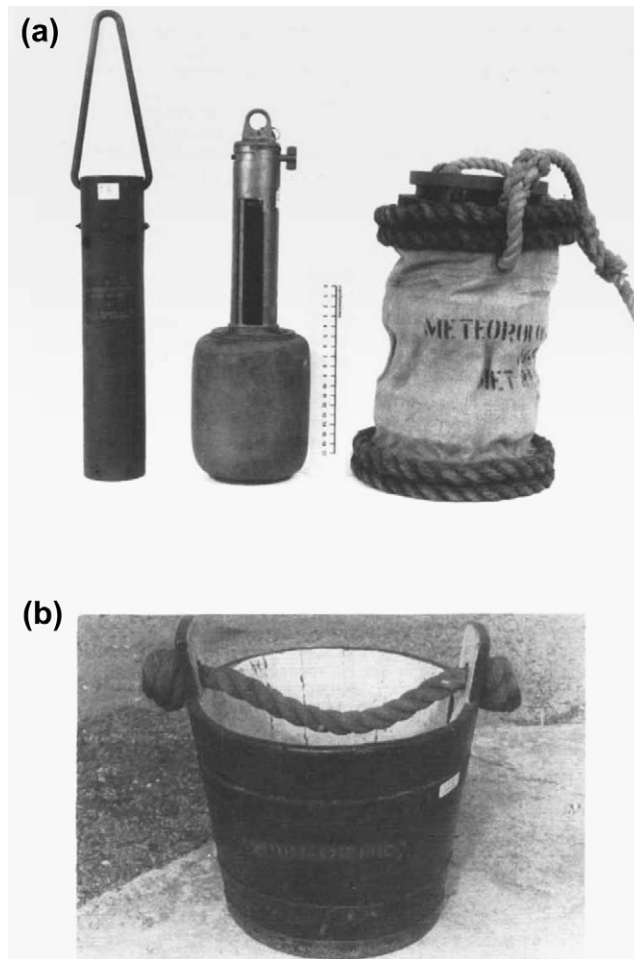


FIGURE S16.8 (a) Special bucket samplers for SST measurements. The rightmost is a canvas bucket and the other two are metal containers. (b) Traditional wooden bucket used to collect surface samples. *Source: From Folland and Parker (1995).*

& Parker, 1995). Standard buckets are small, holding only about a liter.

For the past several decades, surface samples have been routinely collected continuously through clean water intake lines. A thermistor in the intake line measures the water temperature. These temperatures differ from a surface bucket temperature or a satellite infrared temperature, depending on the depth of the intake. For research purposes, separate intake lines can bring water directly and continuously

to the laboratory, where surface properties in addition to temperature can also be measured. Such properties include salinity and concentrations of dissolved gases such as oxygen and CO_2 .

For subsurface samples, different types of water-sampling “bottles” have been used. These are generally metal or plastic tubes with either plug valves at each end (“Nansen bottle,” Figure S16.9) or spring-loaded end-caps with rubber washers (“Niskin bottle,” Figure S16.10). Materials for the bottles and parts are carefully



**Nansen water bottles
before (I), during (II), and
after (III) reversing.
(From Dietrich et al. 1980)**

FIGURE S16.9 Nansen bottle, circa 1960, for mounting individually on a wire with reversing thermometer racks. *Source: From Dietrich, Kalle, Krauss, and Siedler (1980); Ocean World (2009).*

chosen to avoid contamination of the samples. Prior to the 1980s, the sample bottle was attached to the wire with the ends open and lowered to the desired depth. This remains the practice for analyses that require exceptionally large water samples, for which a rosette sampler such as that shown in [Figure S16.10](#) is

impractical. The bottles are closed by the tripping action of a “messenger,” which is a small metal weight that slides down the wire. Generally a number of bottles (12 to 24) are attached in series at predetermined intervals along the wire (a “bottle cast”) and closed in succession. Each in turn releases a messenger to close the next bottle below it. When the bottles are brought back on deck, the water samples are drawn through a tap, following a routine designed to obtain a pure sample. In some older designs, the tripped bottle was released at its upper end and rotated through 180 degrees about a hinge at its lower end where it was clamped to the wire. These “reversing water

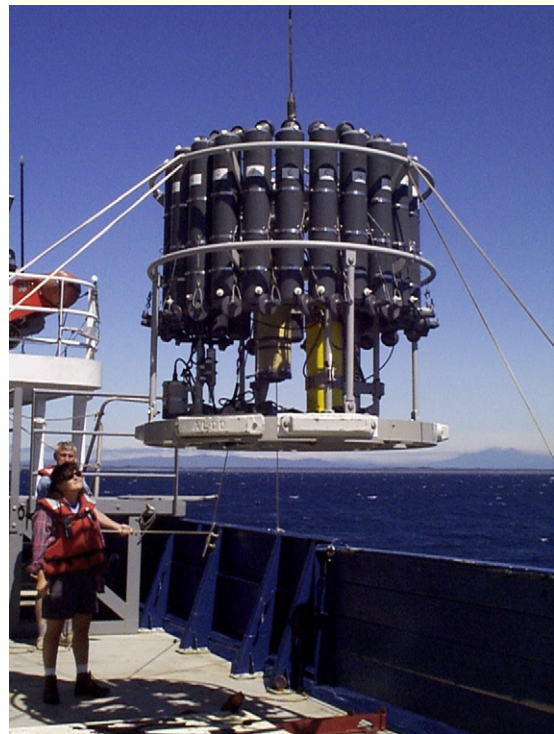


FIGURE S16.10 Rosette sampler. Large sampler used in the World Ocean Circulation Experiment, with 36 10-liter Niskin bottles, an acoustic pinger (lower left), an LADCP (center, yellow long), a CTD (bottom, horizontal), and transmissometer (center, yellow short). *(Photo courtesy of L. Talley.)*

bottles” permitted operation of the reversing thermometers described in Section S16.4.2.2. In other designs, the bottle remains stationary while a frame carrying the reversing thermometers rotates 180 degrees. A capacity of 1.25 L was common for bottles prior to development of the rosette sampler, which now typically collects up to 10 L per bottle. For special purposes, such as ^{39}Ar analyses, or radiocarbon analyses prior to the 1990s, much larger bottles are used with up to several hundred liters capacity.

The most commonly used bottle is the Niskin bottle. It is used with most rosette samplers (Figure S16.10). These are plastic bottles with stoppers at each end. The stoppers are held together by a rubber cord or spring that pulls them together from inside the bottle. To “cock” these bottles, lanyards are used to pull the stoppers away from the bottle, leaving the bottle wide open for water to flow through. The bottle is “tripped” by activating a firing mechanism that releases the lanyard, allowing the stoppers to close on the bottle trapping the seawater sample. Niskin bottles can capture a much larger volume of seawater than the older Nansen bottles. Reversing thermometers on Niskin bottles are mounted in a spring-loaded frame that rotates the thermometers at the same time that the Niskin bottle stoppers are closed.

The “rosette sampler” (Figure S16.10) is now the most common arrangement for water bottles. A single frame usually carries 24 sample bottles, and might hold up to 36. The frame is attached to the end of an oceanographic wire that contains electrical conductors. The bottles can be closed when desired by electrical command from on deck. This rosette arrangement is generally used with a continuously profiling CTD, measuring pressure, temperature, and conductivity (Section S16.4.2.3). CTD profiles can be plotted while the sampler is in the water and can be used to adjust rosette bottle sampling depths. Rosette bottles are always open on the way down and are closed on the way up because the tremendous pressure at depth would cause

the bottles to leak if they were first closed and then moved to a greater depth. The sampler is usually stopped before each rosette bottle is tripped so that the up and down movement of the ship can help to flush the bottle out. Reversing mercury thermometers are no longer used on rosette samplers since CTD thermistor accuracy is now higher than the accuracy of the thermometers.

After sample bottles are brought back to the ship’s deck, water samples are drawn for immediate analysis or storage. At this stage, any problems with sample collection should be noted for future reference. Bottles suspected of leaking can be checked to see if the measurements (e.g., salinity) are consistent with the CTD. Samples for dissolved oxygen and other dissolved gases are collected as soon as possible after the sample bottle is available to avoid contamination from the air. Samples for other properties are collected thereafter.

S16.4.2. Temperature Measurement

The concepts of temperature and heat were discussed in Section 3.3, which also included brief mention of measurement methods. Typical distributions were shown in Section 4.2. Here we describe thermometry methods in much greater detail. In situ temperature is measured using thermistors of various accuracies and precisions. Historically, it was measured using mercury thermometers. Satellite instruments measure SST remotely, using radiometry (Section S16.9).

S16.4.2.1. Sea-Surface Temperature

SST on research ships is measured either from engine intake water, dedicated intake water lines, surface seawater samples collected in buckets or Niskin bottles, or thermistors mounted in probes such as XBTs (S16.4.2.5) or CTDs (S16.4.2.3). SST on buoys is measured using thermistors. Satellites measure SST using infrared or microwave radiometry (Section

S16.9.5). We describe these methods from the oldest to the most recent.

The oldest method for measuring temperature is from bucket samples (Section S16.4.1 and Figure S16.8). Prior to the advent of digital thermometers (thermistors), an ordinary mercury-in-glass thermometer was used, taking care not to expose the bucket to the sun (heating) or to the evaporating influence of the wind (cooling). For faster moving powered vessels, special bucket samplers have smaller openings to reduce the tension on the bucket support line when collecting a sample. The thermometer is usually installed and insulated as part of the bucket. This type of SST measurement is limited by the accuracy and readability of the thermometer along with the ability of the sampling system to meet the requirements for sample isolation

The change from wooden to canvas bucket samplers around 1880 to 1890 resulted in an overall cool bias (drop in the mean SST to a low just after 1900 from the level between 1850 and 1880; Figure S16.11), due to the wind cooling of the less well insulated canvas buckets on the ship's deck (Folland & Parker, 1995). This low bias continued up through 1940 when the mean SST again began to rise. Part of the work in computing the most accurate heat budgets (Section 5.4) was to correct for this bucket bias. The Hadley Centre in England has modeled the effects of using a wooden bucket for the SST sample versus using a canvas bucket and found a relationship between the temperature anomaly and the wind speed. This made it possible to adjust for this bias to create temperature records useful for studying climate variability.

Bucket samples for surface temperature have been mainly replaced by "injection temperature" measurements in the engine cooling intake water. This shift in measurements began in the 1940s and continued through the 1950s. By the early 1950s, almost all ship SST measurements were made in this way. Because these measurements are made in the warm engine room, they tend to be biased high even though the engine

intake is usually 2 to 5 m below the sea surface. An upward trend in global SST anomalies after 1940 was partially due to this change in method, resulting in a need for correction for data sets used to track climate trends (Folland & Parker, 1995). A separate bias results from the location of the engine intake below the waterline. An alternative is to measure the temperature of the ship's hull below the waterline (Emery, Cherkauer, Shannon, & Reynolds, 1997). Since the ship's steel hull is a good thermal conductor, it responds quickly to changes in the surrounding SST. Due to changes in ship loading, it is important to install a series of thermistors in the vertical to ensure that a sensor is below the ship's waterline.

SST is also commonly measured on research ships using a "thermosalinograph," which measures the properties of water collected through a special inlet located on the ship's hull somewhere below the sea surface (Figure S16.12). This intake is usually located as close to the ship's bow as possible to collect a sample with little influence from the ship. The intake is usually a few meters below the mean waterline, so it is representative of the "bulk" SST. This method avoids the engine room heating problem that plagues the "ship injection" temperatures. The research-oriented sensors are also generally more accurate than those used in engine intake lines and record internally rather than having to be read by a ship's officer (a possible source of SST error). In addition, thermosalinographs are often integrated with other underway data collection systems.

SST measurement has been revolutionized in terms of geographic and temporal coverage with the advent of satellite remote sensing, using thermal infrared (IR) sensors (1 km resolution) and with passive microwave sensors (25 km resolution, but can observe through clouds). These instruments are described in Section S16.9.5. Using satellite SSTs and all available in situ measurements of bulk SST, a "blended SST analysis" with 100 km resolution

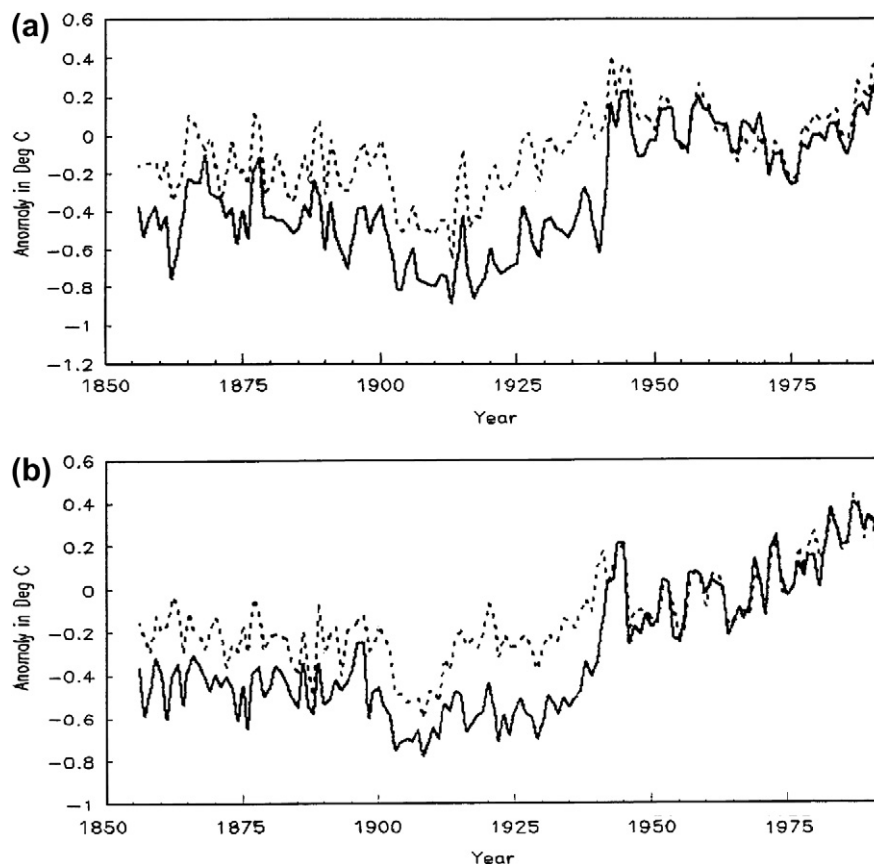


FIGURE S16.11 Time series from 1856 to 1992 of Northern (a) and Southern (b) Hemisphere anomalies of SSTs from the 1951 to 1980 average. The dashed line is a correction to the canvas bucket SST measurements for the wind cooling, developed by the British Hadley Centre. Source: From *Folland and Parker (1995)*.

is distributed routinely (Reynolds, 1988; Reynolds & Smith, 1994, 1995). This SST product is used for many different applications, including the initialization and boundary conditions for ocean, weather forecasting, and coupled climate numerical models.

Satellite systems measure the temperature of the very thin (<1 mm) “skin” layer of the surface of the ocean. This skin layer is the molecular layer between a turbulent ocean and the overlying turbulent atmosphere that affects the heat and momentum exchange between the two. Unfortunately it is not possible for

drifting buoys and ships to measure this skin SST. As a result, the blended SST analysis is a mix of skin and bulk SSTs. These generally differ by more than 0.3°C , with the skin generally cooler than the bulk SST. The effects of diurnal heating strongly influence the relationship between the skin and bulk SSTs, particularly under low wind, high solar insolation conditions. Higher wind speeds decrease the mean difference between skin and bulk SSTs. Shipboard and airborne radiometers are being developed to routinely and accurately measure the skin SST for satellite sensor validation.

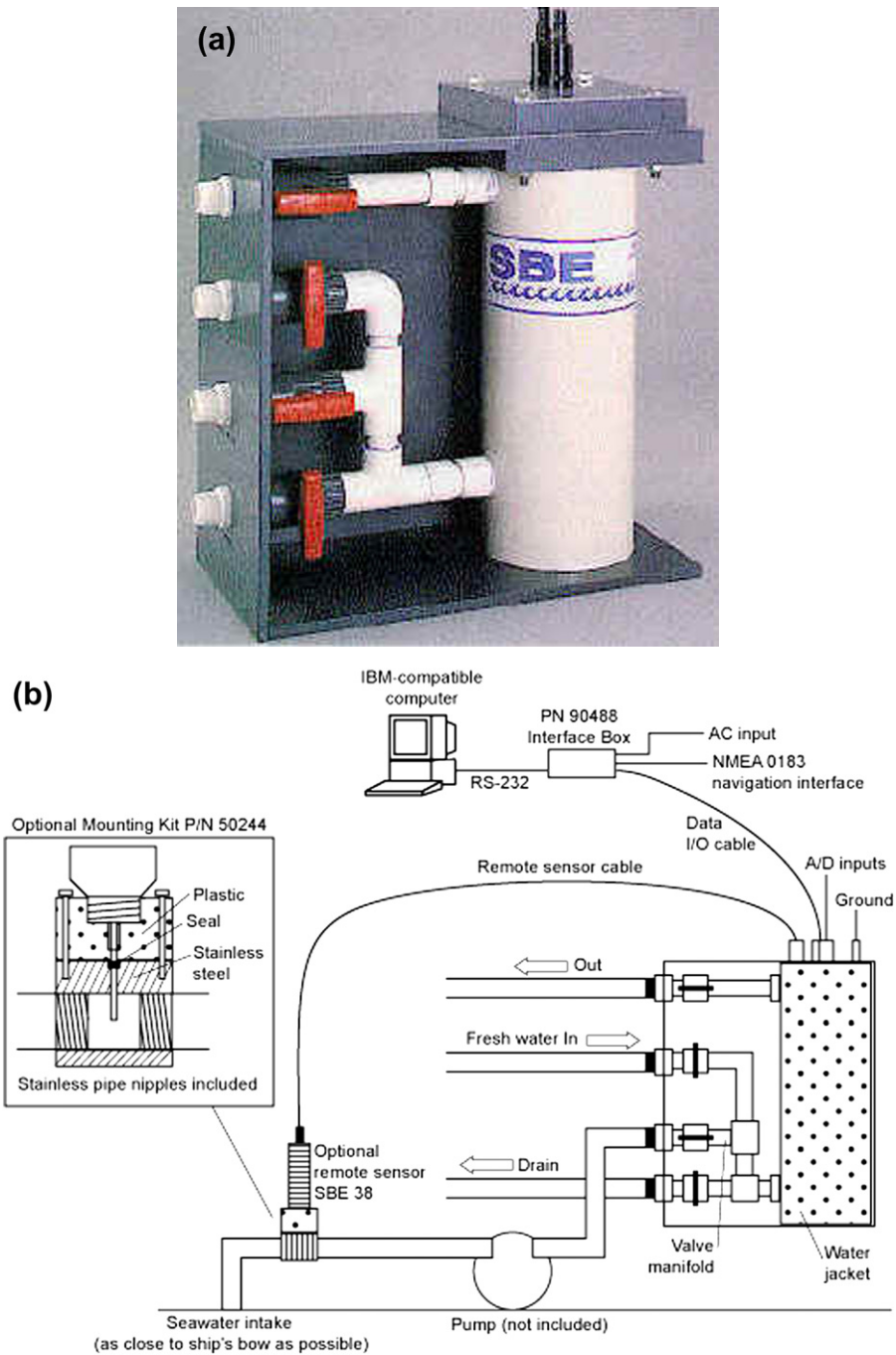


FIGURE S16.12 Thermosalinograph: (a) Sea-Bird unit and (b) schematic of its operation. Source: Sea-Bird Electronics, Inc. (2009a).

Most in situ comparisons with satellite SSTs use temperatures measured at 0.5 to 1.5 m below the surface by the buoys and down to 5 m by the ships, since these are the most available, with a long historical record and reasonably good accuracy. Skin SST algorithms are being improved and the connections between skin and bulk temperature continue to be explored with the goal of understanding the connections between these temperature differences and wind speed and air–sea heat flux. Critical in this understanding is the development of methods to assimilate both skin and bulk SST into ocean and coupled ocean-atmosphere numerical models.

Aircraft also use radiation methods to measure SST. In practice the temperature of the sea is not measured absolutely but is compared with that of two black bodies, one at a constant temperature and one allowed to “float” with the ambient temperature by a parabolic mirror that rotates to view the sea and two black bodies. The same principle is used on shipboard radiometers.

S16.4.2.2. Mercury Reversing Thermometers

Mercury thermometers were the traditional method for measuring subsurface temperatures prior to the 1980s. This method has been almost completely replaced with digital thermometry using thermistors. Most present oceanographic instruments incorporate thermistors, including vertically profiling instruments, single point time series instruments, and floating instruments. For sampling in the most traditional mode with reversing thermometers, highly accurate digital reversing thermometers have been developed. For historical interest, the description of mercury reversing thermometers is retained here, since they were the basis of oceanographic data sets prior to the advent of CTDs with highly accurate thermistors (Section S16.4.2.3). Reversing mercury thermometer

precision and accuracy was much lower (0.01 and 0.02°C) than is now possible with high-quality thermistors (0.001 and 0.005°C). However, lower quality thermistors, such as are used on many expendable instruments such as XBTs (Section S16.4.2.5), may also have a low precision of 0.01 °C.

The protected reversing thermometer (Figure S16.13) was developed especially for oceanographic use to record temperature at depth and then remain unchanged while the instrument was brought back up through the water column to the ship. It is a mercury-in-glass thermometer, which is attached to a water-sampling bottle. It is protected from temperature change due to ambient water pressure by a surrounding glass jacket with a vacuum. When the reversing thermometer rack is flipped during collection of a water sample, the mercury in the inverted thermometer “breaks” and runs down to the other end of the capillary, thus recording the temperature at the depth of reversal. The break occurs in the capillary stem above the bulb at a point where a short side-arm (called the “pigtail” appendix) is placed. It is really rather surprising that the mercury should break consistently — to better than ± 0.01 K — in a good thermometer in laboratory tests.

The mercury thermometer is read when brought back on deck. After corrections for scale errors and for the small change in reading due to any difference between the in situ temperature and that on deck, the reversing thermometer yields water temperature to an accuracy of about ± 0.02 K in routine use. This final correction is made possible by the presence of an “auxiliary” thermometer parallel to the reversing thermometer in the same enclosed glass housing. The auxiliary thermometer senses the ambient deck temperature, which is then used to correct the reversing thermometer for the temperature on the ship when it is read. Normal practice is for each thermometer (reversing and auxiliary) to be read twice by two different persons using a microscope lens

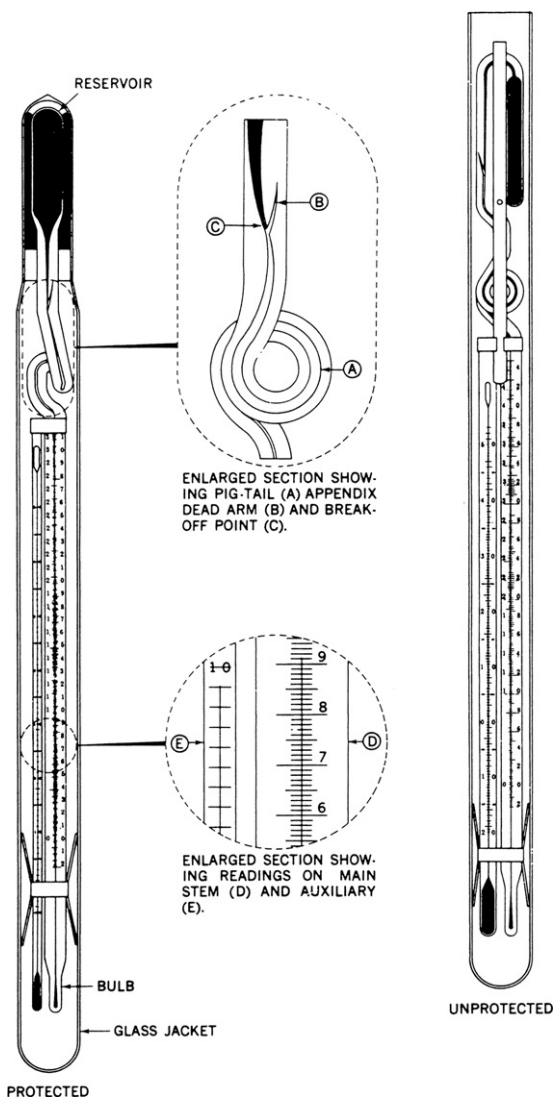


FIGURE S16.13 Protected and unprotected reversing thermometers. Source: *Emery and Thomson (2001)*.

(Figure S16.14). Reading these thermometers takes some skill since it is necessary to interpolate between gradations on the thermometers. Good practice for reversing thermometers includes regular calibration and maintenance of a calibration history. With these calibration values it is possible to correct for any “creep”

deformations that might take place in the glass thermometers. An older thermometer with an accurate calibration history is more valuable than a new thermometer with no calibration history.

The most common way to accurately determine the depth of a sampling bottle prior to the use of continuously profiling devices with pressure sensors such as CTDs (Section S16.4.2.3) was to use an unprotected reversing thermometer (Figure S16.13) together with the protected one that recorded the temperature. The unprotected thermometer differs from the protected thermometer due to the absence of a vacuum, thus allowing the ocean pressure to alter the mercury column height and the recorded temperature. The reading depends on the thermometer’s compressibility and the ambient water pressure when it was reversed. Use of the protected and unprotected thermometer measurements together yields the pressure and hence depth, the latter to about $\pm 0.5\%$ or to ± 5 m, whichever is greater.

Mercury reversing thermometers have been almost completely replaced by digital thermometers, which use calibrated thermistors. These are usually incorporated in a profiling device such as a CTD (next section) or XBT (S16.4.2.5). Reversing digital thermometers are also available for use with Niskin bottles.

S16.4.2.3. Conductivity, Temperature, and Depth Profiler

Continuous profiles of temperature (and salinity) are more desirable than values at discrete sample bottle depths. Sensor packages known as STDs (Salinity-Temperature-Depth) were developed in the 1950s, incorporating newly developed seawater conductivity sensors and thermistors. (Salinity calculation requires concurrent temperature and conductivity measurement, see Sections 3.4 and S16.4.3.) As experience developed with processing STD data, it became apparent that it would be best to record the seawater conductivity directly



FIGURE S16.14 Reading reversing thermometers. (Photo courtesy of W. Emery.)

along with temperature and pressure to permit post-cruise processing to improve the salinity accuracy. The device that replaced the STD by the mid-1970s was known as the CTD (Conductivity-Temperature-Depth).

The standard CTD sensor includes high precision thermistors (often two, either for redundancy or to provide different response times for processing the conductivity measurements), a conductivity sensor and a pressure sensor (Section S16.3), and often an oxygen sensor (Figure S16.15). The unit is lowered through the water on the end of an electrical conductor cable that transmits the information to computers or recorders onboard ship. The Guildline and Neil Brown CTDs were the original instruments; Neil Brown MK3 CTDs were used extensively in the World Ocean Circulation Experiment (WOCE) and are no longer produced. Sea-Bird added a high-capacity pumping system to flush the conductivity cell at a known rate, which improves sensor response.

Internally recording CTDs eliminate the complex infrastructure of having a conducting wire to transfer the signal from the CTD to the ship. This type of unit can be used with a simple support cable or on a mooring. Upon return to

the surface, this CTD is plugged into a computer and these data are downloaded for processing and display. Internally recording CTDs are used on all profiling floats, such as in the Argo program (Section S16.5.2), and can be mounted on moorings.

For highly accurate measurements, CTD sensors, including thermistors and pressure transducers, must be calibrated. Prior to the 1990s, thermistor calibration was accomplished by adjusting laboratory calibrations of the sensors with estimates of shifts and drifts monitored at sea via reversing thermometers on the rosette bottles that usually accompanied a CTD profile. Since the early 1990s, improvements in the stability of calibrated, precision CTD thermistors has superseded the use of reversing thermometers for calibration. This has shifted best practice to using CTD thermistors in redundant pairs, calibrated pre- and post-cruise in the laboratory. This provides both detection and correction for sensor drift and now-rare sudden offsets. Pressure transducer calibration is entirely accomplished in specially equipped calibration facilities. Salinity and oxygen calibration are more complicated because these sensors are not stable; water

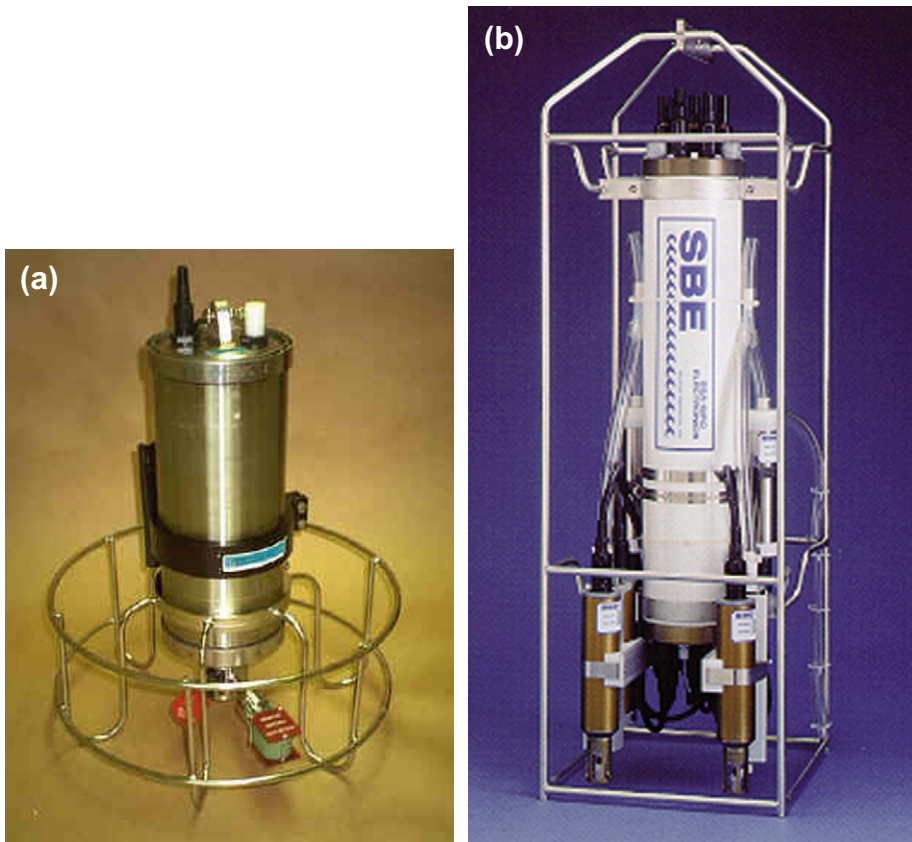


FIGURE S16.15 (a) Neil-Brown Mark III CTD. Source: From *General Oceanics* (2009). (b) Sea-Bird 911plus CTD. Source: *Sea-Bird Electronics, Inc.* (2009b).

sample values are required for the highest accuracy.

Modern CTD accuracy in ocean deployments is approximately $\pm 0.001^\circ\text{C}$ in temperature, ± 0.001 psu in salinity if routinely calibrated with seawater sample salinity (in practice, on every station), and ± 0.5 db in pressure.

S16.4.2.4. Mechanical Bathythermograph

Vertical profiles of temperature alone have been collected from research and merchant ships since the early 1950s. The first profiling instrument in wide use from approximately 1951 to 1975, prior to the widespread use of

thermistors, was the mechanical bathythermograph (MBT; [Figure S16.16](#)). Given the large number of MBT temperature profiles in the historical data records, it is important to describe this instrument and its limitations. In addition to providing upper layer temperature profiles, the MBT could be operated while a ship was underway. In the MBT, a liquid-in-metal thermometer caused a metal point to move in one direction over a smoked or gold-plated glass slide that was moved at right angles to this direction by a pressure-sensitive bellows. The instrument was lowered to its permitted limit in the water (60, 140, or 270 m) and then

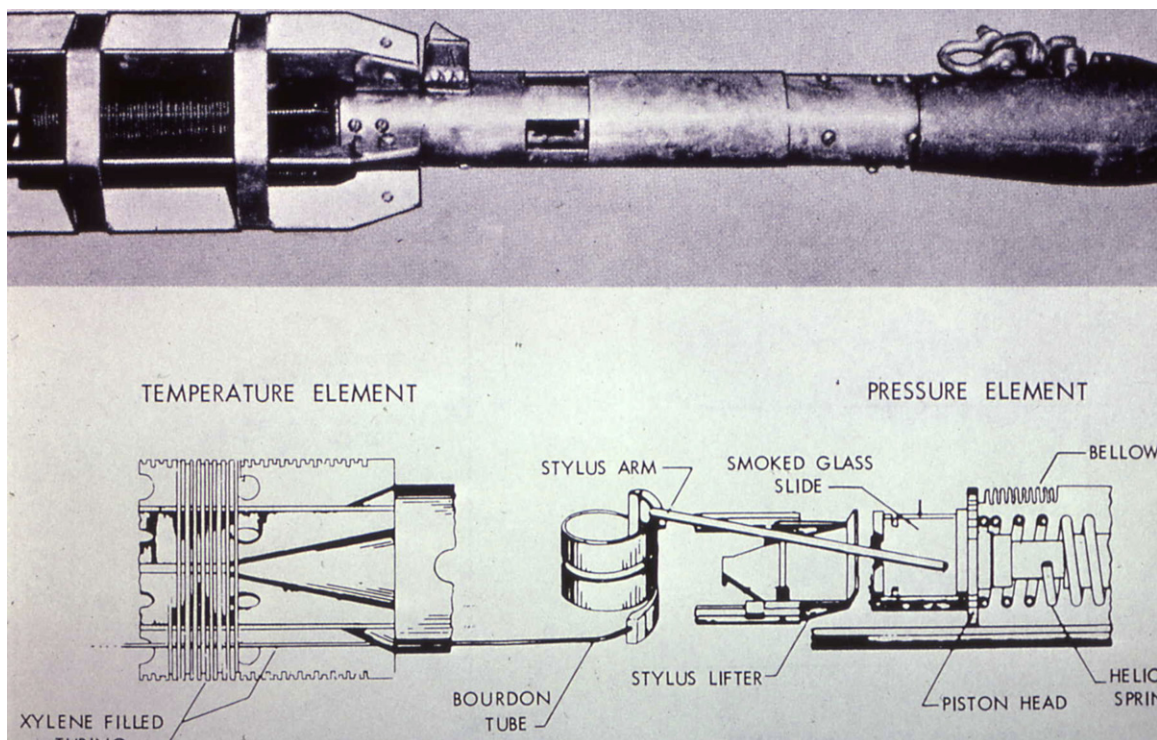


FIGURE S16.16 Mechanical bathythermograph (MBT), in use from 1951 to 1975. Source: *Neumann and Pierson (1966)*.

brought back using a very fast electric winch. Since pressure is directly related to depth, the line scratched on the slide formed a graph of temperature against depth. It was read against a calibration grid to an accuracy of ± 0.2 K (0.1°F) and ± 2 m if well calibrated. Since each instrument had a nonlinear relationship between the sensors and temperature, each instrument was coupled with its own reader to convert the scribed profiles to a temperature profile.

The MBT had a “torpedo-like” profile intended to provide minimal water resistance as the probe was hauled in to the ship. Unfortunately the MBT was hydrodynamically unstable and would “swim” on its return, often announcing its presence by a thud against the hull of the ship. The high-speed electric winch

had a “neutral position” between up and brake that would cause the probe to fall back into the water. As a consequence most MBT probes were hauled up by hand for the last few meters.

Most MBTs were in units of $^\circ\text{F}$ rather than $^\circ\text{C}$ and in feet rather than meters, since the U.S. Navy developed them. A sample temperature profile is shown in Figure S16.17. Note the nonlinear temperature and depth scales. Each temperature profile had to be read by eye, resulting in numerous data transcription errors.

S16.4.2.5. Expendable Bathythermograph and Expendable CTD

The MBT was replaced by the expendable bathythermograph (XBT; Figure S16.18), which was introduced in 1966 and remains in wide use, especially for profiling from volunteer

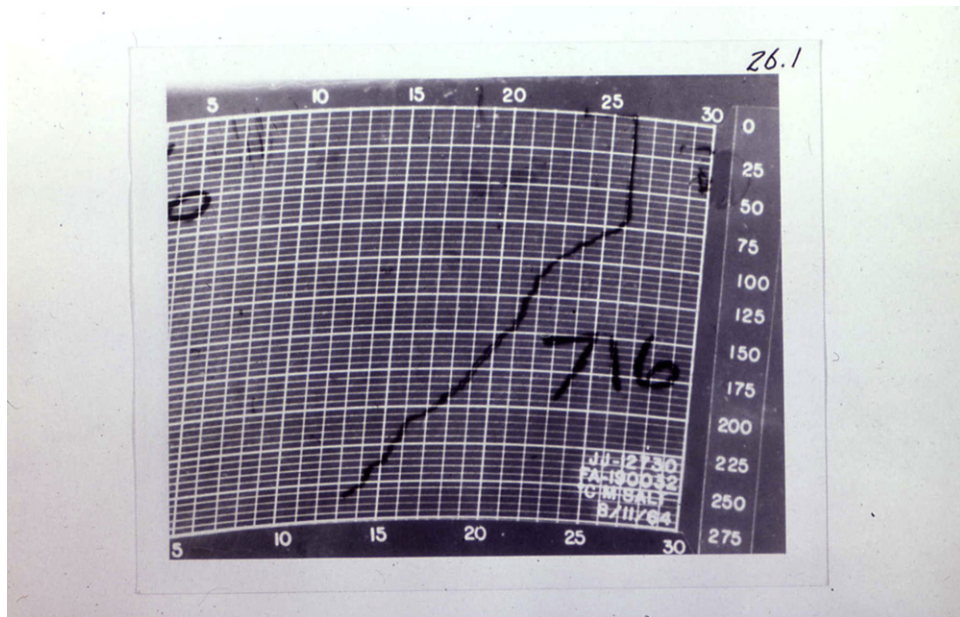


FIGURE S16.17 MBT temperature profile. Source: *Neumann and Pierson (1966)*.

observing ships. The XBT has a thermistor and electronic data acquisition system. A conductivity sensor is included in the XCTD, which is otherwise essentially the same as an XBT. XBT profiles are deeper (400, 800, or 1500 m) than MBT profiles. They can be launched from ships moving at up to 30 knots. The XBT has a thin, two-element wire insulated by clear resin. This dual element wire pays out from a spool on the probe as the probe falls, transferring the temperature signal from a thermistor installed on the head of the XBT probe back to the ship. At the same time a spool of the same wire on the ship pays out as the ship travels, thus mechanically disconnecting the probe from the ship while still retaining the electrical connection. When all of the wire is out, the wire breaks and the XBT is lost (hence “expendable”).

The probe is assumed to fall at a known and constant rate thus making it possible to infer the depth from the time the probe hit the sea surface. Early versions of the XBT deck unit recorded the temperature profiles on pressure-

sensitive paper that rolled forward at the assumed rate of fall for the XBT. More recent systems are digital, but an assumed fall rate is again used to estimate depth. The fall rate is determined by a limited number of measurements in a tower that is 250 feet high and then extrapolated to the full XBT depth. This is known to introduce some error in depth. In addition, changes in the density of the probe as the wire pays out alter the fall rate and introduce depth errors. The present error in XBT depth, using the most recent fall rates, is approximately 20%.

XBT probes are usually not individually calibrated. Instead, a lot of about 2000 thermistors is purchased by the manufacturer and about 250 of these are “calibrated” for accuracy. The accuracy reported for the group of 250 thermistors is then assigned to all of the 2000 thermistors. Thermistors that do not meet the stated accuracy of the XBT probes are discarded.

XBTs and XCTDs are launched from portable or fixed launchers (Figure S16.19). For occasional use, the portable unit is useful and

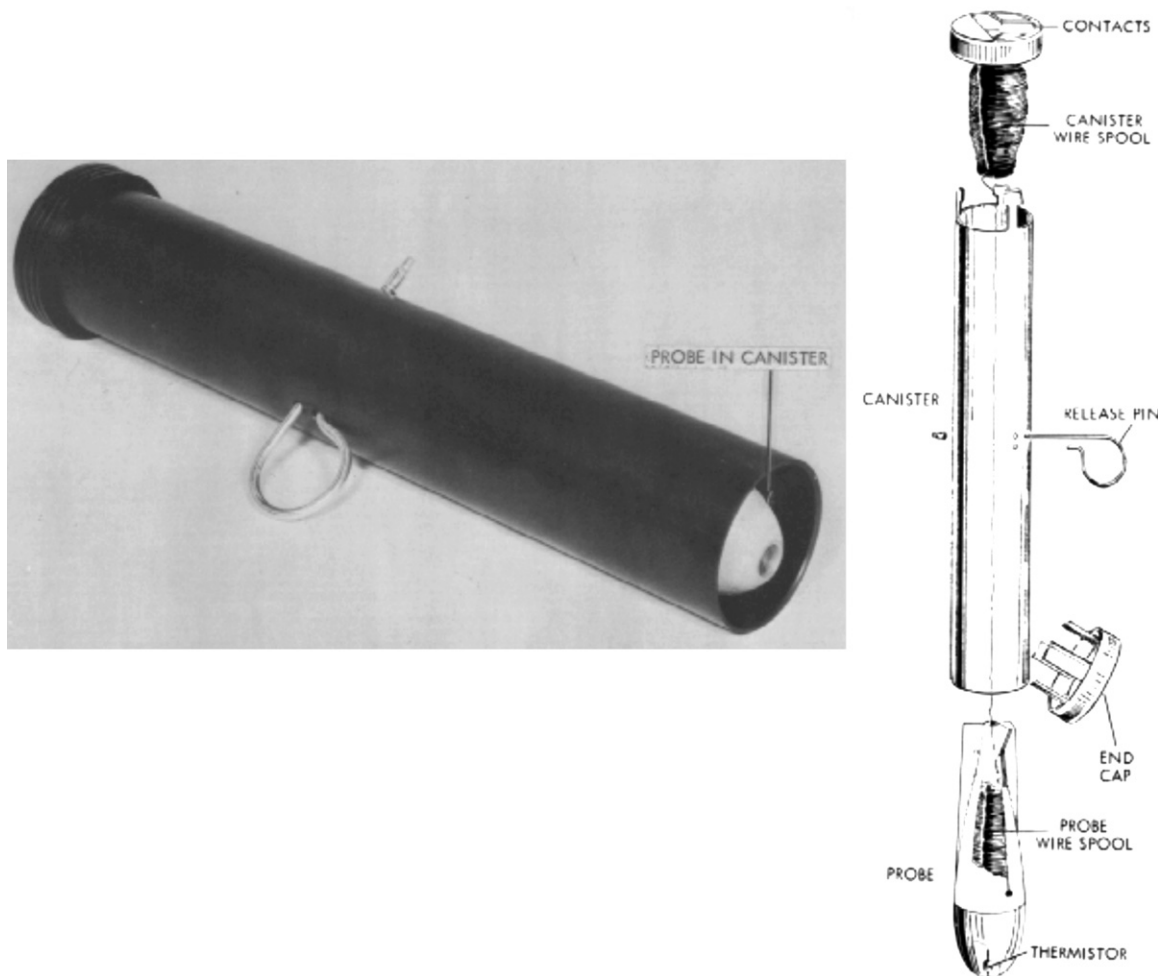


FIGURE S16.18 An expendable bathythermograph (XBT). *Source: From NOAA UOTC (2009).*

flexible. For volunteer observing ships operating XBTs every hour, fixed launchers holding multiple probes have been developed.

XBT's have been developed for platforms other than moving ships. One type can be deployed from a submarine, with the buoy floating up to the surface and then dropping the probe. XBTs can also be dropped from aircraft (AXBT). The AXBT deploys a small surface buoy, which contains a radio transmitter to

send the temperature/depth information (from 300 to 800 m) to the aircraft, which continues its flight. AXBT probes are usually dropped from altitudes between 300 and 1000 m, but testing has shown that they can survive the impact of being dropped from 6000 m. AXBT designs from different manufacturers vary, but all have some type of atmospheric drag element (parachute, wings, etc.) to slow their descent and soften the impact with the sea. The combined

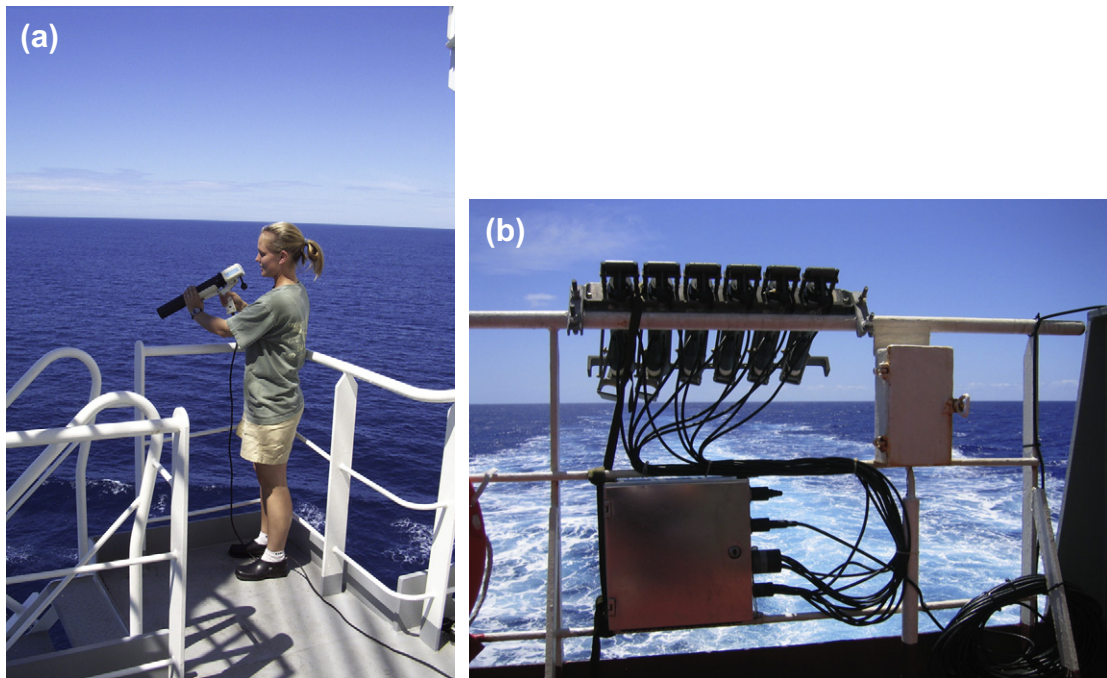


FIGURE S16.19 (a) Portable (hand-held) XBT launcher. (Photo courtesy of Valerie Cannon.) (b) XBT autolauncher developed for multiple probes by Scripps Institution of Oceanography. (Photo courtesy of G. Pezzoli and D. Roemmich.)

XBT probe and radio transmitter makes the cost per AXBT much higher than that of the normal ship XBT, but the relatively lower cost per area surveyed of using an aircraft often offsets the higher cost per probe. Also, if near-simultaneity is a requirement of the sampling program, AXBT observations are one of only a very few methods of carrying out this type of sampling.

Expendable instruments have provided the oceanographer with simple tools for rapid sampling. This has proved important for synoptic sampling from multi-ship or aircraft surveys and has led to wider use of ships of opportunity. In an effort to extend such technology to other important parameters, developments in the 1980s produced an expendable velocimeter (speed of sound) and an expendable current profiler, using the electromagnetic principle. These more exotic expendables are

considerably more expensive than the XBT and are less widely used.

S16.4.2.6. Subsurface Temperature Measurements from Floating and Moored Instruments

Valuable temperature records with long temporal coverage are collected on subsurface instruments. Thermistors are robust, and can maintain an acceptable calibration for years.

Most moored instruments (Sections S16.5.4 and S16.5.5) employ thermistors. Thermistors spaced closely together in the vertical are sometimes deployed as “thermistor chains” to obtain dense vertical coverage, particularly useful for studies of internal waves and smaller scale phenomena. Most surface drifters and subsurface floats also have thermistors, providing valuable records that complement or sometimes

supersede the usefulness of the actual velocity measurement.

Freely drifting subsurface floats are becoming routine vehicles for temperature and salinity profiling. Profiling floats are described in Section S16.5.2. The “pop-up” type of float typically includes a thermistor, and preferably also a conductivity sensor. Every time the float surfaces, it transmits a profile of temperature (and conductivity if available) to a communications satellite, which then relays the information to a data acquisition center. A global deployment of such profiling floats is now in progress (Argo). Argo has reached a full global sampling capacity of 3000 floats, providing profiles to 1800 m depth every 10 days. This network is replacing much of the current XBT ship of opportunity sampling for temperature, since volunteer ships do not cross many areas of the ocean.

S16.4.3. Salinity Measurement

As already described in Section 3.4, salinity is presently determined from conductivity, relative to the conductivity of an international standard seawater prepared in the UK. Prior to the widespread use of conductivity methods beginning in the 1960s, salinities were calculated by titration with much lower precision and accuracy than is achievable with conductivity methods. Salinity is measured both on seawater samples collected from bottles such as on a rosette sampler, and through paired conductivity and temperature sensors deployed in the water. Conductivity sensors in CTDs are relatively unstable and usually require frequent calibration. Therefore highly accurate salinity observation (especially in the open ocean) requires calibration with measurements on seawater samples in the laboratory. On research cruises, salinity samples are analyzed onboard within a day of sample collection to minimize evaporation from the sample. However, the stability of conductivity sensors is improving steadily to the point where sensors can be moored and

measured for about a year, or can be deployed on drifting floats, and produce reasonable salinity values. All profiling floats now deployed globally as part of the Argo array (Section S16.5.2) include internally recording CTDs to provide temperature and salinity profiles.

When measuring salinity from seawater samples, water from sampling bottles is drawn into 200 ml glass bottles (Figure S16.20) after several “rinses” done with a minimal amount of water from the sample bottle. These rinses remove residue from earlier salinity samples. The subsamples are then carefully capped and left in the wet lab to reach the equilibrium temperature of the lab, which can take about 12 hours, since conductivity is foremost a function of temperature and secondarily of salinity. The salinity samples are then processed with a laboratory salinometer that measures the conductivity of each sample in comparison with a carefully prepared standard. The conductivity and temperature of the lab sample are then used to calculate the salinity of the sample.

S16.4.3.1. Salinity Measurements Using Titration

As described in Section 3.4, the classical (Knudsen) method of salinity measurement, in general use prior to about 1960, determined the chlorinity by titration with standard silver nitrate solution (Strickland & Parsons, 1972) and calculated salinity from the formula (3.3). In routine use, an accuracy of ± 0.02 is considered reasonable, with rather better accuracy with special care and replicate titrations. A careful operator could titrate 50 samples per day. This method was volumetric, whereas salinity is defined gravimetrically (i.e., by mass). As a consequence, it was necessary either to correct for deviations of the temperature of the solutions from the standard, or preferably to carry out the titrations in a temperature-controlled room. This titration method was not very convenient to use onboard ship. It is also less precise



FIGURE S16.20 Drawing a salinity sample from a Nansen bottle. (Photo courtesy of W. Emery.)

than electronic methods, which are based on the relationship between salinity and conductivity.

S16.4.3.2. Salinity Measurements Using Conductivity

Salinity has been estimated through its relation to electrical conductivity since about 1930, when the U.S. Coast Guard introduced the measurement for the International Ice Patrol in the western North Atlantic. The method was not widely used for many years because of the bulk and expense of the equipment required. This is because the conductivity is as much a function of temperature as of salinity, which necessitates stabilizing the temperature of the

samples to $\pm 0.001^{\circ}\text{C}$ during measurement. However, improvements in circuits and equipment encouraged a number of laboratories to bring this method into wider use from about 1956. An accuracy of ± 0.003 psu or better is obtained in routine use. This is substantially better than the titration method.

In 1957, Esterson (1957) of the Chesapeake Bay Institute described an inductive (electrodeless) salinometer, which was later developed by Hamon (1955) and Hamon and Brown (1958). Hamon and Brown's inductive salinometer design was the basis for modern inductive salinometers. In this instrument, the temperature effect is taken care of by measuring the

temperature while the conductivity is measured and correcting for its effect automatically in the electrical circuit. The salinity may be measured to a precision of ± 0.001 psu over the range from 32 to 39 psu. With a little practice, an operator can measure the salinity of up to 45 samples per hour. The absolute accuracy of the measurement depends on the accuracy of the standard seawater (Section S16.4.3.4). Since the 1990s, this accuracy has been approximately 0.001 psu.

Conductive salinometers such as the "Autosal" from Guildline (Figure S16.21) are more accurate than inductive salinometers and have virtually replaced them. This salinometer uses a four-electrode conductance cell of small dimensions in a thermostat bath (controlled to

± 0.001 K/day) with a precision of ± 0.001 K or better. The seawater flows continuously from the sample bottle through a heat exchanger in the thermostat, to bring it to a specified temperature, and then through the cell. The conductance-bridge is balanced semi-automatically and the conductivity ratio of the sample relative to that of Standard Seawater (see Section 16.4.3.4) is displayed digitally. Salinity is then obtained from the conductivity ratio and the temperature using the UNESCO/N.I.O International Oceanographic Tables or the Practical Salinity Scale 1978 Formula or Tables referred to in Section 3.4 (UNESCO, 1981). The circuits are such that variations of electrode surface conditions do not affect the measurement. The size of the instrument is about $60 \times 50 \times 55$ cm and it may



FIGURE S16.21 Autosal inductive salinometer in common use in laboratories for salinity analyses. Source: From Guildline (2009).

be used on shipboard as well as in a shore laboratory.

In situ conductivity measurements are made by CTDs (and their predecessors the STDs) and on other subsurface devices where salinity observations are desired, such as moorings and floats. Conductivity sensors are far less stable than thermistors, primarily because they are open cells, often with ceramic coatings, and changes in the geometry of the cells affect the calibration. Therefore, relatively frequent calibration of these sensors using water samples is required for high accuracy.

To obtain salinity measurements from CTDs and similar instruments, temperature must be measured simultaneously with conductivity, since conductivity depends primarily on temperature and only secondarily on salinity. The conductivity and temperature are then combined during processing that takes in account the time lag in sensor response. Different sensors usually have different response times to changes in temperature; a conductivity cell responds faster than the high precision thermistors. Therefore, when processing CTD data, it is important to account for the sensor response time mismatch. Erroneous spiking in the derived salinity is usually a result of this mismatch. Some CTDs overcome the temperature response time by combining a fast but less accurate thermistor with a slower but more accurate precision resistance thermometer (PRT) to yield a rapid and accurate temperature estimate at each level in the vertical.

S16.4.3.3. Salinity Measurements Using Refractive Index

The refractive index of seawater is also related to salinity (and to temperature). The interference type of refractometer has been used in the past for salinity measurements with a claimed accuracy of ± 0.02 psu. A refractometer that can be installed in a profiling instrument to measure salinity in situ rather than in a laboratory setting has been developed.

S16.4.3.4. Standard Seawater

All of the above conductivity methods are comparative rather than absolute, and require a chemical standard for calibration. The current standard is set by the international body, IAPSO, with documentation published by UNESCO (1981). Practical Salinity is defined by the ratio of the electrical conductivity of the seawater sample to that of a standard potassium chloride (KCl) solution, at 15°C and 1 atmosphere (Section 3.4; Lewis, 1980). The standard solution is known as Standard Seawater (SSW), since it actually was seawater collected from a given location near Copenhagen for many years. Defined now as a KCl solution, salinity calibration is much more robust and stable. Oceanographic laboratories throughout the world use samples of SSW, sealed in glass ampoules, to standardize electrical conductivity salinometers. The use of a common standard for salinity reduces the possibility of systematic errors making it possible to combine data from different expeditions or surveys in the same area or worldwide.

S16.4.4. Density Measurement

Standard laboratory methods to determine density directly are not practical at sea because of the motion of the ship, and are far too slow for routine use on shore. Thus density is calculated indirectly from salinity, temperature, and pressure using the equation of state. The most widely used modification to the internationally recognized equation of state was made in 1980, and is referred to as EOS 80. The method for determining this equation of state was described in Section 3.5, along with the newly developed equation of state, TEOS-10, which is replacing EOS 80.

S16.4.5. Other Water Properties

Many properties of seawater are measured in addition to temperature and salinity.

Nutrient concentrations (nitrate, phosphate, silicic acid, nitrite, and sometimes ammonium) are routinely measured using relatively small samples drawn from the rosette sampler with a simple rinse to remove residue from previous analyses. Samples are run using auto-analyzers that mix the samples with chemical reagents. This produces a colored compound whose light absorbance is proportional to the nutrient concentration being measured. The absorbance is measured with a colorimeter. Separate analyses are run for each nutrient.

Oxygen content is even more routinely measured from water samples, and increasingly from oxygen sensors incorporated in a CTD. Sampling of dissolved gases such as oxygen requires care to avoid contamination from the atmosphere. The standard method for oxygen is to rinse nominal 125 ml volume-calibrated flasks with a cone-shaped neck once with minimal agitation followed by a 10 second inverted rinse (to minimize the amount of air/oxygen getting in) with laminar flow from the sample drawing tube (Figure S16.22), allowing the sample to overflow for at least three flask volumes. Reagents are then added to fix the

oxygen before stoppering the flask. Flasks are shaken immediately after drawing, and then again after 20 minutes to assure the dispersion of the $\text{MnO}(\text{OH})_2$ precipitate. These samples are then analyzed for oxygen content within 4 to 36 hours of their collection. This processing uses a Winkler titration with a colorimetric end point to find the oxygen content of the sample. Automated titration rigs are commonly used to reduce the variability in end point detection that can occur between human operators.

CFC analyses were introduced in the 1980s and have become routine for large oceanographic expeditions such as those in the WOCE. Because extreme care must be taken to avoid contamination, not just from the atmosphere but also from shipboard sources, the ships and laboratories must be scrupulously free of refrigerants and propellants that contain CFCs. Samples are drawn from the rosette sample bottles into large syringes, which are filled, ejected, and then refilled. Samples are run in the shipboard laboratory using a gas chromatograph.

Dissolved helium sampling has also become widespread. These samples are drawn into



FIGURE S16.22 Drawing an O_2 sample from a Niskin bottle. (Photo courtesy of J. Swift.)

sample containers, which might be special, nearly impermeable glass flasks or narrow copper tubes, and overfilled to eject any air or air bubbles. The samples are sealed tightly and then taken to the laboratory for later analysis.

In addition to the dissolved gases, nutrients, and salinity, a number of other types of analyses are regularly run. These include dissolved inorganic carbon, pH, alkalinity, tritium, and isotopes of carbon, nitrogen, and oxygen. These require clean samples of seawater, but without the extreme care to exclude air from the samples.

In Section S16.5.3 as well as in Chapter 4 and throughout the ocean basin chapters, the use of some of these chemicals as tracers of circulation and mixing is discussed.

S16.5. CURRENT MEASUREMENTS

There are two basic ways to describe fluid flow: the *Eulerian* method in which the velocity (i.e., speed and direction) is given or observed at every point in the fluid, and the *Lagrangian* method in which the path followed by each fluid particle is given or observed as a function of time (Section 7.2). Both approaches are used to map ocean currents and it is possible to connect the two methods using some approximations.

Typical horizontal current speeds in the ocean range from about 200 cm/sec (about 200 km/day or about 2 knots) in the swift western boundary currents (Gulf Stream, Kuroshio), in the Antarctic Circumpolar Current, and in the upper ocean equatorial currents to a fraction of 1 cm/sec in much of the surface layer and in the deep waters. Vertical speeds associated with the large-scale circulation are very much less, on the order of 10^{-5} cm/sec or 1 cm/day; these are essentially unmeasurable except with extremely good instruments and data filtering. On the other hand, vertical speeds associated with surface and internal waves and tides are easily

measured as they are of the same order as horizontal speeds for the same phenomena.

S16.5.1. Lagrangian Methods for Surface Currents

The simplest Lagrangian current indicator is an object floating in the water, carried by the ocean current with a minimum of surface exposed to the wind, or below the surface of the water. The so-called drift pole, a wooden pole a few meters long (also called a spar buoy) and weighted to float with only 0.5 to 1 m emergent, was historically used to determine surface currents close to landmarks (where the movement of the pole can be measured relative to the landmarks). Such a pole was simply allowed to drift with the water, its position determined at intervals either from the shore or by approaching it in a boat and fixing its position relative to the shore. Sheets of paper or patches of dye, such as sodium fluorescein, which can be photographed at intervals from a high point of land or from an aircraft, have also been used. Glass drift bottles of about 10 cm length, with small cards inside to be returned to the agency that deployed them, were deployed in large numbers prior to the 1930s to map surface currents. Other near-shore drifters have been built as wooden crosses or even "hula hoops" covered with plastic garbage bags. The latter have been found to closely simulate oil being carried along by currents on the surface of the ocean.

Historically, surface currents were mapped using information about how much a ship drifted from its intended course due to surface currents. This information is a by-product of sailing ship navigation. A comparison of the actual track (checked by astronomical navigation, landfall, etc.) with the intended track gives a measure of the surface current every time a positional fix is obtained from the ship. Maury, in about 1853, first suggested examining ships' navigation logs to extract

such information on currents. In his case he first examined the logs for the Gulf Stream region off the eastern United States. The method was subsequently extended worldwide. Most of the maps of surface currents presented in marine atlases are based on the accumulation of such ship-drift data. The modern version of the Maury ship-drift surface current compilation is [Mariano, Ryan, Perkins, and Smithers \(1995\)](#), from which the Gulf Stream map in Figure 1.1b was obtained. The error is +10 cm/sec.

Modern measurements of surface currents are made with freely drifting buoys (or *surface drifters*) with a radio transmitter for satellite tracking. Thousands of tracked surface drifters have been used since the 1970s ([Figure S16.23](#)), most with a lifetime of at least a year. There are three items to consider for the instrument: the surface buoy, the drogue, and the tracking system.

Surface buoys were initially quite large and made of such hardy materials as aluminum or fiberglass. Smaller buoys were then developed to reduce the “windage” or extent to which the drifter was pushed by the wind versus following the current. Thus, the floats became small glass spheres or plastic platters ([Figure S16.24](#)). Another popular alternative was a very small spar buoy that was ballasted to ride with most of the buoy below the surface. As mentioned previously in Section S16.4.2 on temperature, most surface drifters also include a thermistor on the buoy to measure surface temperature. Many, particularly in very remote regions rarely visited by research ships, carry other instruments used for meteorological models and weather prediction, such as air pressure sensors.

The surface drifter’s drogue is attached beneath the buoy with a sturdy line. Usually the connection at the bottom of the buoy float is some form of hydraulic hose capable of flexing a great number of times without breaking. The drogue acts like a parachute, and the

buoy moves at the speed of the water at the drogue depth. Most surface drifters deployed in the 1990s and 2000s were drogued between 15 and 100 m depth and had lifetimes of 1 to 2 years. Measurements of buoy slip through the water have shown that the “holey sock” drogues follow the water better than any of the other drogue configurations. These drogues are wire cylinders covered with fabric with several holes ([Figure S16.24](#)). Measurements also showed that a larger diameter cylinder is better than a longer cylinder of smaller diameter.

Modern surface drifters report their positions and data via satellite. Initially all communication and location was accomplished by the Argos system, carried on the National Oceanic and Atmospheric Administration (NOAA) polar orbiter satellite. This communications system predates the global subsurface float program Argo (Section S16.5.2), and should not be confused with it. A French system with an American subsidiary, Argos is able to communicate with a large number of transmitters at the same time. From the Doppler shift of the radio signal, the satellite is able to compute a fairly accurate position (± 2 km) for the buoy’s location. In addition, Argos is capable of transferring 250 data words, which is enough for the SST samples and barometric pressure if available. With the advent of the GPS satellite navigation system, it is possible to have the buoy calculate its position independently using GPS. Modern communications satellites have much wider bandwidths than available through Argos, allowing transmission of much more detailed data streams. However, many observational programs such as the Global Drifter Program continue to use Argos for continuity and reliability.

In the United States, surface drifter data are collected and processed by the Global Drifter Data Center at NOAA Atlantic Oceanographic and Meteorological Laboratory in Miami,

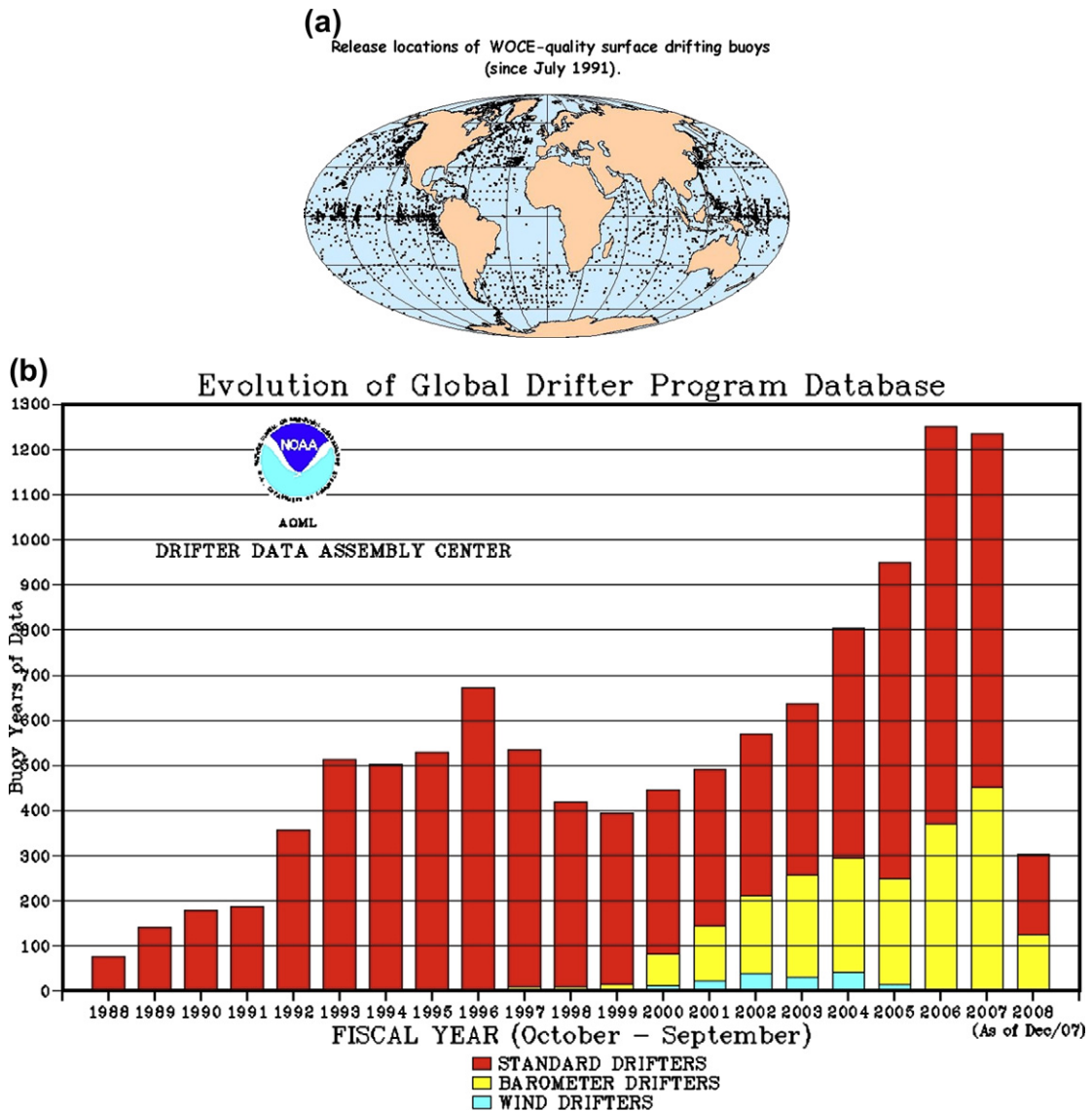


FIGURE S16.23 Starting points of surface drifter tracks from 1991 to 1997. Source: From WOCE (2009). (b) Number of years of drifter data per year since 1988. Source: From NOAA Global Drifter Program (2009).

which currently serves as the international data center for drifting buoy data. Another global drifter data center is located in Ottawa, Canada, at the Marine Environmental Data Service.

S16.5.2. Lagrangian Methods for Subsurface Currents

Subsurface currents are also observed using Lagrangian instruments that follow the water,

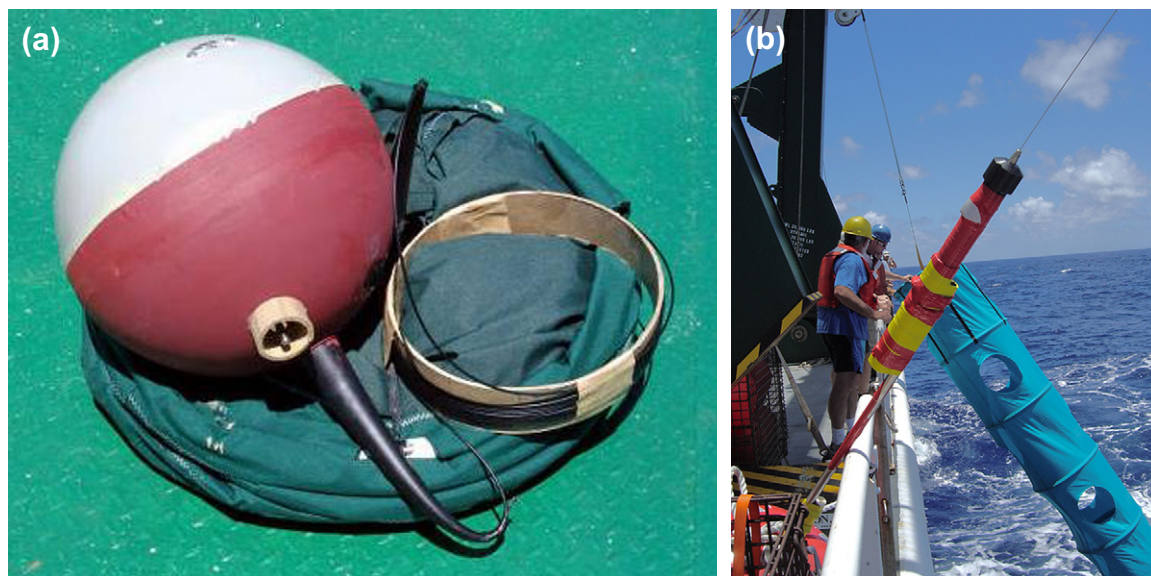


FIGURE S16.24 Lagrangian free-drifting buoy elements: (a) drifter ready to deploy with buoy, coiled wire, and collapsed holey sock drogue. *Source: From NOAA Global Drifter Program (2009).* (b) Holey sock drogue (blue cylinder) being recovered. *(Photo courtesy of K. Buesseler.) Source: From WHOI Image Galleries (2009).*

at least approximately. The first category of subsurface floats that we consider are acoustically tracked. A great advantage of acoustically tracked floats is that they can be followed continuously, hence obtaining information at eddy scales, which is not the case for the pop-up floats described in the next section. John Swallow of the National Institute of Oceanography in England developed the first float in the 1950s (Swallow, 1955). The “Swallow float” (Figure S16.25a) and its modern derivatives are neutrally buoyant, which means that the float’s mass is adjusted before launching so that it will sink to a selected density. Actual seawater density is primarily a function of pressure, hence depth, since the compressibility of seawater causes a larger density range than either temperature or salinity (Section 3.5). The float then remains at this depth and drifts with the water around it. The Swallow float sent out sound pulses at intervals, which was followed by listening to it through hydrophones from the ship that chased the float and simultaneously determined its own position. In

doing this, the direction and speed of drift of the float was determined.

Subsequently, floats were developed that could be tracked by moored instruments or by satellite, removing the need to chase them, permitting long deployments. A research ship is needed to deploy and retrieve the moorings and to deploy specialized floats. The first development, by Rossby and Webb (1970), was the “SOFAR float” (Figure S16.25b), which emitted a signal that was picked up by at least three moored hydrophones, so that the position of the float could be continuously monitored through triangulation. The word SOFAR refers to the main sound channel in the ocean, which is at the depth of the minimum in sound velocity (Section 3.7).

A reversed system called RAFOS (SOFAR spelled backwards) was developed in the 1980s (Rossby, Dorson, & Fontaine, 1986), in which the buoy is a simple listening device and the moored stations are low frequency acoustic sources (Figure S16.25c). This greatly reduces the cost of the (much smaller)

expendable floats and puts the higher cost into the moorings that are retrieved and reused. The RAFOS float is much smaller than the SOFAR float since the sound source is a very long tube that resonates like an organ pipe (Figure S16.25c). The RAFOS system is currently the basis for all acoustically tracked subsurface floats. At intervals, the buoy comes to the surface, reports its data over the same satellite system used to track surface drifters, and then returns to its pre-selected depth to collect more information. (Often this interval is just the beginning and end of the experiment, so it might take several years to obtain the data.) RAFOS and SOFAR systems are restricted to the region of the ocean that isinsonified for the experiments, which is typically no larger than about 1000 km radius because of the range of the tracking. RAFOS deployments in the North Atlantic at various depths have been used extensively to map the circulation and its eddy statistics (Figure S16.26).

Other acoustically tracked floats that have been developed and deployed in special experiments, primarily in the North Atlantic, include floats that continuously re-ballast themselves to follow an isothermal or isopycnal surface (isopycnal floats; Figure S16.26) and floats that move up and down to sample a layer in the ocean, usually to profile temperature and salinity in that layer (“bobber floats”).

A lower cost alternative to acoustically tracked floats, with the additional advantage of permitting coverage everywhere in the (ice-free) ocean because they do not require moorings, was developed by R. Davis and D. Webb in the 1990s (Davis, Killworth, & Blundell, 1996) as part of the WOCE. These pop-up floats, more commonly called “profiling floats” (Figure S16.27), are neutrally ballasted for a pre-assigned depth, and are tracked only by coming up to the surface at regular, pre-assigned intervals and transmitting to a satellite. The satellite then records the float position and also any temperature or salinity or other observations

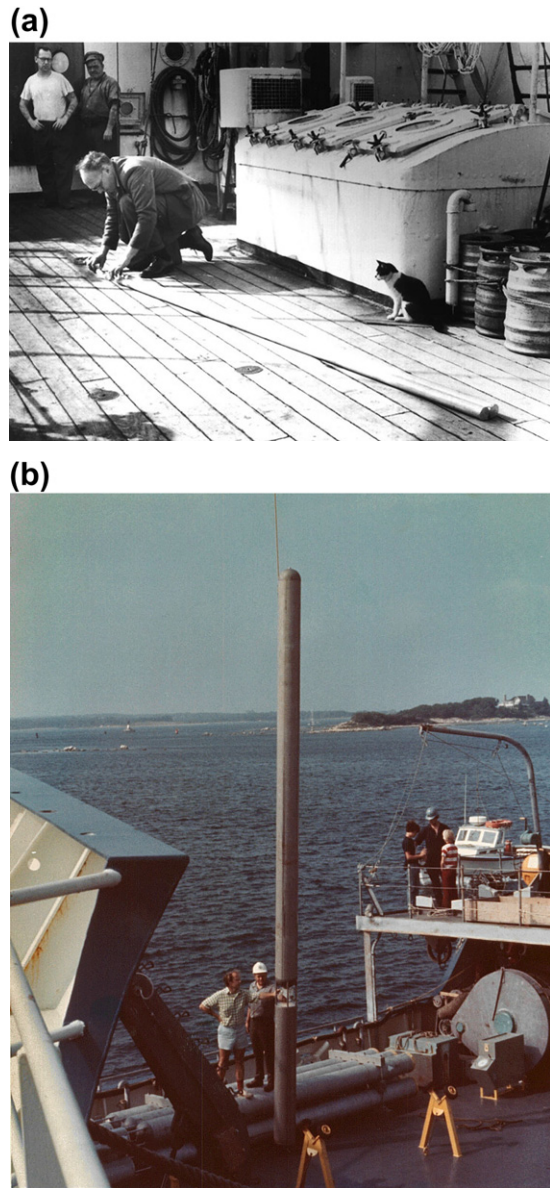


FIGURE S16.25 Acoustically tracked floats: (a) Swallow float, (b) SOFAR float, and (c) RAFOS float. Source: From University of Rhode Island Graduate School of Oceanography (2009). See also Rossby (2007).

that are profiled by the float (Section S16.4.2.6). After reporting to the satellite and perhaps remaining at the surface for half a day or more

(c)



FIGURE S16.25 (Continued).

to ensure the satellite transmission, the floats return to their original depth. Because these floats are only discretely tracked when they pop to the surface, say every 10 days, the velocity field is more coarsely resolved than

from acoustically tracked floats. The latter therefore are preferable for experiments requiring resolution of the ocean's eddies, while the pop-up floats are useful for studying larger scale circulation with its longer timescales. They are

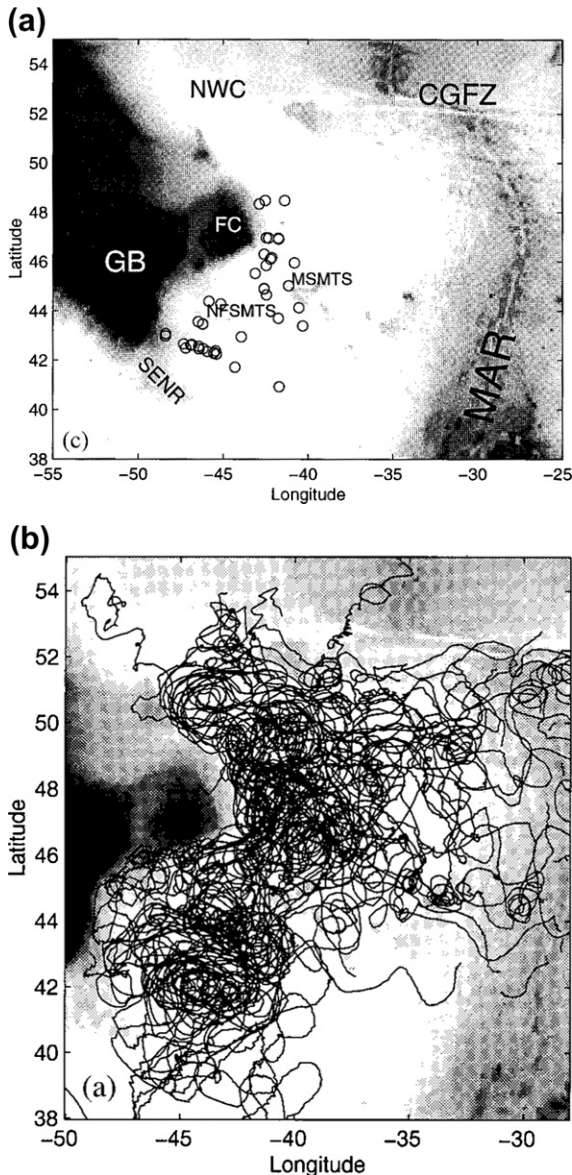


FIGURE S16.26 RAFOS floats on the isopycnal surface $27.2 \sigma_0$ in the North Atlantic for 1993 through 1995: (a) release locations and (b) tracks. Source: From Zhang, Prater, and Rossby. (2001).

also proving to be extremely useful for providing global temperature/salinity profiling when they pop to the surface.

The profiling floats ascend and descend by using oil in a small cavity to control buoyancy. When the float ascends, the oil is pumped into an external bladder. When it descends, the oil is pumped back inside the solid body of the float. The floats are carefully ballasted for the desired “parking depth”; for 20 m accuracy, the ballast must be accurate to within a gram compared with the much greater weight of the float.

Profiling floats commonly carry a thermistor and often a conductivity sensor so that temperature and salinity can be vertically profiled and measured during the full-submersed track if desired. Additional sensors continue to be desired; a popular add-on is an oxygen sensor. The floats can be “parked” at one depth, say 1000 m, if this is the depth where the velocity field is desired, and then profile down to say 2000 m just before popping to the surface to provide a deeper profile. This vertical transit is now used to measure oceanographic profiles, which are then reported via satellite giving an autonomous ocean profiling system.

Large-scale deployments of profiling floats were made in the 1990s at 1000 m depth. A global network called Argo (not to be confused with the satellite communication service Argos) consisting of the most recent designs of these floats is now underway (Figure S16.27c) as part of the long-term global ocean observing system. It is intended that this kind of observational system will remain in place for the foreseeable future as a means of regularly mapping the temperature, salinity, and velocity structure of the upper half of the ocean. In the recent Argo program, the floats are parked at 1000 m for 10 days, then sink to 2000 m before they rise to the surface, collecting temperature and salinity profiles along the way. These floats carry GPS units for precise geolocation while they are at the surface. The position and profile data are then relayed via satellite.

Another advantage of the Argo floats is that they can be deployed by a variety of methods. Traditional deployments from research vessels

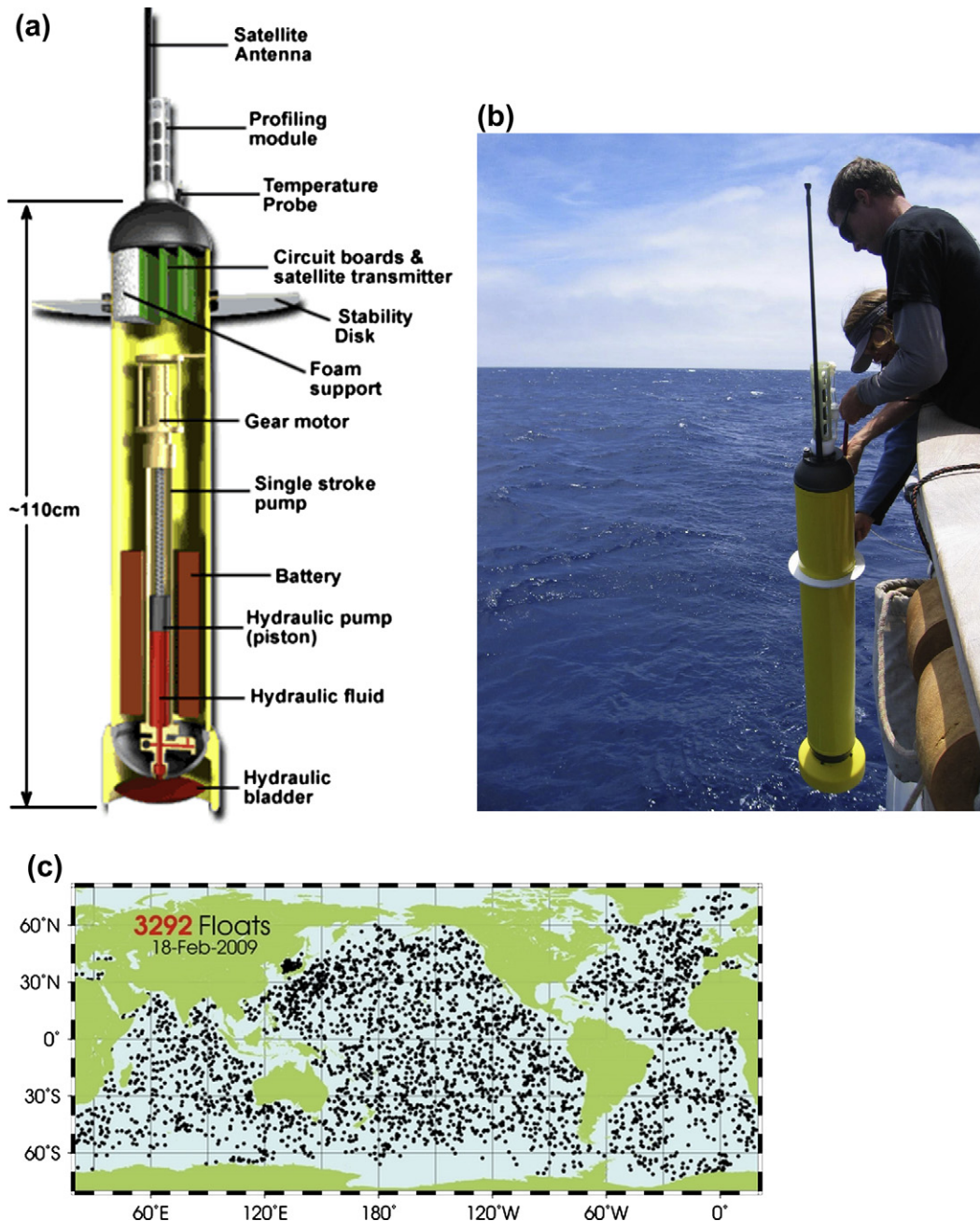


FIGURE S16.27 (a) Schematic of an Argo float. (b) The 3000th Argo float being deployed in July 2007. (Photo courtesy of Kara Lavender.) *Source: From Argo 3000 (2007).* (c) Argo float profile locations in February, 2009. *Source: From U.S. Argo Program (2009) for a and c.*

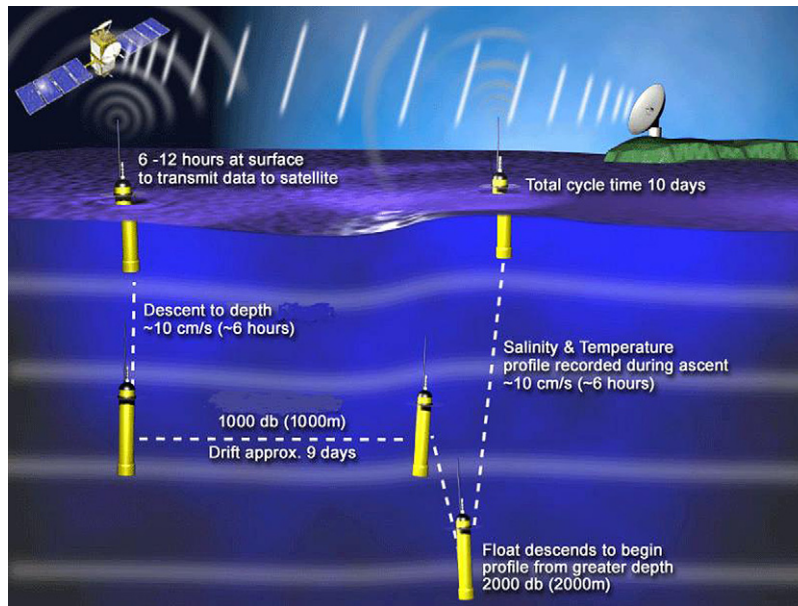


FIGURE S16.28 Operation of an Argo float in “park and profile” mode. Source: From U.S. Argo Program (2009).

can be augmented by deployments from merchant vessels of opportunity and from aircraft. This capability is particularly important for regions such as the Southern Ocean where visits by research vessels and merchant ships are infrequent.

The operation of an Argo float is summarized in Figure S16.28, which demonstrates the 10-day repetition cycle, including its hours at the surface, descent, 9 days at its “parking” depth, and ascent. Not included in the diagram is the possibility of parking at one depth for most of the nine days and profiling over a larger range of the water column.

S16.5.3. Lagrangian Methods Employing Tracers

While they are not direct measurements of current, we discuss flow tracers here, since they provide direct evidence of some average of the circulation and diffusion. Tracers are

useful if they have known regional or temporal sources, such as intentional dyes or an actual pollutant like sewage or industrial waste. Samples of water are collected from a grid of positions near the source and in likely directions of flow. The tracer concentration is determined by chemical analysis. In all tracer release studies both advection and eddy diffusion are acting three dimensionally to spread the tracer, thus results cannot be interpreted solely in terms of advection by currents.

Intentional tracers that have been used are red dye rhodamine-B and sulfur hexafluoride (SF_6). Rhodamine-B can be detected at extremely small concentrations (less than 1 part in 10^{10} of water) by its fluorescence, using relatively simple instruments, and it is also non-toxic at such dilutions. It is only of practical use in coastal waters. SF_6 can be detected at much lower levels and has been used in the open ocean to study stirring and mixing of ocean waters over periods of up to a year (Figure

S16.29). Eddy diffusivities in the horizontal and vertical directions (Sections 5.1 and 7.3.2) have been derived from this intentional tracer.

Materials released unintentionally in small amounts for reasons other than oceanographic research have been exploited as artificial tracers of water movement. These materials are known as “transient tracers” (Section 3.6). Primary examples of radioactive or unstable materials are tritium (decaying to ^3He) and $\Delta^{14}\text{C}$ (radioactive) released into the Northern Hemisphere atmosphere in the early 1960s during atomic bomb testing in the Pacific, and iodine (^{129}I) (radioactive) released from a nuclear plant in western England. $\Delta^{14}\text{C}$ also occurs naturally and is useful for relative dating of the ocean’s deep waters. However, its anthropogenic concentrations are much larger than its natural concentrations, making $\Delta^{14}\text{C}$ useful for following surface waters into the subsurface ocean. Primary examples of stable materials created for industrial use are the CFCs, which have been used as cleaning compounds, refrigerants, and propellants. With known production rates since their invention and introduction in the twentieth century, and recent curtailment because of their major impact on Earth’s ozone layer, CFCs have been useful for determining ventilation pathways. Because these tracers have temporal source functions that are well understood, they can also be used for bulk dating of the tagged subsurface waters (Section 4.7).

Tritium, enhanced levels of $\Delta^{14}\text{C}$, and CFCs have been traced through all the upper ocean waters of the world. In the Pacific example of Figure 4.25b, tritium is higher in the Northern Hemisphere, demonstrating the predominantly Northern Hemisphere atmospheric source (primarily in the 1960s). Low values in the Antarctic result from upwelling of deep waters. Penetration of the purely anthropogenic tracers to the ocean bottom in the Antarctic and North Atlantic shows that these are regions of deep water formation. ^{129}I has been traced through much of the northern North Atlantic, following

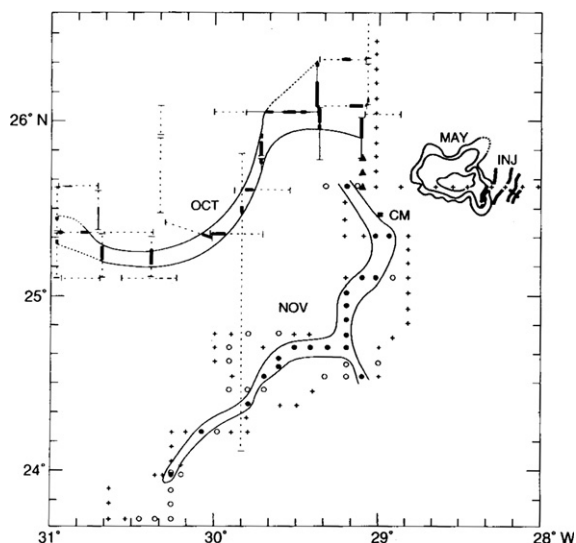


FIGURE S16.29 Horizontal region covered by an intentional release of sulfur hexafluoride after release at a point in the subtropical North Atlantic. Source: From Ledwell, Watson, and Law (1993).

the subpolar circulation. The concentration of these released tracers is extremely low. They are useful because there is either no natural source or the natural source creates a much lower concentration than the anthropogenic source.

S16.5.4. Eulerian Current Measurement: Mechanical Sensors

Current meters are deployed at a fixed location and record the current speed and direction over time. The instruments described in this section have mechanical moving parts, and are more subject to fouling than the acoustic and electromagnetic current meters described in Section S16.5.5.1. As a result, acoustic methods have largely superseded mechanical sensors, but we describe the most common mechanical current meters because of the abundance of historical data records.

All current meters have a sensor for speed, a sensor for direction, and ideally a sensor for

pressure to detect mooring deflections in the vertical. Ideal speed sensors have low inertia. Compasses are used for direction, and must be extremely well calibrated especially if used where the horizontal component of Earth's magnetic field is small. The technology for mooring and recovering the instrument is also important. Most current meter systems record internally and are retrieved by a research vessel to recover the data, although some modern moorings are equipped to transmit their data via communications satellite.

Before 1960, the most widely used Eulerian instrument was the Ekman current meter (shown in a unique "repeating" form in Figure S1.4). This consisted of a 10-cm-diameter ducted propeller mounted in a frame with a large "tail" to orient the meter with the current. The assembly was attached to the end of a wire and lowered to the desired depth. A metal weight (messenger similar to that used for a hydrographic "bottle" cast) was dropped down the wire to free the propeller to rotate and a second one was dropped after a measured time to stop it. The number of revolutions was recorded by a mechanical counter. The water speed was then proportional to the number of revolutions per minute. The current direction on an Ekman current meter was recorded by the rotating counting mechanism dropping small metal balls at even intervals (controlled by the rotation of the propeller) into a magnetic compass tray with 100 sectors. Thus, the number of balls in each tray gave a statistical view of the directions. This instrument had to be lowered and raised for each measurement — a tedious business.

The Robert's current meter was an improved version of the Ekman current meter, and is the forerunner of most current meters today. In the Robert's meter, speed (from a propeller) and direction (from a compass) were transmitted electrically to the surface and recorded ship-board or transmitted by radio from the supporting buoy to a mother ship. Since this required

considerable ship time to collect the measurements, these current meters were eliminated in favor of internally recording instruments that can be moored for considerable periods of time.

One disadvantage of most propeller-type current meters is that up-and-down motion (when the ship rolls or the mooring moves), which may cause the propeller to turn and cause inaccuracies in the speed measurement. A hollow cylinder (ducting) with its axis mounted horizontally around the propeller minimizes this effect. An alternative to the propeller is the Savonius rotor (Figure S16.30), which is less sensitive to vertical motion. It consists of two half hollow cylinders mounted on a vertical axis with flat end plates and produces a large torque even in small horizontal currents. The rotor is made of plastic to be neutrally buoyant to reduce bearing friction so that it is sensitive to currents of as little as 2 cm/sec. Even this low threshold value can be a problem in parts of the ocean where currents of this order prevail. The rotor carries several small magnets. As each magnet passes a coil on the frame it induces a momentary electrical current pulse. The number of pulses per second is proportional to the current speed. The current direction is determined electrically with reference to a magnetic compass.

The Savonius rotor was used in Aanderaa current meters (Figure S16.31, which were widely used for several decades. (Aanderaa now sells only acoustic sensors.) The Savonius rotor on the Aanderaa current meter is affected by vertical mooring motion, which causes an alternating artificial current by what is called "rotor pumping." This effect can double the recorded current speed and is most severe on shallow meters and in coastal regions where wave action is significant. To reduce this effect, Aanderaa now mounts a semi-cylindrical shroud around one-half of the rotor and uses flat rotor blades rather than curved ones.

Note in Figure S16.31 that the current meter is mounted on the mooring line with a hard bar

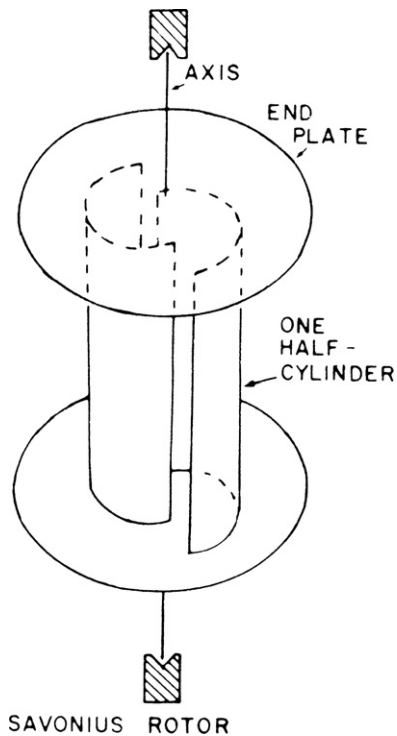


FIGURE S16.30 Savonius rotor current meter.

while the current meter is supported by a gimble that allows complete azimuth change with limited vertical variation. Thus, the current meter is expected to align itself with the current that then measures the current direction with an internal compass. All of the external sensors are at the top of the current meter. These can include temperature, pressure, and inductive salinity. In the earlier Aanderaa current meters, current speeds and directions were averaged over a fixed period of time and stored internally.

The Vector Averaging Current Meter (VACM) (Figure S16.32a) was designed in the 1960s to measure the velocity frequently, resolve it into components, and record averages of these components separately to give a more complete record of the velocity. Presently available Aanderaa meters follow this protocol as well. Like

Aanderaa current meters, VACMs use a Savonius rotor and vane. They were made by EG&G Marine Instruments and remained in wide use through the 1990s.

The Vector Measuring Current Meter (VMCM) was developed in the 1970s (Weller & Davis, 1980) to compensate for the rotor pumping problem that affects Savonius rotors. The VMCM (Figure S16.32) uses two orthogonal propellers. The open fan-type rotors of the VMCM are susceptible to fouling, and so, like Savonius rotor current meters, VMCMs are gradually being replaced with acoustic current meters.

S16.5.5. Eulerian Methods: Acoustic and Electromagnetic Current Meters

Non-mechanical current-measuring devices include acoustic and electrical-field and magnetic-field sensing tools. These methods are replacing mechanical current meters because they are less subject to inaccuracies resulting from fouling.

S16.5.5.1. Acoustic Current Measurements

The most widespread non-mechanical Eulerian current measurement technology is acoustic, which measures the travel time of pulses of high-frequency sound reflecting off particles in the water. The Doppler shift in frequency gives a measure of fluid speed along the sound path. These Doppler sonar profilers (Figure S16.33) are equivalent to sonic anemometers used to measure winds. Acoustic systems have no moving parts that can foul or provide inertial resistance to changes in ocean currents. Fouling on transducer heads reduces instrument range but not accuracy. Acoustic instruments can also provide current measurements at numerous depths within the range of the instrument, which is usually several hundred meters.

Acoustic instruments in wide use include acoustic Doppler current profilers (ADCPs), acoustic Doppler velocimeters (ADVs), and acoustic current meters (ACMs) (Figure 16.33).

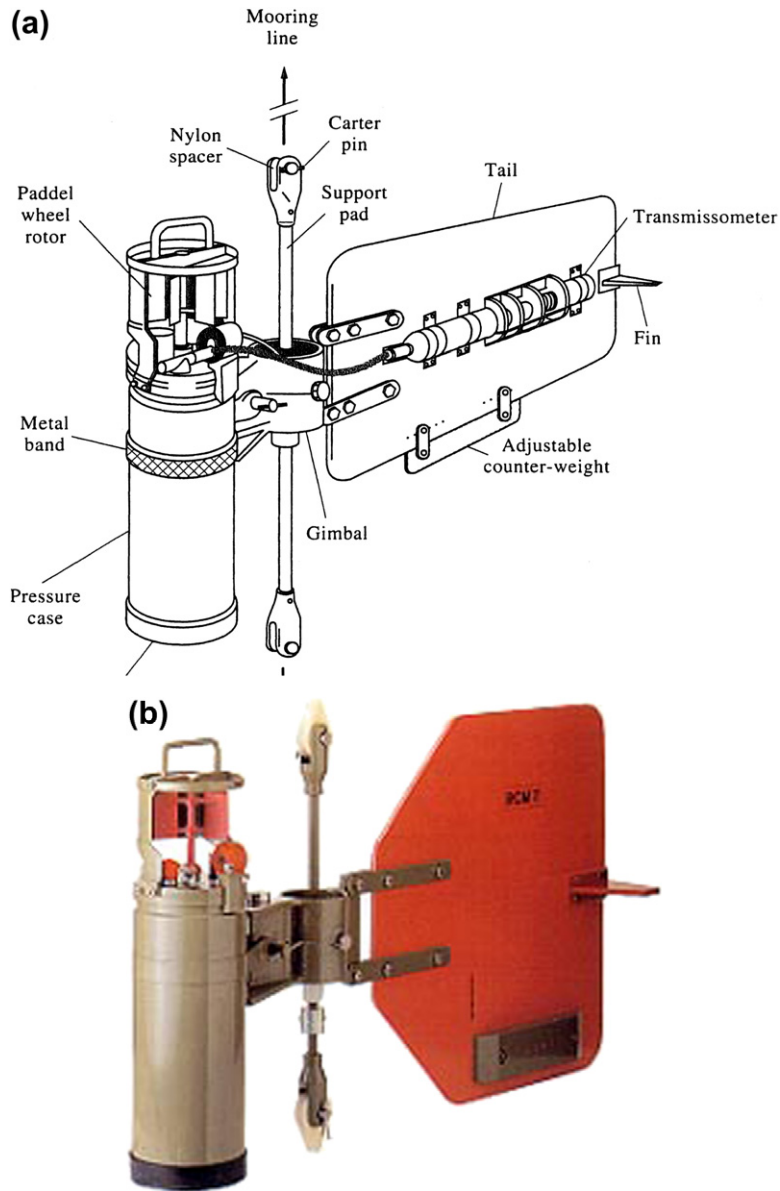


FIGURE S16.31 Aanderaa RCM-7/8. Source: From Aanderaa Instruments (2000).

Acoustic current profilers are used both from ship installations and as moored current meters. For mooring use, both ADCPs and ACMs are available. ADCPs are also sometimes incorporated in a CTD/rosette package

and used to profile velocities in the water column along with the temperature and salinity profile from the CTD. In this configuration they are known as Lowered ADCPs (LADCPs).

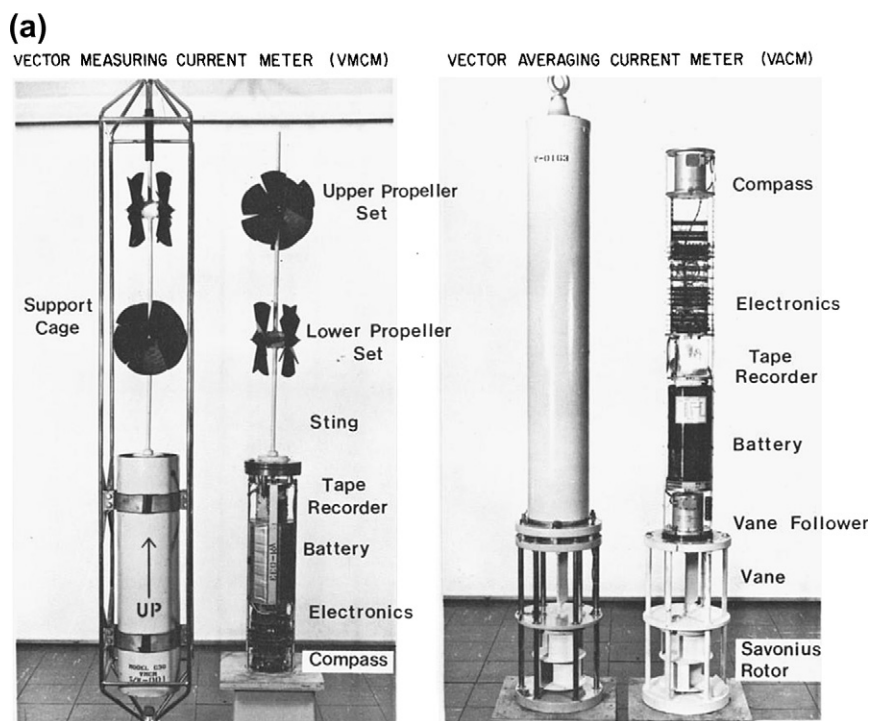


FIGURE S16.32 (a) Vector Measuring Current Meter (VMCM) and Vector Averaging Current Meter (VACM). *Source: From Beardsley (1987).* (b) Deploying a VMCM with some other instruments. *Source: From USGS (2005).*

The ADCP was developed in the 1970s from the “Doppler log,” which measures currents relative to a moving ship to yield ship speed. (Originally, the speed of a sailing ship was measured by measuring the travel time of a log thrown into the water as it went from the ship’s bow to its stern. From this practice, any speed-measuring device from a ship became known as a log.) The Doppler log measures the speed of the ship by sending out an acoustic pulse that is reflected back to the ship by particles in the water (such as plankton). The Doppler shift of the returned signal’s frequency compared with the original pulse makes it possible to compute the ship’s speed relative to the water.

The use of ADCPs for oceanographic research was pioneered by Rowe and Young (1979) and Pinkel (1979). This same Doppler technology allows the water motion relative to

the ship to be measured if the ship’s motion can be accurately computed from an external navigation system, such as the satellite Global Positioning System (GPS). By controlling the direction of the acoustic beam, the Doppler system reflects the currents at different depths below the ship. The principals of operation are described in Howe and Chereskin (2007).

Using a three- or four-element sensor head, an ADCP (Figure S16.33) is capable of resolving both speed and direction of the water movements relative to the sensor. Most oceanographic research vessels carry an ADCP system on board and may operate it continuously. The ADCP profiling depth depends on the sound frequency used in a given instrument. There is a trade-off in depth coverage versus vertical resolution. Greater depth coverage requires a lower frequency, which results in lower vertical

(b)



FIGURE S16.32 (Continued).

resolution. Commonly employed ADCPs profile over 300 m. Lower frequency Doppler instruments are becoming more common, profiling to 800 or even 1500 m.

ADCP ACCURACY IS LIMITED BY

1. The accuracy of the frequency shift measurement used to obtain the relative velocity; this estimate is conducted by software within the instrument and strongly depends on the signal/noise ratio and the velocity distribution among the scatters.

2. The size of the footprint and the homogeneity of the flow field; at a distance of 300 m from the transducer, the spatial separation between sampling volumes for opposite beams is 300 m so that they are seeing different parts of the water column, which may have different velocities.
3. The actual passiveness of the drifters (i.e., how representative are they of the in situ current?) and the concentration of the drifters (limiting range in regions of exceptionally clear water).

In the shipboard system, the ADCP can track the bottom and obtain absolute velocity, provided the acoustic beam ranges to the bottom. Once out of range of the bottom, only the velocity relative to the ship can be measured. Erroneous velocity and backscatter data are commonly obtained from shipboard ADCP measurements due to vessel motions in moderate to heavy seas; the transducer head can be exposed and the acoustic signal attenuated by air bubbles under the ship's hull or through the upper portion of the water column. Much better data are collected from a ship "running" with the seas than one lying in the trough or hove-to in heavy seas. In deep water, zooplankton aggregations can lead to the formation of "false bottoms" in which the instrument mistakes the high reflectivity from the scattering layer as the seafloor.

ACMs and ADVs typically measure currents at a point. Different instruments have been developed for the wide range of fluid conditions from rivers, lakes, and surf zones, to shallow water and the deep ocean. Different instruments have been developed for different conditions, ranging from very shallow to deep water. Commercial ADVs use three beams focused a short distance from the instrument (tens of centimeters); they measure all three components of the velocity at one point with high spatial resolution useful for studying turbulence and waves.



FIGURE S16.33 Acoustic Doppler Current Profiler with a 4-transducer head. Source: From *Teledyne RD Instruments (2011)*.

S16.5.5.2. Electrical and Magnetic Field Current Measurements

A second technique for non-mechanical current measurement is the *hotwire anemometer*, commonly used to measure wind speed. In this instrument, the rate of cooling of an electrically heated wire is a measure of the fluid speed past it. A thin wire or metal film about a millimeter long is exposed to the flow and maintained at a constant temperature by automatically adjusting the electric current through it so that the joule heating is exactly equal to the rate of loss to the fluid. The magnitude of the electric current is then a measure of the fluid speed. This device is small and responds rapidly to flow variations, which makes it particularly suitable for the measurement of turbulent fluctuations of flow speeds. Problems with this system include its sensitivity and tendency to foul. As a result, no reliable moored version has been developed.

A third technique, the *electromagnetic method*, uses a fundamentally different principle first suggested by *Faraday (1832)*. With this technique an electromagnetic force (EMF) is induced in a conductor when it moves through a magnetic field. In oceanographic applications, seawater is the conductor. When seawater flows across the

lines of force of a magnetic field, an EMF is generated:

$$E = B \cdot L \cdot v \quad (\text{S16.1})$$

where v is the water speed, L is the width of the current between the measurement points, and B is the strength of the magnetic field component in a direction mutually perpendicular to the direction of both v and L . Depending on the application and instrument, the magnetic field can be that of Earth, or it can be generated internally in the instrument. For a horizontal current and a method that uses Earth's magnetic field, B is the local vertical component of the magnetic field.

Faraday attempted to measure the flow of the Thames using this method, but was unsuccessful because of problems with copper electrodes. Some of the earliest reported successful measurements by this technique were of tidal currents in the English Channel (*Young, Gerard, & Jevons, 1920*); a long series of measurements was made of the Florida Current between Key West and Havana (*Wertheim, 1954*). The basic equipment required is a recording milli-voltmeter and two electrodes to dip in the sea. An example of a modern electromagnetic current meter, with two pairs of electrodes on opposing sides of a small plastic sphere (25 cm or 10 inch diameter), is pictured in *Figure S16.34*; this particular instrument generates its own magnetic field internally and the "current width" is the distance between the opposing electrodes. Because there are two pairs of sensors mounted perpendicular to each other, two orthogonal velocity components can be measured.

Unused commercial *undersea cables* are often used to make electromagnetic measurements of currents. A very long time series of current measurements through Florida Strait, between Florida and the Bahamas, has been collected using this method with abandoned telephone cables that have easily accessible terminations

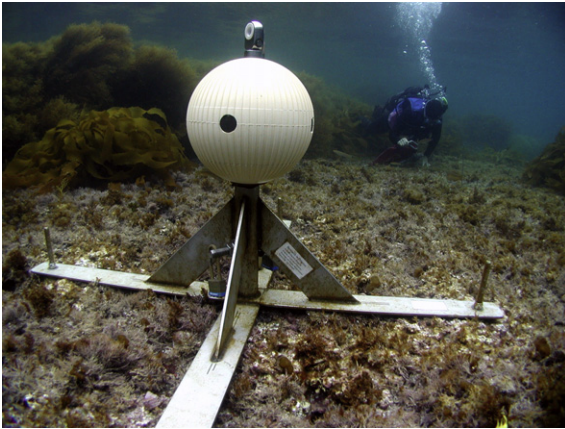


FIGURE S16.34 Electromagnetic current meter (S4 model). Source: From *InterOcean Systems* (2011).

on either end (Larsen & Sanford, 1985). Undersea cables that have been used for such transport measurements are shown in Figure S16.35 and are monitored by ICPC (2007).

One source of error in the EMF method is the finite, but usually unknown, electrical conductivity of the sea bottom, allowing an electrical current to flow due to the induced EMF and thus reducing the observed EMF below the level expected from the formula and speed of the water. This introduces a constant scaling factor, which must be determined by making some water-current measurements with another type of meter while the electromagnetic system is in operation.

The *Geomagnetic Electrokinetograph* (GEK) was an early adaptation of the electromagnetic technique to permit underway shipboard current measurement (Longuet-Higgins, Stern, & Stommel, 1954; Von Arx, 1950). Two electrodes were towed behind the ship with a cable strung between the electrodes. The EMF induced in the cable was recorded as a measure of the component of the water velocity perpendicular to the ship's track. To obtain the total water velocity, the ship was then turned at right angles to the original track and a second component measured. Combining the two

components gave the water velocity relative to the solid earth. The difficulty of reducing and interpreting GEK data led to a rapid decline in its use. The small magnitude of Earth's magnetic field together with electrical noise always present in nature makes the geoelectromagnetic method practical only with electrode separations of tens of meters or more. Recently current meters employing this principle with even smaller electrode spacing have become available commercially. They have no moving parts but do need a significant electrical power supply.

Most electromagnetic current meters allow for additional measurements of temperature, conductivity, and pressure. Data can be averaged over regular intervals of a few seconds to tens of minutes, or set to burst sampling with a specified number of samples per burst at a given sampling interval. For example, one can set the number of samples per burst (say continuous sampling for two minutes every hour) and set the number of times velocity is sampled compared with conductivity and temperature. The limitations are the storage capacity of the instrument (thousands of kilobytes) and the amount of power consumption. For some electromagnetic current meters, the surface of the housing is grooved to maintain a turbulent boundary layer to prevent flow separation at higher speeds.

S16.5.6. Mooring Technology

S16.5.6.1. Subsurface Current Meter Moorings

Even with the development of improved instruments, the measurement of currents from a ship has several disadvantages. A major one is that a ship cannot remain at sea for very long, whereas it is very useful to obtain long records of currents. A second, but minor problem is that ship movement introduces spurious components into the measured currents, which must be

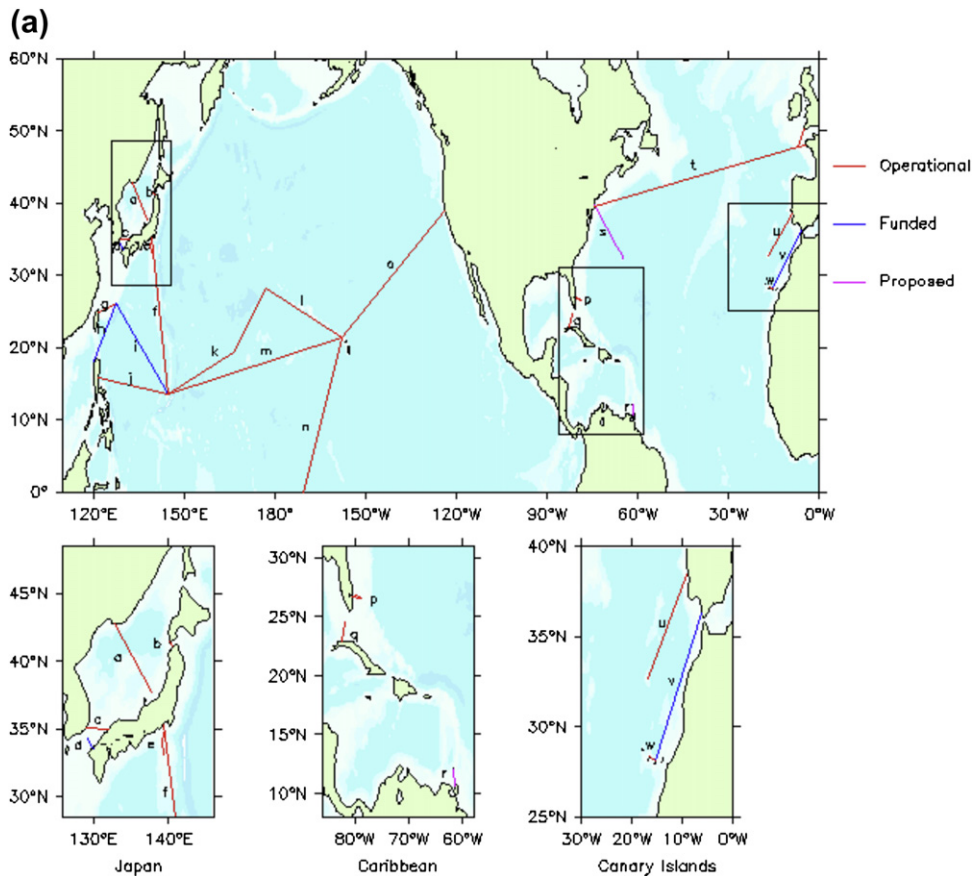


FIGURE S16.35 (a) Map showing abandoned commercial undersea cables that have been exploited for observations of transports. This map was prepared in 1998. (b) Close-up of Florida Current cable measurement locations. *Source: From Flosadottir (2004) and ICPC (2007).*

filtered. (However, moored measurements can have their own problems with motion.)

For these reasons, techniques for the successful mooring and recovery of strings of current meters in the deep ocean, supported on a cable from a buoy beneath the surface to an anchor weight on the bottom, have been developed since the mid-1960s. There are still problems associated with the movement of the mooring in strong currents, but an autonomous, moored string of current meters is nevertheless an efficient way to resolve and monitor ocean current behavior over a period of time. Instruments

can also be mounted on a frame that is fixed on the bottom, which eliminates mooring motion that is useful in shallow water or for instrument types such as ADCPs or inverted echo sounders that sample a large part of the water column from a single instrument.

Moorings can be primarily surface or subsurface, depending on location of the uppermost instruments and mooring flotation (Figure S16.36). Surface moorings have a surface float with the instruments suspended below it on a line. There is a loose tether to a bottom anchor. Surface buoys are commonly used for surface

(b)

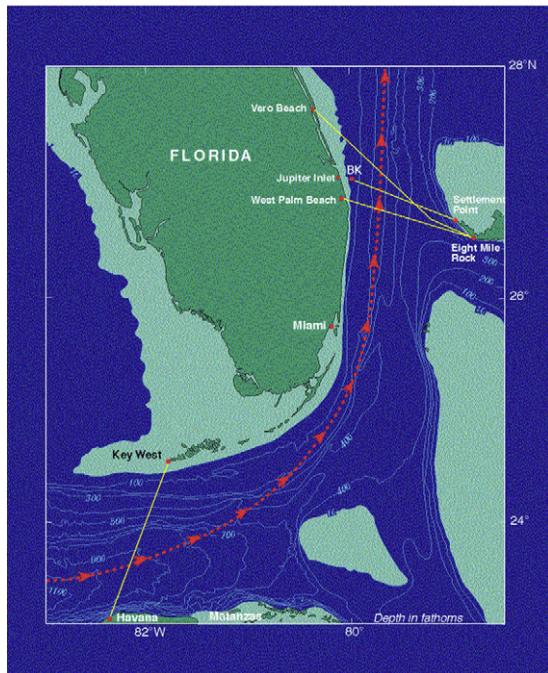


FIGURE S16.35 (Continued).

meteorological observations, such as wind, pressure, and so forth; for surface layer observations with a downward-looking ADCP; and when regular data telemetry is desired. On a subsurface mooring the uppermost flotation for the line of instruments is below the sea surface and includes clusters of intermediate floats (Figure S16.37a) that provide buoyancy to the mooring to keep it tight and provide the buoyancy needed for recovery. The floats are attached at intervals in the mooring to give intermediate buoyancy making the mooring tighter so that it resists being displaced by currents. Mooring lines consist of steel cable, nylon rope, or a synthetic called Kevlar. Steel cable is very strong and inexpensive but is subject to kinking while being deployed, which can dramatically weaken the cable. Nylon rope and Kevlar are most commonly used, because both are pliable and thus unaffected by kinking

but are more expensive. Mooring anchors are usually a set of used, hence low cost, railroad wheels (Figure S16.37b,c).

To recover a mooring after it has been in the water for the length of the experiment, it is necessary to find it and release it. With GPS navigation, it is now straightforward to return to the deployment location for recovery. The most common release method is an acoustic release (Figure S16.37d) mounted between the anchor and the end of the line; when it receives an acoustic signal from the recovery ship, it releases the line and the mooring surfaces. Battery lifetime is the primary limiting factor for acoustic releases. An early recovery technique was a double anchor with a float at the surface marking the second anchor. This second anchor could be recovered and the system brought in, ending with the current meters and flotation. With this system, subsurface flotation could be used, which greatly reduced mooring motion from surface effects. A modification of this system eliminated the surface marker for the second anchor but required the ship to grapple to find the cable between the two anchors. The absence of a surface marker is advantageous when there are ships or icebergs in the area. These recovery methods were time-consuming and risky compared with the acoustic release method.

For deployment, a mooring is laid out behind the ship, starting with the float that will be nearest the surface. The top float usually has a light and radio transmitter that activates when the float reaches the surface during retrieval. The top float is often equipped with a radar reflector to make it easier to see on the ship's radar. After the near surface float is in the water the rest of the mooring is played out one segment at a time with current meters, thermistor chains, and intermediate floats installed along the line as planned. At the end, the acoustic release is mounted above the anchor with the entire mooring floating out away from the ship. The ship is then maneuvered into position so that when the anchor is

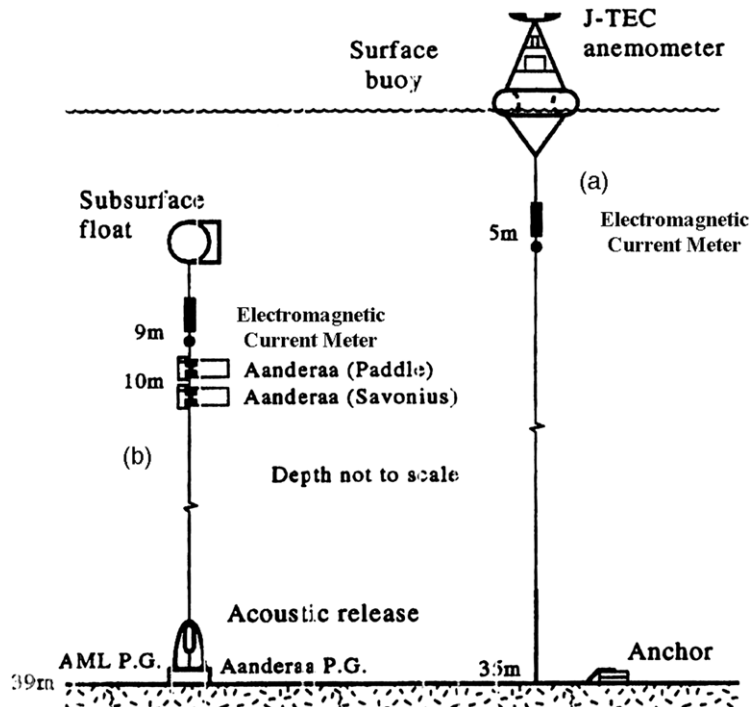


FIGURE S16.36 Two current meter mooring configurations: (a) Surface mooring and (b) subsurface mooring. Internal mooring flotation on the subsurface mooring is not shown. Source: From Emery and Thomson (2001).

dropped the mooring will fall to the position desired. This is usually done by cutting a separate line that has been used to support the anchor when the ship is brought to the correct location. When the mooring is recovered, it includes a surface float with a radio transmitter and a light to assist in locating it. Once spotted, the ship is maneuvered so as to approach the buoy with the working deck exposed to carefully get hold of the line to pull the mooring in. The current meters are strung out along the surface, supported by the surface float and the various intermediate floats. The mooring line is brought on board, disconnecting the current meters from the line.

S16.5.6.2. Deep-Sea Surface Moorings

Surface moorings have been used in coastal oceans for many decades to measure

atmospheric conditions and sometimes the currents and conditions in the water column. In the past several decades, surface buoys have also been moored in the deep ocean to measure air–sea interactions, particularly in the tropical Pacific, which is the location of the El Niño–Southern Oscillation (ENSO). The tropical Pacific moorings were started as part of the Tropical Ocean–Global Atmosphere (TOGA) program, and are called the TOGA Atmosphere Ocean (TAO) buoys (Section 10.8; Figure S16.38; TAO, 2009). The TAO buoys relay their data in real time and measure surface atmospheric conditions as well as the water column. The tropical measurements have proven so important for interannual climate prediction that the arrays have been extended into the tropical Atlantic and Indian Oceans in arrays referred to as

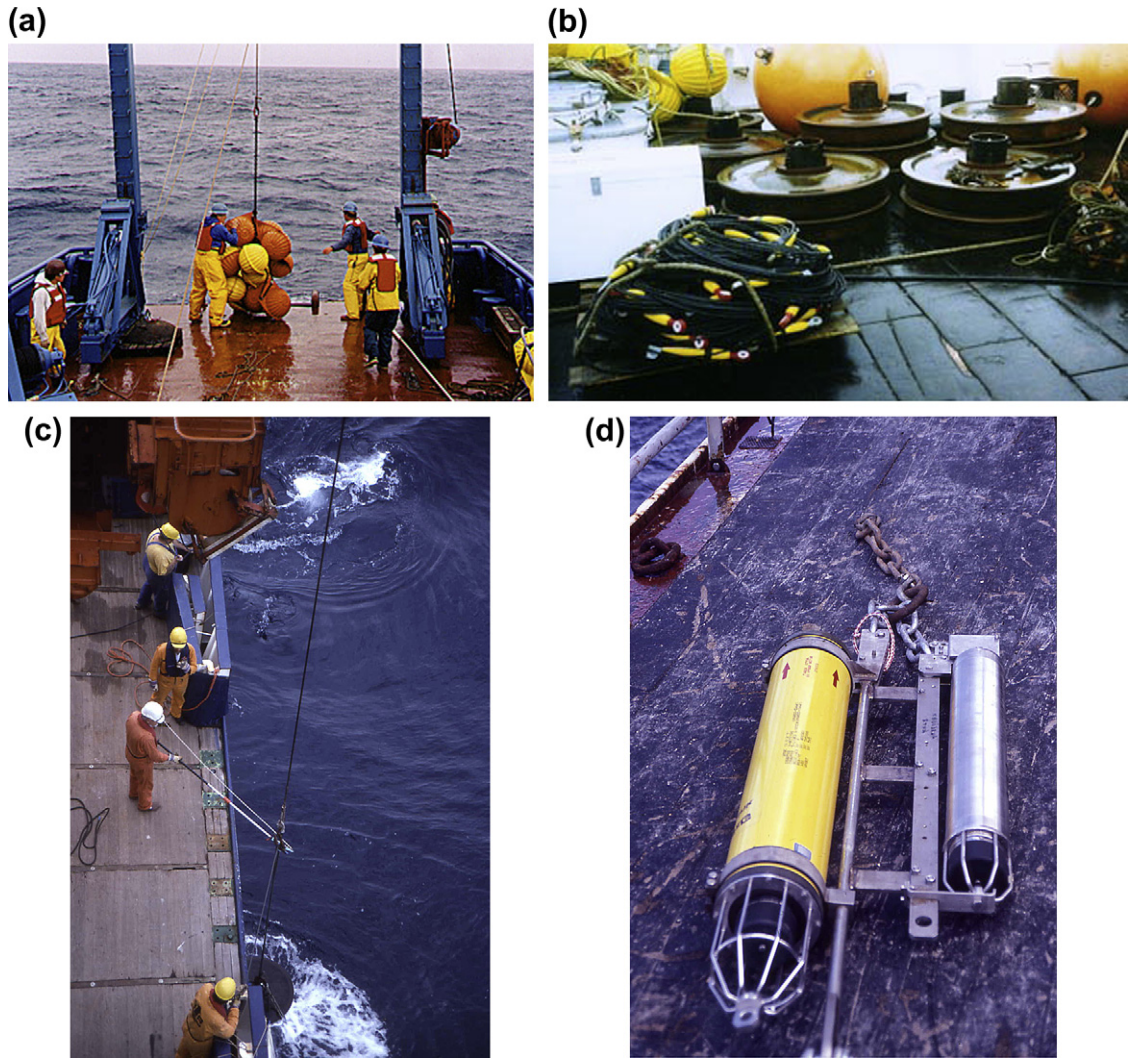


FIGURE S16.37 (a) Intermediate floats being attached to a mooring line. (b) Railroad wheel anchors. (c) Cutting the support line to drop anchor on a mooring. (d) Two different acoustic releases at the bottom of a mooring. (Photos courtesy of W. Emery.)

PIRATA and RAMA respectively (Figure S16.38).

A TAO surface float is shown in Figure S16.39 while it is being serviced. Because their data is central to ENSO prediction, the floats carry redundant sensors and are serviced on a regular basis, at least once per year, requiring

a dedicated research vessel because of the large number of moorings.

S16.5.6.3. Large Moored Buoy Programs

Prior to the TAO buoy program there were a number of large buoys that were deployed to measure primarily meteorological parameters

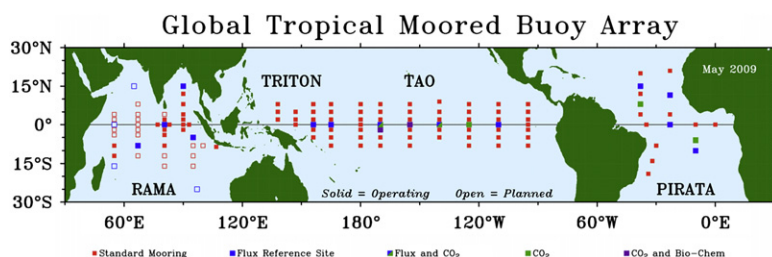


FIGURE S16.38 Tropical moored buoy array. Source: From NOAA PMEL (2009a); Bourlès et al. (2008); McPhaden et al. (2009).

over the ocean, particularly in areas of critical ocean operations such as the tanker route between Alaska’s North Slope and Seattle. Some of the earliest moored surface buoys were the “bumble bee buoys” moored in the North Pacific (Figure S16.40a) in the late 1960s and early 1970s. These buoys were constructed from old fuel tanks and fitted with meteorological instrumentation. On the early buoys the recording systems were optical with film cameras recording the analog readings. This meant that data processing was done by eye, introducing the potential for errors.

Following the success of these programs in collecting useful data from unvisited portions of the North Pacific, there were plans to install a large number of 12 m discus “monster buoys” (Figure S16.40b) throughout the northern oceans. The high cost of these buoys made this expansive plan impractical. The National Data Buoy Center (NDBC) was created within NOAA; it operates monster buoys in the Bering Sea, the Gulf of Mexico, and the western North Atlantic. At this time there are seven such buoys. There is also a set of five 10 m discus buoys in the Caribbean and off the California coast. A much larger number of 6- and 3-m buoys have also been deployed. At present the monster buoys report their data via satellite, which makes them available both for operations and for research applications. These are primarily meteorological data that provide needed forecast information for ship operations.

These data are available online from NDBC (www.ndbc.noaa.gov/mooredbuoy.shtml).

S16.6. ACOUSTIC METHODS FOR OBSERVING CHANGES IN TEMPERATURE OR DENSITY

S16.6.1. Acoustic Tomography

As discussed in Section 3.8, electromagnetic radiation penetrates only short distances in the ocean, ~100–200 m for light. However, as discussed in Section 3.7, the ocean is essentially transparent to sound waves. The speed of sound in seawater mainly depends on temperature and pressure. Temperature changes are of great interest, both at the short range and short time-scale of eddies and winter convection (tens to hundreds of kilometers over several weeks or months), and at the long range and long time-scales of basin-averaged temperature changes. Thus the travel times of sound pulses between a source and a receiver in a particular region might be used to obtain information on the changing temperature distribution. A technique developed to take advantage of this is called *acoustic tomography* (Munk & Wunsch, 1979; Munk, Worcester, & Wunsch, 1995). It is analogous with medical tomography in which brains are mapped using radiation applied from outside the head. Howe and Chereskin (2007) provided a good review of this technique.

(a)



(b)

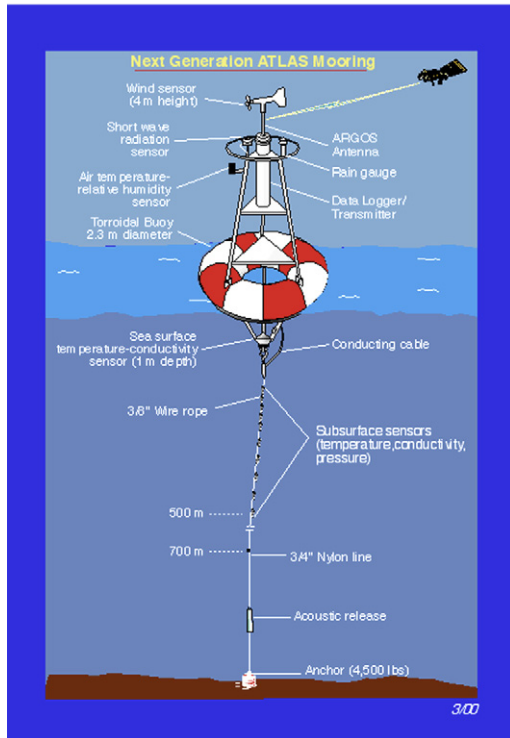


FIGURE 16.39 (a) TAO buoys being serviced. (b) Layout of TAO ATLAS mooring. *Source: From NOAA PMEL (2009b).*

The first large-scale acoustic tomography experiment used a moored array of sound sources and receivers in a 300 km square (Figure S16.41; Cornuelle et al., 1985). Each source and receiver had accurate clocks so that travel times for sound pulses could be determined along each of the 20 possible paths joining the sources and receivers, which were situated at about 2000 m depth in the sound channel. Along each of the source/receiver directions, there were 5 to 10 possible sound paths in the vertical plane so that information about sound speeds was available over a range of depths between about 500 m and 3500 m. Analysis of travel-time data by “inverse methods” (Chapter 6) then yielded changes in sound speed. From this the temperature structure in the volume within the array is derived. Sound speed variations of about 2 m/sec corresponded to temperature variations of 0.4 °C at 700 m depth. The temperature structure derived from the tomography corresponded well with CTD surveys, which of course did not have the temporal coverage of the tomographic array.

Ocean acoustic velocity tomography uses measurements of the differences in travel time between pairs of transceivers (co-located transmitter/receiver pairs) to provide information about the velocity of the water (Howe, Worcester, & Spindel, 1987). For instance, if the water between locations A and B is moving from A toward B, then the travel time for a sound pulse is less from A to B than from B to A. The difference in travel time is proportional to the water speed along the path AB with an accuracy of a few centimeters per second. With three moorings in a triangle, the velocities measured along each leg of the triangle provide the relative vorticity (rotation about a vertical axis) of the water (Section 7.7). If extended to four, five, and more moorings at the vertices of a square, pentagon, and so forth, transmissions across the area can also add information on the water motion within the area.



FIGURE S16.40 (a) Bumble bee buoys used in the North Pacific. (Photo courtesy of W. Emery.) (b) 12 meter disc buoy. Source: From NOAA NDBC (2008).

Acoustic tomography lends itself well to intense regional studies for which repeated cruises are impractical and for which traditional moorings or floats would not provide the required spatial and temporal coverage. Similar regional tomographic arrays have been used successfully to study winter convection in the Greenland, Labrador, and Mediterranean Seas (Morawitz et al., 1996; Avsic, Send, & Skarsoullis, 2005; Send, Schott, Gaillard, & Desaubies, 1995). Acoustic tomography is proving very useful for monitoring straits as well (Denmark Strait, Fram Strait, Strait of Gibraltar).

Acoustic tomography has also been implemented for basin scales in the ocean to detect very large scale warming or cooling (Acoustic Thermometry of Ocean Climate, ATOC; Dushaw, 2002). Sound sources of sufficient strength can be heard around the world since acoustic waves propagate so easily in water. Changes in travel time for acoustic waves along the extremely long paths are related to changes in the total temperature change (“integrated temperature”) along the path. A test of the concept was made with a sound source in the southern Indian Ocean, which was readily heard at receivers on both the east and west coasts of the United States. An array of sources and receivers around the North Pacific (Figure S16.41b) is presently monitoring basin-scale

variations in temperature. A global-scale deployment would be feasible (Figure S16.41c).

S16.6.2. Inverted Echo Sounder

Rosby (1969) suggested that variations in travel times of acoustic pulses from the seafloor to the sea surface could be related to changes in the density structure and hence depth of the thermocline. Moreover, since these travel times are integrated measurements over the water column, they effectively filter out all but the fundamental mode of any vertical oscillations. This led to the development of the *inverted echo sounder* (IES; Watts & Rossby, 1977), in which the round-trip travel times of regularly spaced acoustic pulses from the seafloor are used to determine temporal variability in the vertically integrated heat content. This can be related to thermocline depth and dynamic height if the temperature–salinity relationship is stable. With an array of IESs, it is possible to map the changing dynamic height field and hence changes in geostrophic currents. This has good regional application, especially for studying the evolving eddy field. IES arrays have been used in studies of the Gulf Stream, Antarctic Circumpolar Current, Japan Sea, and Malvinas Current as well as other regions.

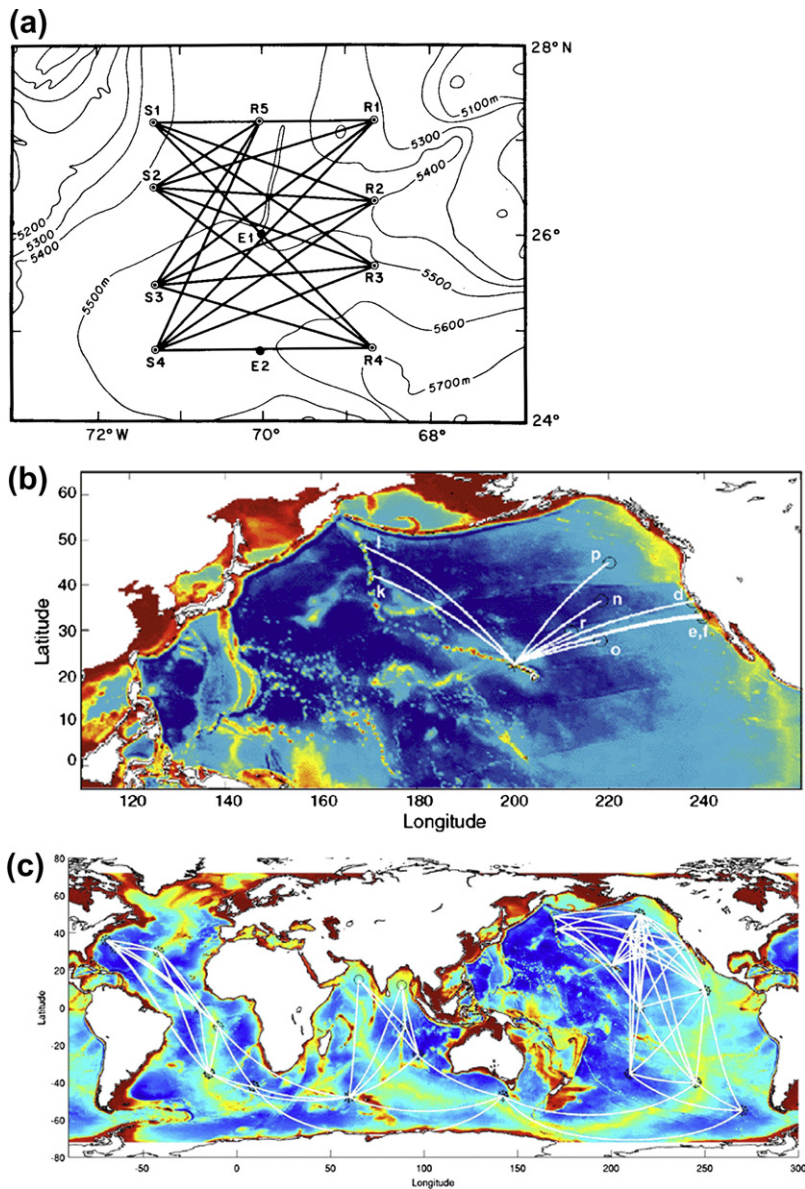


FIGURE S16.41 (a) Moored array of sound sources (S), receivers (R), and “environmental moorings” (E) for the first large-scale acoustic tomography trial in the western North Atlantic. *Source: From Cornuelle et al. (1985).* (b) Existing North Pacific ATOC acoustic array. *Source: From Dushaw (2003).* (c) Prototypical ATOC long-distance acoustic array. *Source: From Dushaw (2002).*

S16.7. SEA-LEVEL MEASUREMENT

Like SST, the measurement of sea level is one of the oldest oceanographic observations. Observations and increasing understanding of the tides occupied ancient scientists from Greece to India, Arabia, and China (Cartwright, 1999). Nineteenth century sea level studies were related to vertical movements of the coastal boundaries in the belief that, averaged over time, the height of the mean sea level was related to movements of the land. Today sea level data are used to resolve the tides, monitor wind-driven storm surges and events such as El Niño in the western tropical Pacific, monitor global sea level rise, and calibrate/validate satellite altimeters (Section S16.9.9). Tide gauges also form the backbone of the tsunami warning system that alerts coastal residents to seismically generated waves.

In addition to measuring the effects of coastal erosion and global sea level rise, long-term sea level changes are also related to changes in global ocean currents. A map of sea-surface topography is analogous to a meteorologist's map of surface pressure from which winds are inferred. For this reason satellite-based radar and laser altimeters can be related to the geostrophic components of the ocean circulation (Section S16.9.9 and Section 7.6).

Most operating tide gauges consist of a float sitting in a "stilling well" (usually a pipe) with a counterweight on the other side of a shaft

that rotates as the float (sea) level changes (Figure S16.42). The system includes careful benchmarking to measure changes in the land level. Float tide gauges are the most standard. In areas with large wave and wind action that creates oscillations even within the stilling well, a "bubbler" gauge can be used. With this gauge a bubble is released at the bottom and variations in pressure due to oscillations of the sea level can be sensed by changes in the bubble. Bubbler gauges actually measure the combined effects of sea level and atmospheric pressure, so it is necessary to correct for atmospheric pressure when processing these data. Data within the global network of sea level stations are digitally encoded and transmitted by satellite to data collection centers.

In the distant past, sea level was measured with a staff installed so that the level of the ocean's surface moved up and down the graded staff, and the level was read by eye. This was then scribed on to a recording chart that moved with time.

Satellite altimetry is an important new tool for observing global sea level changes. (Altimetry is not useful for observing tides, since it does not have the correct temporal sampling.) For the ocean interior far from the islands and coastlines where tide gauges can be mounted, altimetry is the only available tool for observing sea level change. Its uncertainty is 3–4 mm, with larger error near coastlines. Tide gauges

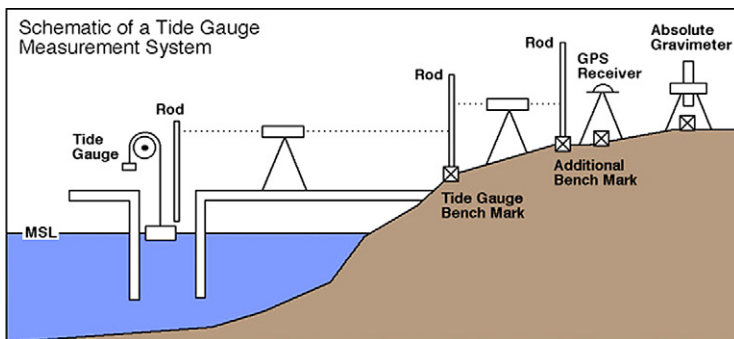


FIGURE S16.42 Tide gauge measurement system. Source: From Nerem (2009).

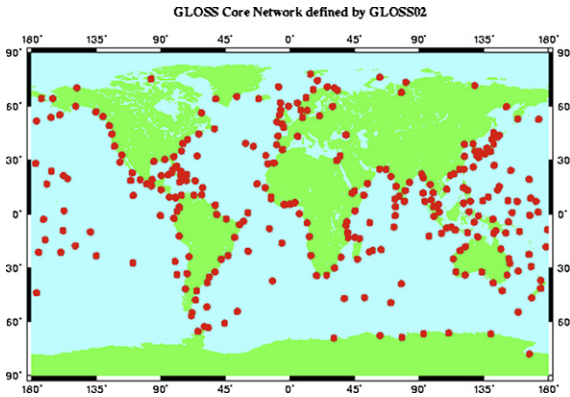


FIGURE S16.43 The global sea level observing system (GLOSS) tide gauge network. Source: From WMO JCOMM (2009).

serve as altimetric calibration points, so they continue to be essential for observing global sea level change. The Global Sea Level Observing System (GLOSS) is the international focal point for tide gauge data (WMO JCOMM, 2009). The tide gauge network currently comprises 290 stations (Figure S16.43).

S16.8. RADIATION AND OPTICAL MEASUREMENTS

In Chapter 5 we discussed methods for computing shortwave and longwave radiation indirectly using bulk formulae and observations of external quantities such as cloud cover and albedo. These formulae are based on direct measurements of shortwave and longwave radiation (Q_s and Q_b). Such direct measurements are made at high-quality weather stations and meteorological instrument packages (Figure S16.44), which are often carried by research ships. In Chapters 3 and 4 the inherent and apparent optical properties of seawater, which are observed in situ using various optical instruments, were described. (Satellite observations relevant to these quantities are described in the next section.)

Observations of shortwave radiation are made with a *pyranometer*. The sensing element of the Eppley pyranometer consists of two flat plates of copper, one painted with a flat black paint and the other whitened with magnesium oxide. The two plates are placed horizontally with a clear view of the sun and sky and are shielded from draughts by a clear hemispherical cover. The black paint absorbs all shortwave and longwave radiant energy falling upon it and is heated above the surrounding temperature. The white plate reflects practically all of the energy between 0.3 and 5 μm (shortwave radiation) but absorbs all longwave energy. The white plate is consequently heated less than the black one and the difference in temperature between them is a measure of the shortwave radiation (Q_s) falling on a horizontal surface in the locality of the instrument. The difference in temperature is measured by connecting the “hot” junctions of a group of

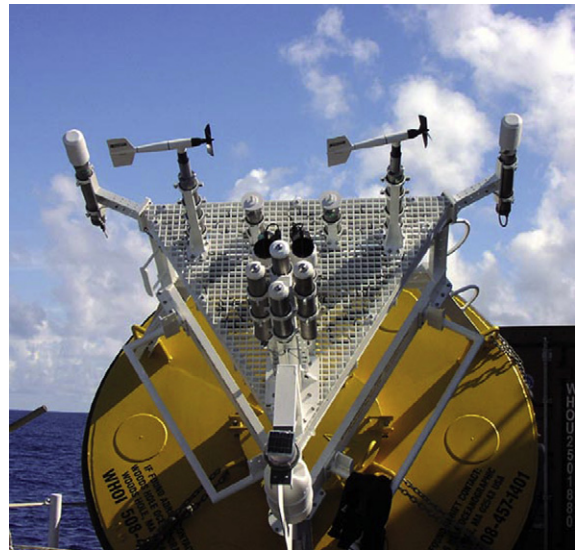


FIGURE S16.44 Meteorological sensor package: ASIMET system with dual sets of sensors for shortwave radiation (pyranometer), longwave radiation (infrared radiometer), barometric pressure, relative humidity and air temperature, precipitation, and wind. Source: From WHOI (2010).

thermocouples to the black plate and the “cold” junctions to the white plate. The difference in temperature gives rise to a thermoelectric EMF, which is measured by a recording galvanometer. This instrument is calibrated by exposing it to a standard source of energy, such as a standard electric filament lamp.

The downward-directed component of the longwave radiation Q_b in the atmosphere is measured with a *radiometer*. This Gier and Dunkle instrument consists of two horizontal plates of black material separated by a layer of material of known heat conductivity. The upper sheet of black material absorbs all the radiation falling upon it from above and is heated above the temperature of the lower sheet, which is screened from radiation from below by a sheet of polished metal. The difference in temperature between the upper and lower sheets is measured by thermocouples and is a measure of the rate at which the sum total of longwave and shortwave energy is coming down from above. To determine the value of just the longwave component, it is necessary to subtract the shortwave radiation rate as measured with a pyranometer. An alternative procedure is to omit the polished metal screen from below the black horizontal plate and arrange the instrument so that the upper plate “looks at” the atmosphere and the lower plate “looks at” the sea below. In this “net radiometer” arrangement the difference in temperature between the upper and lower plates is a measure of the net amount of radiant energy reaching a horizontal surface, that is, it is a direct measure of $(Q_s - Q_b)$.

The *Secchi disk* is the simplest device used to determine the transmission of visible light through the water, hence its clarity (Tyler, 1968; Preisendorfer, 1986). The Secchi disk used for marine applications is a plate with a 20 to 40 cm diameter that hangs horizontally on the end of a rope marked in meters (Figure S16.45); smaller disks are used for lakes (Carlson, 2011). The upper surface is usually painted white or with alternating white and

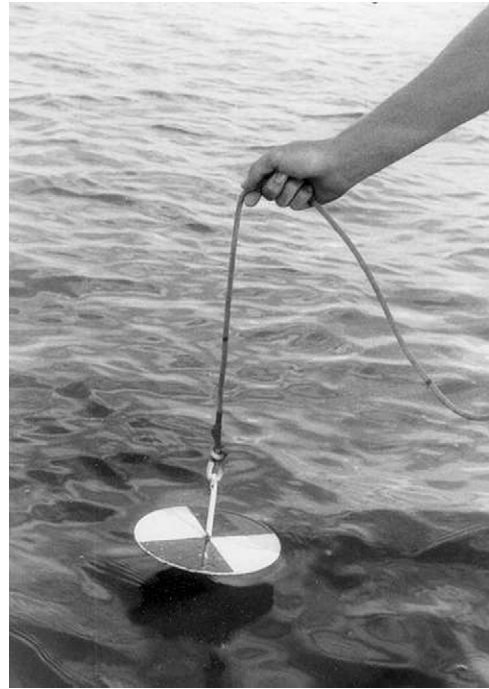


FIGURE S16.45 Secchi disk with alternating black and white quadrants, which is typically used for lake applications. Secchi disks for marine applications are larger and usually all white. Source: From Carlson (2011).

black segments. The disk is lowered into the sea and the depth at which it is lost to sight is noted. This depth decreases as the vertical attenuation coefficient of the seawater increases. In very clear water the depth may be over 50 m, in coastal waters 1 to 2 m, and in some river estuaries less than 1 m. The Secchi disk measurement is only semiquantitative, but has often been used because it is so simple. After just a little practice, it is possible to obtain consistent readings to better than 10%, with little variation from individual to individual. Secchi disks are also used to estimate attenuation coefficients resulting from dissolved and particulate material. However, Preisendorfer (1986) cautioned against using Secchi disks for quantitative estimates. Secchi depths for the Atlantic and Pacific range from less than 15 m

to more than 35 m (Figure 4.26), and are inversely correlated with chlorophyll-a content.

Modern electronic instruments measure optical properties directly and quantitatively. There are many useful instruments, including those measuring beam attenuation as a function of depth and wavelength (*transmissometer*), fluorescence (*fluorometer*), light scattering (*optical backscattering meter*), and *radiance* and *irradiance sensors*. The first three sensors are active instruments, which emit their own light and measure the response. The latter sensors are passive, measuring the ambient light.

Transmissometers (Figure S16.46) measure beam attenuation. The instrument emits light at a specified wavelength, and then detects how much light passed through the intervening water to be intercepted at the other end of the instrument. The wavelengths are chosen based on what is being studied, such as chlorophyll, dissolved organic matter, and other particles (Richardson & Gardner, 1997). Transmissometers compatible with full-depth CTD casts were used throughout the WOCE to gather full-depth profiles of attenuation. Typically there is high attenuation in the surface layer as

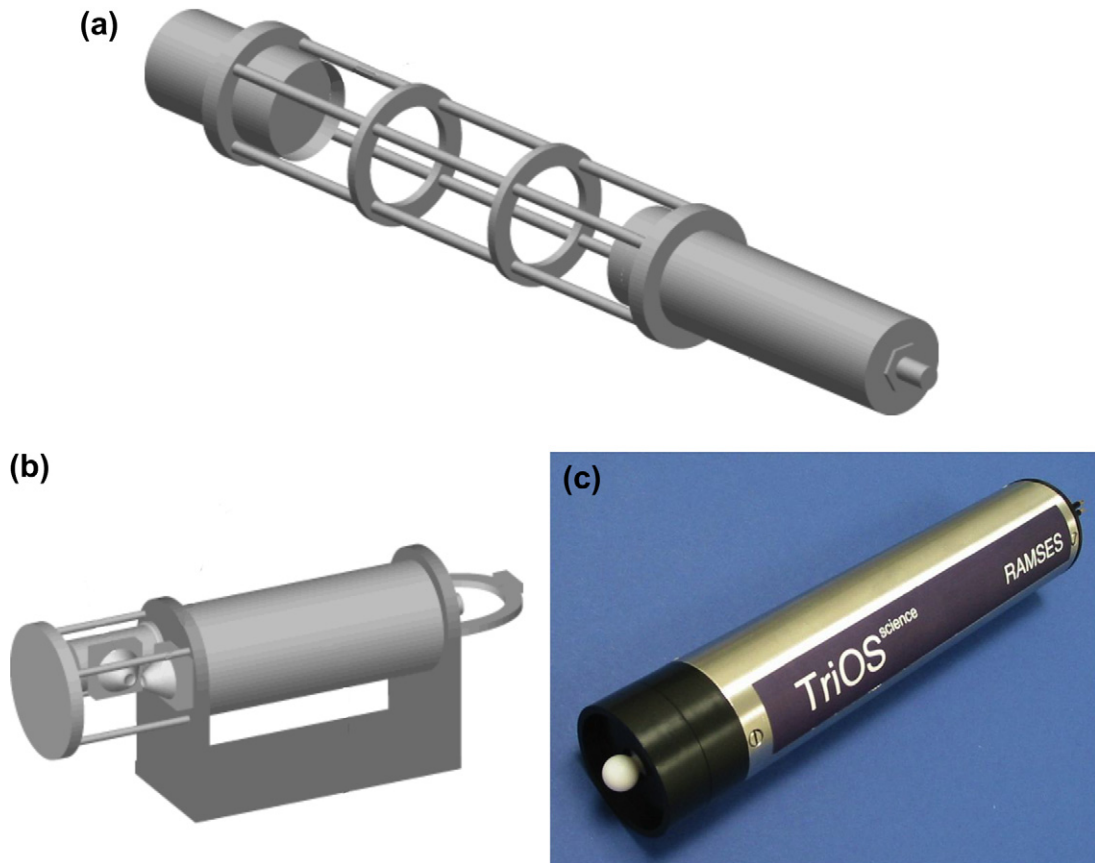


FIGURE S16.46 (a) Transmissometer schematic. (b) Fluorometer schematic. Source: From Richardson and Gardner (1997). (c) Irradiance radiometer. Source: From TriOS (2009).

well as in a boundary layer of about 100 m thickness at the ocean bottom where sediment is stirred up.

Fluorometers measure fluorescence, which indicates the presence of chlorophyll. They emit flashes of light at specified wavelengths to excite fluorescence and measure the emitted light (which is at another wavelength). The light and the receiver are located close together in contrast to the setup on the transmissometer (Figure S16.46).

Backscattering instruments emit a beam of light and measure the backscattered light with a sensor located next to the light.

Radiance sensors (radiometers) measure visible light at a range of wavelengths within a narrow field of view (e.g., 7 degrees), while irradiance sensors measure the same within a wide field of view (TriOS, 2009).

S16.9. SATELLITES

S16.9.1. Satellite Remote Sensing

One of the biggest problems in physical oceanography is the mixture of time and space sampling that results from the normal ship-based measurement system. Because of ship speed limitations (10–12 knots), it is impossible to observe a large area in a “synoptic” (i.e., near simultaneous) fashion. Thus oceanographers once had to be satisfied with data collected over some period of time. For many stationary and longer period phenomena, such averages are adequate, but as the study of time-variable oceanographic processes has intensified, the need for more nearly simultaneous sampling has increased. One solution is the use of Earth-orbiting satellite data to sense the ocean’s surface. While satellite measurements are limited to near the ocean’s surface, the large-scale, almost-synoptic sampling (minutes for areas of thousands of square kilometers) is an essential component of the global observing system. This is complemented by the increasing deployment of autonomous in situ

instruments as part of the Global Ocean Observing System, including subsurface floats and surface drifters (Section S16.5).

Oceanographic parameters that are routinely measured by satellites include surface temperature, sea ice distribution, wave height, surface height, radar backscatter, and ocean color. A sea-surface salinity sensor is set to be launched in 2011. Meteorological parameters measured by satellites that are important for ocean forcing include wind speed, sea level pressure, cloudiness, and water vapor content. The next subsections describe some of the present (around 2004) generation of primarily U.S. satellite sensors used for oceanography.

There are many other satellite-based observational systems not covered here. NASA publishes an online Remote Sensing Tutorial (<http://rst.gsfc.nasa.gov/>) that is an excellent starting point. A good, older textbook is *Methods of Satellite Oceanography* (Stewart, 1985). Many texts address specific aspects of satellite remote sensing. As any textbook presentation of satellite methods is certain to be outdated within just a few years, the student is encouraged to seek the latest information from the space agencies and data archive centers. Web sites — particularly those of NASA, NOAA, the European Space Agency (ESA), and the Japan Aerospace Exploration Agency (JAXA) — provide a large amount of information about these satellites, and are also excellent starting points for data sets. An especially useful gateway to oceanographic data sets is the Web site for the NASA Jet Propulsion Laboratory’s Physical Oceanography DAAC (PO.DAAC), which has been reliably available and updated for a number of years.

S16.9.2. Satellite Orbits

At present much satellite-based information comes from operational weather satellites in both *polar* and *geostationary* orbits. A geostationary satellite remains fixed over one location on

Earth's surface orbiting Earth at the same rate as Earth rotates. This specific orbit necessitates an altitude of 35,800 km. The geostationary system scans about one-third of Earth's surface under the satellite. Geostationary operational environmental satellites (GOES) for weather analysis and forecast purposes are operated by NOAA (GOES East and GOES West), providing full coverage of the American continents and most of the Pacific and Atlantic Oceans. The principal instruments on GOES are an imager (visible and infrared radiation) and atmospheric sounder. Among other products, these provide the familiar satellite images of cloud cover used in weather reporting (Figure S16.47).

ESA has operated geostationary satellites for the same weather purposes since the 1970s. The first ESA satellite was Meteosat (1977), stationed over western Africa (intersection of the equator and the Greenwich meridian). The series of Meteosats was followed in 2000 by the Meteosat Second Generation (MSG) satellites with 1 km resolution in the visible light and 15 minute reporting intervals as well as a number of new sensors.

At much lower altitudes of about 800 km, polar-orbiting weather satellites are generally deployed in "sun-synchronous" orbits to maintain the same local equatorial crossing time on each orbit. Thus each polar orbiter passes over a location at least twice per day (once at night and once during the day). At higher latitudes the approximately 2000 km scan width of these instruments leads to overlap, providing many more views of the surface. Polar-orbiting weather satellites have progressed dramatically since 1960, when the television camera on the first Television Infrared Observing Satellite (TIROS) could point only at North American latitudes due to the spin stabilization of the spacecraft. This first series of ten weather satellites ended in 1966. The next TIROS spacecraft series mounted a camera looking out along the radius of the spinning satellite (called the wheel satellite) and took a successive set of

pictures to provide the first global view of Earth's surface. Today, three-axis stabilization on the TIROS-N (N for new) satellites makes it possible to keep instruments such as the Advanced Very High Resolution Radiometer (AVHRR), which senses surface temperature as described in Section S16.9.5, pointed continuously at Earth's surface. As of 2011 there have been nineteen TIROS-N satellites, known as NOAA 1 through 9. The first was launched in 1970 and the most recent in 2009, with new launches every two to four years. The AVHRR is the principal instrument of oceanographic interest on these satellites.

Another series of American polar-orbiting satellites that collect data useful for oceanography is the Defense Meteorological Satellite Program (DMSP). They use essentially the same spacecraft as the NOAA polar orbiters but they carry different payloads. The principal instruments useful for oceanographic studies are visible and infrared sensors for SST and a microwave sensor that has been especially useful for sea ice. These data are collected by an instrument called the Operational Line Scanner (OLS). It has poorer spatial and radiometric sensitivity than the AVHRR, but has a unique characteristic. The OLS has a "low-light" capability, which makes it possible to view Earth lights from cities, polar Aurora, and other low intensity light phenomena. This capability was specified for the DMSP by the U.S. military that wanted the ability to operate even at night when the visible solar radiation was not available. Currently there are four DMSP satellites in operation.

ESA has launched numerous Earth observing satellites. Polar-orbiting satellites include ERS-1 (1991–2000), ERS-2 (1995–present), and Envisat (2002–present). Each of these satellites has carried a wide range of sensors useful to oceanographic applications such as imagers, radar altimeters, scatterometers, and synthetic aperture radars.

The present approach to earth science from satellites within NASA and ESA is to fly many

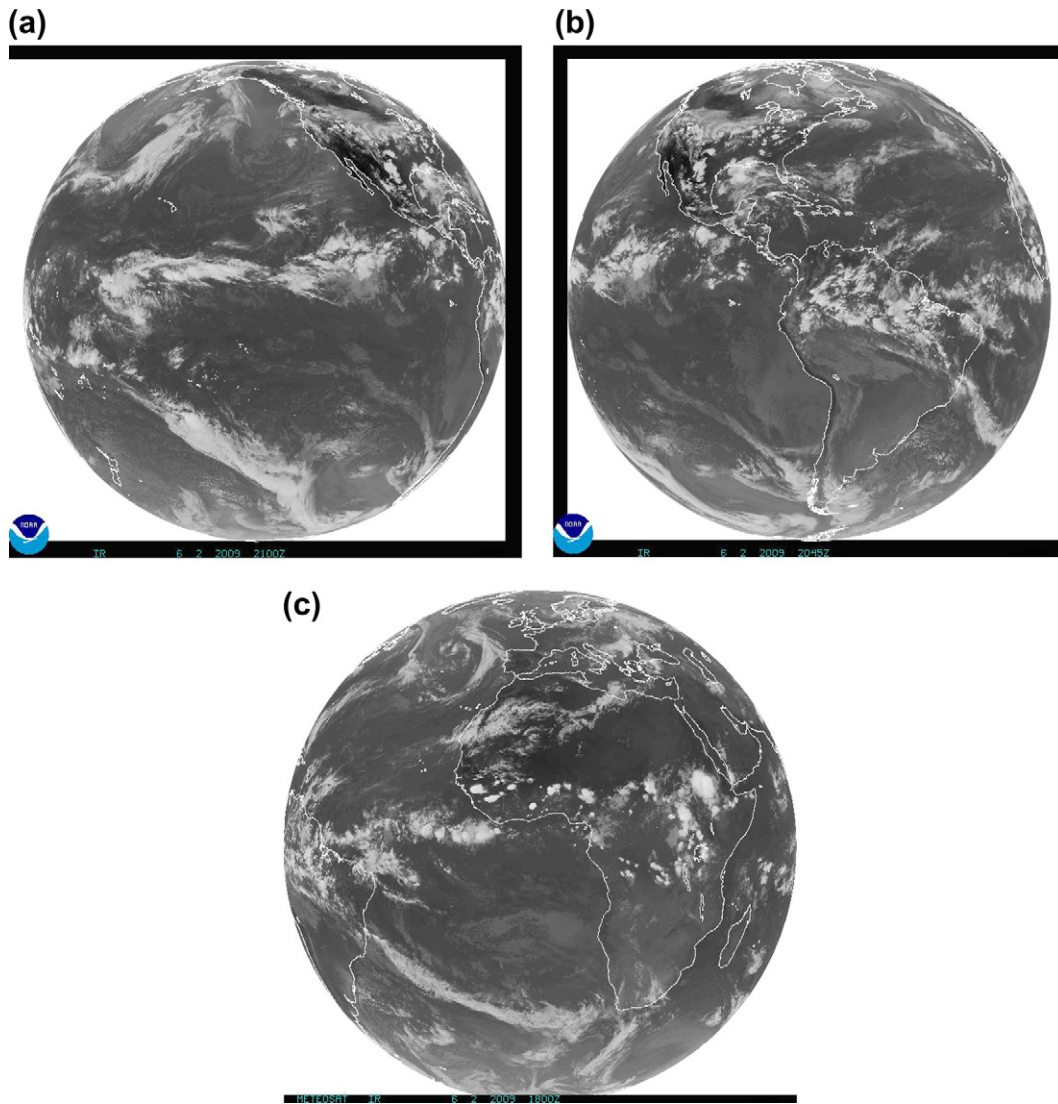


FIGURE S16.47 Infrared image for June 2, 2009 from (a) NOAA GOES_East, (b) NOAA GOES_West, and (c) Meteosat. Source: From NOAA NESDIS (2009).

small missions, each dedicated to one or just a few parameters. Almost all of the many NASA satellites in the Earth Science Mission are polar orbiters in various orbits that depend on the desired frequency, repetition, and spatial resolution and range. A summary of these missions can be found on NASA's Earth

Observing System (EOS) Web site (<http://eosps.gsfc.nasa.gov/>).

S16.9.3. Sensor Types

All satellite sensing is "remote," most using electromagnetic radiation at various wavelengths

and extensive signal processing to assemble images and digital data sets of physical parameters. (One notable exception to the dominance of radiation sensors for oceanographic purposes is the NASA GRACE satellite, which is used to sense Earth's gravitational field through measuring its actual displacement as a function

of that field.) The radiation used in satellite systems for oceanography ranges from microwaves through infrared to visible (Figure S16.48 a). Wavelengths for microwaves are between 0.1 and 30 cm, for infrared radiation from 0.7 to 1000 μm (0.1 cm), and for visible light from 400 to 700 nm (0.7 μm). Specifications for

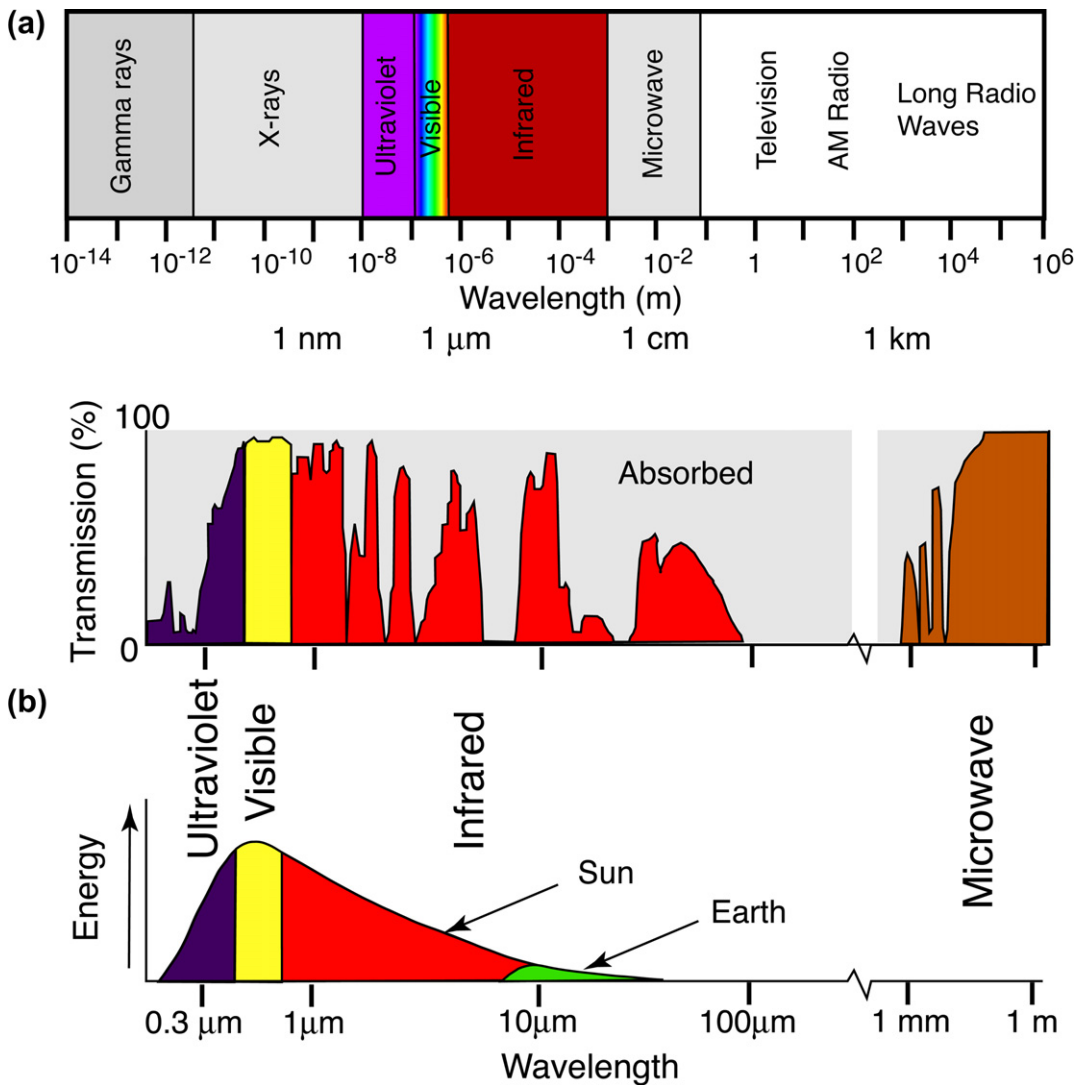


FIGURE S16.48 (a) The electromagnetic spectrum and (b) the atmospheric transmission% and solar spectra; the emission spectrum for Earth is also shown (green). Source: After NASA GSFC (2004).

satellite sensors are often listed in terms of frequency of the radiation rather than wavelength. The frequency ν of electromagnetic radiation is related to wavelength λ through the speed of light c :

$$\lambda\nu = c \quad (\text{S16.2})$$

The speed of light is 3.00×10^8 m/sec. Most satellite instruments measure several different wavelengths. Scientists and engineers then use the measurements at these various wavelengths to construct the physical field.

Satellite radiation sensors are either “active” or “passive.” In *passive* systems, the satellite sensors detect radiation from Earth’s surface or reflected/re-radiated solar energy. In *active* systems, the satellite radiates energy downward and then senses such energy reflected/re-radiated from Earth. The latter is typical of radar and lidar systems that emit radiation to sense surface properties.

The curves in Figure S16.48b represent the atmospheric transmission and the solar emissions spectra. The wavelength axis is expanded compared to Figure S16.48a, but it is possible to compare the main components of the relevant spectra. Transmission through the atmosphere in the visible and near-infrared portions of the EM spectrum is nearly complete; that is, the atmosphere is nearly transparent to these wavelengths. The solar emission maximum is also in the visible range, so that most shortwave energy reaching Earth from the sun is in this and adjoining ranges, including near-infrared.

In the thermal infrared (10–12 μm), transmission is greater in well-defined atmospheric windows. The best (most transparent) long-wave thermal channel is at 10 μm . There is another atmospheric window at about 5 μm . At these wavelengths the solar emission decreases relative to its peak at the visible wavelengths. At the shorter thermal wavelengths Earth emission (green) is quite small. There is another atmospheric window at about

60 to 80 μm where both the solar and Earth emissions are quite low.

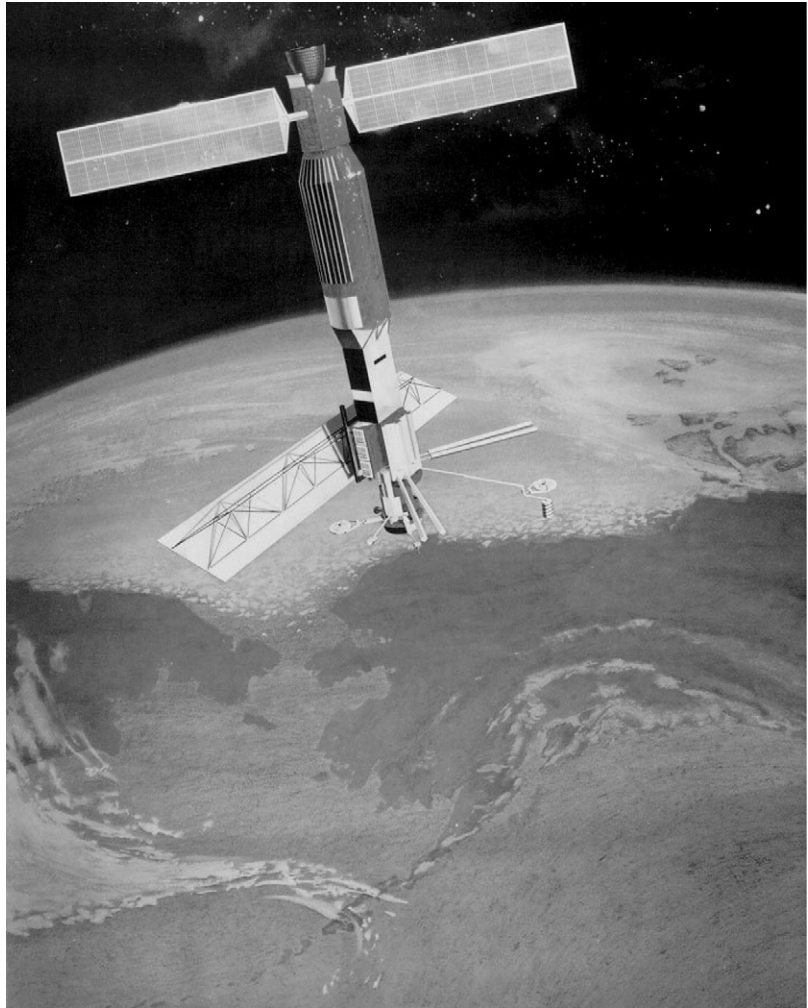
The atmosphere is almost completely transparent for microwave wavelengths greater than about 5 mm.

S16.9.4. SEASAT

The first satellite dedicated to ocean remote sensing was the short-lived SEASAT satellite (Figure S16.49). Because of its special place in the history of satellite techniques for measuring the ocean, we describe it and all of its sensors together. Launched in mid-1978, SEASAT failed after 90 days of operation. Even during its short life, SEASAT proved the concept of a number of unique passive and active microwave instruments designed to measure various parameters of the ocean. The instruments included an altimeter, a visible-infrared radiometer similar to the AVHRR, a Scanning Multi-channel Microwave Radiometer (SMMR), a RADAR scatterometer, and a Synthetic Aperture Radar (SAR). These provided measurements of sea-surface height (altimeter), SST (AVHRR and SMMR), ice distribution (SMMR and SAR), and wind speed and direction (RADAR scatterometer). These SEASAT instruments are described in the following paragraphs.

The passive SMMR on SEASAT provided all-weather images of sea ice and SST. Since microwaves are only slightly attenuated by atmospheric moisture, they are excellent for observing Earth’s surface, which is often obscured by clouds. This is particularly important for the ice-covered polar regions, which are frequently cloud-covered. In addition, the SMMR responds to changes in surface emissivity related to ice age and thickness. A low frequency (6.7 GHz) channel on SMMR was intended to provide SST independent of cloud cover. Unfortunately, calibration and noise problems with the SMMR in this channel resulted in inaccurate SST, a problem that has been solved in more recent microwave sensors.

FIGURE S16.49 SEASAT satellite. Source: From *Fu and Holt (1982)*.



The RADAR Scatterometer on SEASAT was an active microwave instrument, measuring wind speed and direction from the RADAR backscatter from the small wavelets that form at the ocean's surface when the wind blows. This system accurately measures wind stress over the ocean both in terms of magnitude and direction. This is the best way to resolve the wind patterns and their changes over the open ocean. Oceanographers have continued to

pursue the launch and operation of these systems; scatterometry is more completely described in Section S16.9.10.

The (active) SAR on SEASAT was the first SAR flown on a satellite. In its short period of operation the SEASAT SAR produced some very interesting images of the ocean's surface that are still being analyzed today, although it is clear that we do not yet completely understand the SAR signatures of ocean features.

SAR has also proven very useful for the detailed mapping of sea ice and its motion. Again the all-weather capability of an active microwave sensor makes it possible to see through persistent cloud cover. Also the antenna synthesis available with SAR makes it possible to attain high spatial resolution (25 m on SEASAT) with a small satellite antenna. The biggest problem with SAR is the large amount of data processing necessary to retrieve the image of interest from the large volume of data recorded. Originally this was done using optical analog methods, which were very fast but produced brightness inconsistencies. Digital SAR processing was shown to be much more consistent and now all SAR processing is done digitally. In addition, SAR systems have been developed that can actually process the SAR data onboard the spacecraft.

An early satellite altimeter was also flown on SEASAT. *Altimeters* monitor the height of the sea surface and its changes. Again a lot of experience was gained in working with satellite altimetry obtained from the short life of SEASAT. As discussed in Section S16.9.9, because Earth's geoid (gravity field) has not yet been mapped in enough detail to allow use of the altimeter to map absolute sea-surface height, altimeters have been used mainly to study variability in sea-surface height. The SEASAT altimeter also provided the first truly global map (Cheney, Marsh, & Beckley, 1983) of eddy energy from fluctuations of the ocean's surface height.

Finally, SEASAT carried a (passive) visible-infrared radiometer (similar to the AVHRR) to provide single channel visible and thermal infrared imagery simultaneously with the microwave data. All of the SEASAT instruments functioned well during the short lifetime of the satellite. Only failure of the power supply terminated the mission. The concepts behind all of the microwave sensors described below were established by the SEASAT mission.

S16.9.5. Sea-Surface Temperature from Satellite Remote Sensing

SST (Section S16.4.2.1) is measured from satellites with two different methodologies: visible-infrared radiometry and passive microwave sensing. Starting in the early 1970s, procedures were developed to routinely compute SST from satellite infrared measurements. Clouds completely block infrared radiation and normal water vapor seriously attenuates it, resulting in only partial SST coverage. Various methods have been used to correct for clouds and water vapor with most relying on statistics to correct for these effects. A major development was a shift from the 8 km spatial resolution of the SAR to the 1 km resolution of the Very High Resolution Radiometer (VHRR), flying on the same spacecraft, allowing observation of almost the smallest scale phenomena. Later an improved version of this same instrument, the Advanced VHRR (AVHRR), became the standard instrument for satellite SST estimates.

Most archived data are from the AVHRR (see Figure 4.1b). The Global Area Coverage archive, at about 4 km resolution, goes back to late 1978. There are also a number of archives of 1 km AVHRR data from direct readout stations around the globe. Microwave sensors have poorer spatial resolution but provide images even in cloudy conditions. Given that clouds cover a large portion of the ocean at any given time, and given that some regions in some seasons are almost completely cloud covered, microwave SST sensing is indispensable. Unfortunately there have not been as many successful passive microwave sensors with channels appropriate for SST sensing.

The AVHRR is the primary SST sensor on the TIROS-N (NOAA operational) satellites. The AVHRR has five channels: one in the visible (0.58–0.68 μm), one in the near-infrared (0.725–1.10 μm), and three in the thermal infrared (3.55–3.93 μm , 10.3–11.3 μm , and 11.5–12.5 μm) channel. This combination has

proven to be useful in studies of cloud patterns and atmospheric temperatures, land-surface vegetation, and SST. The thermal infrared channels also provide meteorological images at night when there is no visible radiation to reflect from Earth.

The multiple AVHRR thermal infrared channels make it possible to estimate the atmospheric attenuation, by atmospheric water vapor, of the infrared signal emitted from the ocean's surface. Using the difference between the radiation received in channel 4 versus that on channel 5, it is possible to estimate the amount of infrared energy lost to atmospheric moisture before reaching the AVHRR sensor optics. The relatively weak surface temperature gradients in the ocean make it necessary to carry out the best atmospheric moisture correction possible when working with SSTs computed from AVHRR data in an effort to get the precision of the satellite measurement to the 0.3 K accuracy recommended for modern climate studies.

One of the most important aspects of working with the AVHRR data, and any other satellite data, is the correction of imagery for Earth distortion and the remapping of the corrected image to a selected map projection for inter-comparisons between images and with other images or in situ data. This step is generally referred to as "image navigation" and is essential for employing AVHRR imagery quantitatively. Without this image navigation step, satellite infrared imagery can only suggest the complexity of scales on which the ocean varies.

The AVHRR provides three different types of image data. The most commonly available form is the direct readout mode, which is called High Resolution Picture Transmission (HRPT) and is directly read-out by a tracking antenna at a ground station. These data have an approximately 1 km spatial resolution. Each station receives between 4 and 6 passes per satellite per day and, depending on the latitude of the satellite pass relative to Earth station locations,

these passes include between 2000 and 6000 scan lines of 1 km AVHRR data. During each orbit the satellite system records a lower spatial resolution product (approximately 4 km square) called the Global Average Coverage (GAC). These data are only read out at receiving stations at Wallops Island, Virginia, and Gilmore Creek, Alaska. These stations are operated by NOAA, the agency responsible for the U.S. operational weather satellites. The GAC data is valuable because each day a satellite provides a day and night image of the entire globe. Finally, each satellite has a number of tape recorders that can record the full 1 km image data during a short part of the orbit. These Local Area Coverage (LAC) data are recorded at areas selected and commanded by NOAA and are then downloaded, or received at, one of the two NOAA stations. In this way it is possible to "see" parts of Earth that are out of range of the NOAA operated receiving stations.

An example of the 1 km imagery available from the AVHRR is shown in Figure S16.50 which is an infrared (channel 4) AVHRR image of the North American west coast region around San Francisco, California. The color scale indicates that surface temperatures in this image range from about 10°C near the coast to almost 17°C farther offshore. The colder water near the shore reflects the presence of summer upwelling bringing colder water to the surface. The rich patterns of meanders and eddies reflect the well-known instabilities that dominate this area, creating the mesoscale features and what are sometimes known as "jets and squirts" extending out from the coast. Unlike the smooth temperature map of Figure 4.1a, based on averaged historical data, or even the 50 km global SST satellite product in Figure 4.1b, the SST gradients in this image are quite complicated. Mesoscale features populate the boundaries between warm and cold water. This truly synoptic sample clearly indicates the complex spatial variability of many features.

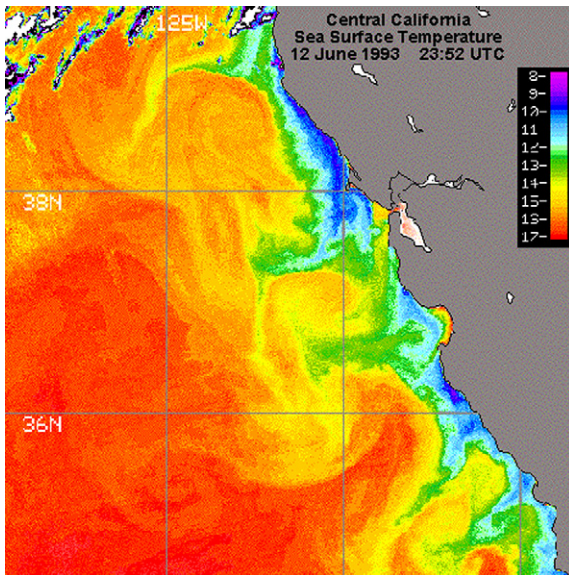


FIGURE S16.50 Thermal infrared image of the West Coast of North America from the Advanced Very High Resolution Radiometer (AVHRR) on June 12, 1993, at 23:52 Universal Time.

The primary SST imager on the DMSP satellites is called the OLS. This is quite different from the AVHRR OLS. In addition to visible and thermal infrared channels, the DMSP satellite OLS has a unique low-light imaging capability designed to make it possible to sense Earth surface conditions at nighttime. There are two levels of spatial resolution: fine (~0.5 nautical mile) and smooth (~2 nm). Unfortunately most of the data archived from the DMSP satellites are stored only in the “smooth” mode (~2 nm resolution) making them marginally useful for oceanographic studies. DMSP data are broadcast in an encrypted format because these are military satellites. Over areas such as the Antarctic the encryption is removed so that the OLS data are available for scientific use. Decrypted versions of the DMSP data are available through NOAA’s National Geophysical Data Center (NGDC) in Boulder, Colorado.

The MODerate resolution Imaging Spectrometer (MODIS), on the Earth Observing TERRA

and AQUA satellites (launched in 1999 and 2002, respectively), has channels to compute infrared SST and ocean color. There are additional channels of optical data, which are now being explored for additional ocean applications (examples in Section 4.8).

A major limitation for SST imaging from AVHRR and other visible-infrared sensors is the presence of cloud cover. Passive microwave sensors can observe through clouds because they use longer wavelengths (6–12 GHz). Early observations were made from 1978 to 1986, using the SMMR, which had calibration and noise problems for SST applications. Later success has come from the use of the Tropical Rainfall Mapping Mission (TRMM) Microwave Imager (TMI). While not intended for measuring SST, TMI has proven very useful for this application (see example in Chapter 4), and has been enhanced by availability of the Advanced Microwave Spectral Radiometer (AMSR).

Unfortunately, spatial resolution for passive microwave SST is 25 to 50 km instead of the 1 km AVHRR resolution. This is too large to “see” SST gradients in detail. However the microwave sensor provides information that would otherwise be impossible to collect because of clouds. A challenge now is to develop techniques for merging passive microwave and infrared satellite measurements of SST.

Many SST products based on satellite data are now available. Some of these are based on individual sensors and others are a blend of different types of data, including AVHRR and microwave sensing. Some include in situ observations as well. The products differ in spatial and temporal resolution and averaging.

S16.9.6. Sea Surface Salinity

Satellite sensing for sea surface salinity (SSS) is on the horizon. A major effort has begun through the NASA EOS to develop a passive microwave radiometer that will provide information on salinity. This mission is called

Aquarius and is scheduled for launch in 2011. The spacecraft will be provided by Argentina. This instrument takes advantage of the dependence of conductivity of seawater on salinity. Variations in conductivity can be sensed by microwave radiometers. Aquarius will carry three radiometers sensitive to salinity and a scatterometer to correct for surface roughness.

S16.9.7. Sea Ice

Sea ice observations have been revolutionized by satellite measurements. Satellite imagery is used to monitor the presence of sea ice cover and to estimate its concentration. Sea ice motion can be mapped from successive images. Optical systems provide extremely high resolution, down to the level of leads in the ice. However, optical sensors are limited by the frequent presence of clouds at polar latitudes. Thus microwave sensors provide comprehensive and routine coverage of sea ice cover and concentration (Gloersen et al., 1992). In addition the microwave imagery can also be used to estimate sea ice parameters such as thickness and ice age.

The original microwave imager used for sea ice was the SMMR, which was launched in 1978. The Special Sensor Microwave Imager (SSM/I) was developed by Hughes Aircraft and has been in operation on DMSP satellites since 1987. The SSM/I was a follow-on to the SMMR and was used to observe a wide variety of atmospheric conditions of interest to the military. The SSM/I was the first “total power radiometer” and has been copied in subsequent microwave radiometers. The earliest passive microwave systems proved to have such weak signals relative to the large electronic “noise” components of the system that it was necessary to have some reference to extract the signal. In 1946 an engineer named Dicke invented a passive microwave system that switched the sensor between Earth’s surface and an internal reference target to measure the surface relative to the known internal target. This became

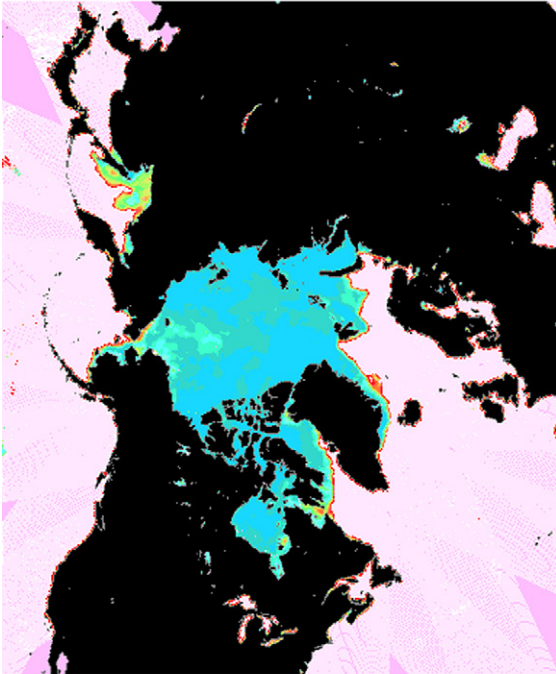
known as the “Dicke radiometer” and is still the predominant design of a passive microwave system. The SSM/I took advantage of the new low-noise amplifiers that overcame the problem of internal instrument noise and was built as a “total power” passive microwave instrument.

Because of the value of SSM/I data for research, the DMSP has released the data as quickly as possible. The data are archived by the National Snow and Ice Data Center. The SSM/I data are processed for ice concentration, ice edge, atmospheric water vapor, atmospheric liquid water, and wind speed. Three of the four frequencies on the SSM/I (19.7 37 85 GHz) are dual polarized (vertical and horizontal) while the 22 GHz frequency has only a vertical polarization. Both polarization and frequency differences are employed in SSM/I algorithms for various parameters. None of the frequencies are low enough to properly sense SST, although some attempts were made. There were also some methods developed to compute wind direction for monthly composites. Ice concentration algorithms have been based on polarization differences in the NASA “team” algorithm while a competing “bootstrap” ice concentration algorithm was developed based on frequency differences. Later the SSM/I channel brightness temperatures have been used to compute all-weather ice motion for both polar regions. Ice maps using SSM/I have been produced routinely for many years (Figure S16.51), and are incorporated in operational ice analyses.

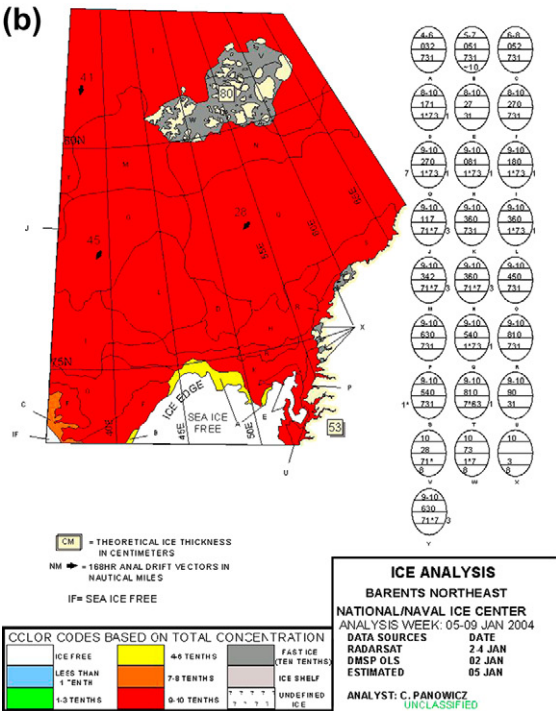
Twenty-two years of sea ice motion from a combination of two successive passive microwave imagers is summarized for both polar regions in Fowler et al. (2004; see Sections 12.4 and 13.7 for the Arctic and Southern Ocean). The motion was computed using the maximum cross correlation (MCC) method applied to SMMR and SSM/I passive microwave data (Emery, Fowler, & Maslanik, 1995).

The SAR flying on Canada’s RADARSAT satellite is also important for sea ice observations. The primary mission of this satellite is to map

(a)



(b)



and monitor Arctic sea ice for ship and shore operations in the Arctic. These data have also been used for land surface and Southern Ocean sea ice applications. Scatterometers are also used for tracking sea ice in the Southern Ocean.

S16.9.8. The Coastal Zone Color Scanner and SeaWiFS

Chlorophyll content in the ocean's surface layer is directly related to the color at the sea surface (Section 3.8), which can be sensed by satellites. Chlorophyll content is related to primary productivity. The Coastal Zone Color Scanner (CZCS) was a pioneering instrument supplying surface imagery in a number of narrow visible bands, which could then be separated into the individual color components. The CZCS was launched in 1978 on the NASA satellite NIMBUS-7 with an expected two-year life-time, but continued to provide useful image data for 8 years, through mid-1986. In spite of some problems with sensor drifts, the CZCS produced some very valuable images of the ocean's productivity, yielding the first global maps of ocean primary productivity, with 1 km spatial resolution (seasonal maps in Figure 4.28).

The follow-on to the successful CZCS was the Wide Field of view System (WiFS) built by the former Hughes Aircraft Santa Barbara Research Systems (now Raytheon). This instrument was integrated with a small satellite system developed by the Orbital Sciences Corporation, which was then called SeaWiFS. NASA arranged with Orbital Sciences to purchase data from this system, but the satellite and its operation

FIGURE S16.51 (a) Sea ice concentration for January 4, 2004 (red – low; dark blue – high) from routine analysis based on the SSMI passive microwave radiometer. *Source: From NOAA Marine Modeling and Analysis Branch (2004).* (b) Operational sea ice analysis, based on a combination of satellite and in situ observations, for the same week for a portion of the Barents Sea. The “egg” codes in the right column are described on the NATICE Web site. *Source: From National Ice Center (2004).*

belonged to and were handled by Orbital Sciences Corporation. This NASA data purchase applied primarily to the GAC data from SeaWiFS (as with the AVHRR 4 km GAC resolution) and some limited amount of 1 km resolution direct readout SeaWiFS data particularly for calibration studies. Orbital Sciences sold the rest of the 1 km data to interested users around the world.

SeaWiFS was launched in 1997 and continues to provide data thirteen years later. Various sites were granted licenses to collect the direct readout data for subsequent transfer to Orbital Sciences Corporation. Initially for six months after launch all of these data were free to any user capable of receiving them. After this time a license was required to receive and process SeaWiFS data. This system continues to provide valuable ocean color imagery to a wide range of investigations. There continue to be challenges regarding the accurate retrieval of chlorophyll and ocean productivity particularly for what is known as case 2 waters, which are markedly productive coastal regions. For the weaker productivity of the open ocean, or case 1 waters, the algorithms all seem to successfully agree.

The launch and operation of MODIS on NASA's Terra (morning) and Aqua (afternoon) satellites in 1999 and 2002 has provided ocean color channels that have also been used successfully for the computation of chlorophyll in the open ocean and coastal waters (Section 4.8). The lack of agreement of ocean color algorithms in coastal waters is emphasized by the fact that three different MODIS chlorophyll algorithms are being used for case 2 waters. With the availability of MODIS data, the future of the SeaWiFS instrument is not clear. The MODIS instruments is expected to be replaced by the Visible Infrared Imaging Radiometer Suite (VIIRS), which is to fly on the next generation of U.S. polar-orbiting operational weather satellites formerly known as the National Polar orbiting Operational Environmental Satellite System (NPOESS), and now the Joint Polar Satellite System; launch is now

scheduled for 2014 and the mission should continue for 12 years.

Numerous other color instruments are also on satellites, prompted by the great utility of ocean color measurements. Several European and Japanese color sensors were launched in 1996 and 1997, at about the same time as SeaWiFS. ESA's Envisat, launched in 2002, includes an ocean color instrument called the Medium Resolution Imaging Spectrometer (MERIS).

S16.9.9. Sea Surface Height: Satellite Altimetry

One of the most important developments in satellite oceanography is the radar altimetric satellite. Altimeters measure the distance from the satellite to Earth's surface. Two major products from these observations include: (1) maps of surface height associated with meso- to large-scale geostrophic circulation and associated with changes in sea level due to thermal expansion and changes in mass, and (2) maps of significant wave height. If the shape of Earth's geoid is known, then the altimeter measurement can be processed to yield sea-surface height. If the geoid is not precisely known, then the altimeter measurements still provide very accurate measurements of sea-surface height variation, since the geoid does not change in time. With corrections to the signal described in the next section, the accuracy of the most recent altimeters in detecting sea-surface height is $\pm 1-2$ cm.

The first test of radar altimetry on SEASAT (Section S16.9.4) showed the possibilities for monitoring the sea surface topography and the estimation of surface geostrophic currents associated with gradients of this surface topography. The next altimeter was on the U.S. Navy's GEOSAT satellite, which was launched in March 1985. After a classified geodetic mapping mission, it was moved to the orbit previously occupied by SEASAT and continued collecting data until 1989 with an accuracy of 5 to 10 cm.

In 1992 a new class of altimetric satellite, called TOPEX/Poseidon (T/P: [Figure S16.52](#)), was launched, with altimeters with much greater accuracy than GEOSAT or SEASAT (~2 cm). It was designed for 3 years, but collected high quality data for 12 years, ending in 2004. T/P carried both an American (NASA) wave-tube altimeter and a French (CNES) solid-state altimeter. These two altimeters shared the same antenna and thus could not be operated in parallel. The TOPEX altimeter was operated about 80% of the time. In addition to its altimeters, T/P carried a radiometer to measure atmospheric water content for corrections to the altimeter measurement. It also carried very precise navigation instruments.

The high accuracy of TOPEX/Poseidon ushered in the new era of quantitative study of the ocean's global eddy variability and was pivotal for development of ocean state estimation (combination of observations with an ocean general circulation model). Interpretation of other oceanographic data sets was greatly enhanced by the availability of altimetric data.

The T/P satellite was followed by the launch in December 2001 of the Jason-1 altimeter satellite ([Figure S16.52b](#)). Jason-1 carries the Poseidon-2 altimeter, which is the successor to the Poseidon altimeter on T/P. After nine months during which Jason-1 and T/P tracked each other about 90 seconds apart for inter-calibration, T/P was shifted to a new orbit halfway between the 110 km cross-track separation of Jason-1's 10-day repeat orbit, which is the old track of T/P. Called the "tandem mission," this pair of parallel satellites made it possible to better resolve the mesoscale ocean surface circulation until the end of the T/P lifetime in 2004. Jason-2 was launched as a follow-on to Jason-1 in June 2008, with the next generation Poseidon-3 altimeter.

Altimetric spatial resolution will be improved with a Wide Swath Ocean Altimeter, which will provide a two-dimensional swath of altimetric measurements 15 km apart over a 250 km swath.

ESA launched its first altimeter mission, ERS-1, in 1991. Its second altimeter mission, ERS-2, was launched in 1995, with nearly identical instrumentation except for an additional

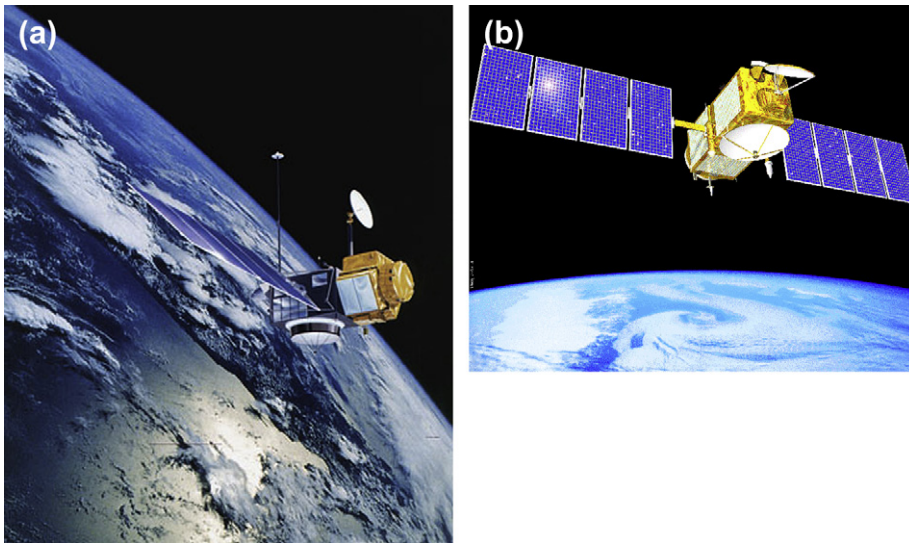


FIGURE S16.52 Artist's renderings of (a) TOPEX/Poseidon altimeter satellite and (b) Jason-1 altimeter satellite. *Source: From NASA/JPL-Caltech (2004a).*

ozone sensor. The third ESA mission with a radar altimeter, Envisat, was launched in 2002 to continue the ERS time series. ERS-1 was retired in 2000. The ERS accuracy is about 5 cm. Both ERS satellites include an SAR for radar images of Earth's surface, a scatterometer for winds, and radiometers for atmospheric water content. The ERS orbits are often in a 35-day repeat cycle, enabling higher spatial resolution than T/P, but coarser temporal resolution at a given location. Thus ERS and T/P complement each other, together providing temporal and spatial coverage. Data sets blended from T/P (now Jason-1 and -2) and ERS altimeter data are proving to be the most accurate in estimating sea-surface height changes (Figure S16.53) associated with changes in geostrophic circulation and with changes in ocean heat content or mass. Sorting out the source of variations requires merging these data with in situ profile data.

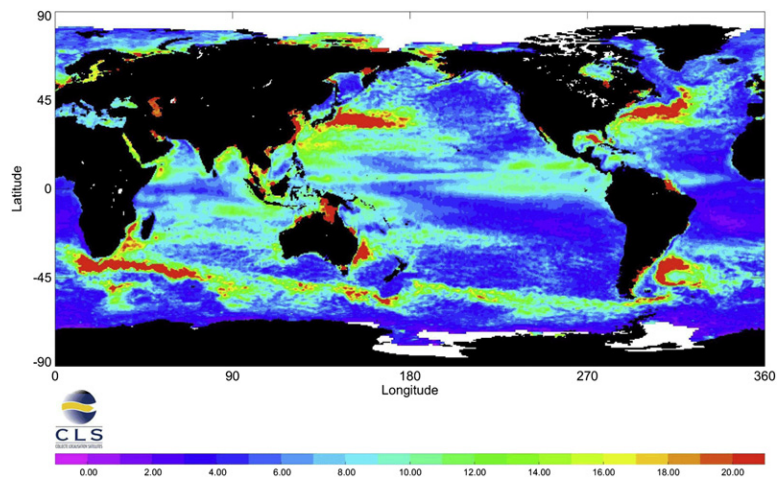
The next major goal for satellite altimetry is to measure Earth's geoid accurately enough that the absolute sea-surface height can be determined from the altimeters. Thus the geoid (mean gravity field) must be mapped at the same spatial scales as the oceanographic phenomena of interest. The Gravity Recovery

and Climate Experiment (GRACE) mission was launched in March 2002 to produce just this map. Satellite gravity missions such as GRACE measure the deflection of the satellite due to the underlying gravity field. GRACE consists of twin satellites orbiting close to each other. Sensors on the satellites very accurately measure the distance between them. Variations in the gravity field are sensed by changes in the distance between the GRACE satellites. The satellites are also precisely navigated with GPS. After extensive processing, a map of the geoid is produced and resolved to 200 km (Figure S16.54). With the advent of GRACE, it is expected that absolute sea-surface topographies will become routine. It should be noted that the energetic boundary currents and meso-scale eddies have spatial scales that are smaller than the 200 km resolved by GRACE.

Aside from its mission to improve the accuracy of altimetric sea-surface height observations, GRACE has been pivotal in detecting changes in ice sheet mass in Greenland and Antarctica. The shrinkage in both hemispheres, with the Antarctic record entirely resulting from GRACE, reflects global change.

The continued success of the various altimeter missions is allowing the physical oceanography

FIGURE S16.53 Mean sea level anomaly (cm) from merged ERS and T/P data (1992–1997). (Courtesy of P. LeTraon/Envisat Data Products.)



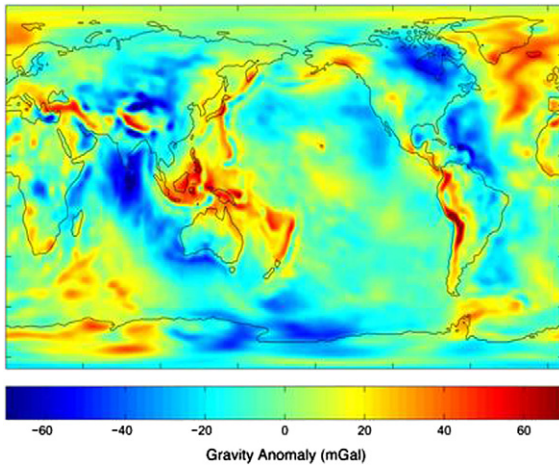


FIGURE S16.54 Gravity anomaly map (mGal where $1 \text{ mGal} = 10^{-5} \text{ m/s}^2$) from the GRACE mission with 363 days of observations (Gravity Model 02). *Source: From NASA/University of Texas (2004).*

community to make significant developments in tide modeling/monitoring, assessing variability in the mean circulation, mapping global eddy energy and planetary waves, and monitoring El Niño events. Altimetric data are used widely in data-assimilating models. These models then provide a diagnosis of ocean circulation and large-scale properties including heat content. Altimeter data alone provide surprisingly good constraints on the models, although in situ profiling of temperature and salinity structure is also needed for accuracy.

S16.9.10. Wave Height and Direction

In addition to mapping sea-surface height, the other primary mission for the altimeters is to provide maps of wave height and direction (Section 8.3.2 in Chapter 8). Mean wave-height estimates accurate to $\pm 1 \text{ m}$ or 25% of the actual wave height are possible from RADAR altimeter backscatter. This measurement is made possible by looking at the waveform returned to the satellite from the altimeter reflection. The slope with which it returns is a function of the significant

wave height on the surface of the ocean. Many experiments have been carried out to verify this assertion.

S16.9.11. Wind Speed and Direction: Scatterometry

Satellite instruments can measure wind vectors over the ocean through radar backscatter, a technique called *scatterometry*. Scatterometers are active radio frequency instruments. The scatterometer on SEASAT used a two-stick antenna configuration, making it possible to resolve the wind direction within a 180 degree directional ambiguity, which is then resolved by a knowledge of the overall atmospheric pressure pattern. The SEASAT scatterometer was an outstanding success, pointing the way toward future measurements of ocean wind speed and direction.

The first opportunity to fly a scatterometer after the short-lived SEASAT (Section S16.9.4) was the first Japanese ADEOS mission in 1996, which included an instrument called NSCAT. Unfortunately this satellite had a massive power failure six months after it started operation. A replacement, stand-alone satellite, QuikSCAT, was launched quickly thereafter in 1999. The scatterometer on QuikSCAT is known as SeaWinds. Another SeaWinds scatterometer was launched on the Japanese ADEOS-II mission in 2002. SeaWinds uses a conically scanning antenna rather than fixed beam antennas. It measures the ocean wind vector with an accuracy of $\pm 2 \text{ m/sec}$ and ± 20 degrees (Figure S16.55).

QuikSCAT data from both satellites are provided through NASA's PO.DAAC (Section S16.10).

Scatterometers are also now flying on the European ERS-2 and Envisat satellites. Launched before QuikSCAT, ERS-2 is a "fan-beam" antenna system capable of resolving two components of the wind vector. Launched after QuikSCAT, Envisat carries a similar scatterometer.

Surface wind speed can also be inferred from microwave brightness values in terms of the

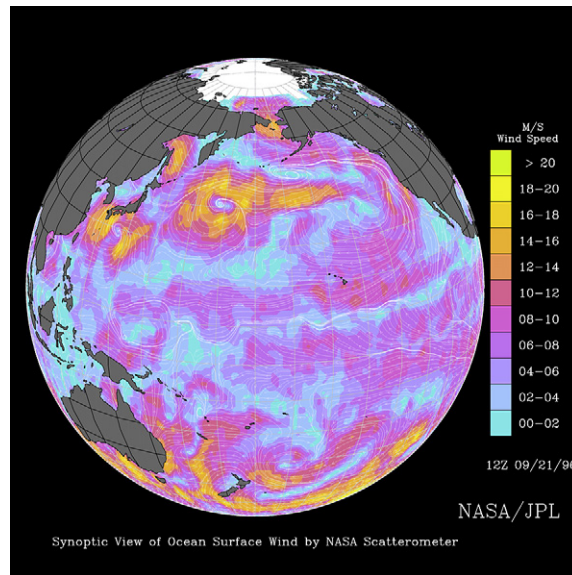


FIGURE S16.55 Pacific wind speed and direction from NSCAT (September 21, 1996). *Source: From NASA/JPL-Caltech (2004b).*

change in emissivity due to the surface roughness. Accuracies are around ± 2.6 m/sec. The scattering cross-section of a nadir RADAR altimeter return also provides an estimate of wind speed at the ocean's surface, accurate to around ± 2.0 m/sec.

S16.9.12. Other Satellite Sensors and Derived Products

Other sensor systems flying on the meteorological satellites are also useful, particularly in the study of air–sea interaction. A list of some of the directly observed or derived quantities important for physical oceanography include:

1. Radiant energy components are estimated to about ± 2 W/m² from both the visible and infrared radiances. Visible radiances are used to estimate the instantaneous effects of clouds on solar insolation to correct for the total amount of incoming radiation from sun and

sky. Infrared imagery can be used to compute outgoing longwave radiation (Q_b).

2. Rainfall over the ocean can be inferred from the presence of highly reflective clouds seen in both geostationary and polar-orbiting satellite imagery. This provides a fairly crude estimate because there is no definite relationship known between the amount of highly reflective cloud present and the level of rainfall experienced. Correlations between reflective cloud and in situ observations of rainfall have suggested excellent correlations in the tropical regions, but such studies have not been as successful in higher latitude regions. Rainfall can also be estimated directly from microwave radiances as cloud liquid water. TRMM integrates an onboard active radar with passive microwave instruments to estimate rainfall and rainfall rates over the tropical ocean.
3. Atmospheric water vapor can be directly measured as a vertical integral by microwave channels or can be computed from a moisture

profile derived from primarily infrared channels. The TIROS Operational Vertical Sounder (TOVS) on the NOAA polar-orbiting weather satellites uses a combination of infrared and microwave channels to measure atmospheric moisture and temperature profiles. Both of the microwave and infrared methods produce atmospheric water vapor values accurate to around 2 g/cm^3 ; the microwave data are cloud independent while the infrared sensors are limited by the amount of cloud cover. Since 1999 the weather satellites carry a profiling radiometer called the Advanced Microwave Sensor Unit (AMSU). As part of NASA's EOS program the Atmospheric Infrared Radiation Spectrometer (AIRS) flies on the afternoon Aqua satellite. AIRS has a large number of narrow infrared channels and is capable of observing very highly resolved atmospheric temperature and water vapor profiles.

4. Upwelling events in the sea can be located and monitored by both their surface thermal signatures and their expression by increased primary productivity in ocean color imagery. One must be careful to separate the in situ effects such as plankton blooms and heating and cooling from changes due to upwelling alone.
5. Currents can be estimated from the displacement of features in sequential imagery. The first studies used the visual method of feature tracking (Vastano & Borders, 1984) while subsequent efforts computed the maximum cross-correlation location between images to estimate advective displacements between the images (Emery et al., 1986). This same procedure can be applied to sequences of visible satellite images to compute the motion of sea ice (Ninnis, Emery, & Collins, 1986). Applied to highly resolved sea ice SAR imagery, this method produces very detailed maps of the ice displacements (Collins & Emery, 1988). Applied to the cloud-independent SMMR and the new SSM/I data,

this method can be used to produce all-weather images of sea ice displacement. The same technique can be applied to sequences of ocean color imagery to estimate surface advection (Bowen et al., 2002; Wilkin, Bowen, & Emery, 2002). It is important to remember that all of these measurements are from remotely sensing platforms and thus are not direct observations of a variable. Thus considerable validation with "ground-truth" data is needed to determine the levels of accuracy and reliability possible with the remote measurements. Still, the advantages of synoptic sampling of large regions make it worthwhile to understand and use these data. We must remember in this validation exercise that the satellite does not often sense the same thing that we measure in situ. For example, infrared satellite sensors are only capable of viewing the micron thick "skin" of the ocean while the in situ ship and buoy SST measurements represent temperatures from 1 to 5 m in depth. In addition a satellite infrared measurement represents the temperature measured over 1 km square of the ocean surface (its "footprint") while the ship or buoy SST is for a single "spot" in the ocean. This is true of most other comparisons that we make between satellite and in situ measurements, becoming an even greater problem when dealing with passive microwave systems with larger footprints. An example is that a moored buoy measurement of wind speed represents a single spot (or the minimum area of a couple of meters) while the passive microwave spot size may range from 12 to 50 km.

S16.9.13. Satellite Communications and Navigation

S16.9.13.1. Satellite Communication

Satellites are important for communications with autonomous instruments and for navigation, as well as for remote sensing. The French system Argos has provided communications

with instrumented platforms such as surface drifters and pop-up floats for many years. Argos is capable of accurately (± 1 km) locating the buoy in the ocean using the Doppler shift of the transmitted signal; the Argos system can also receive data from the buoys at a limited rate of up to 32 data words per transmission. Other satellites with higher data transmission rates, such as the GOES satellites, are gradually coming into use.

Recently constellations of small polar-orbiting satellites have been set up to provide global satellite telecommunication. Best known is Iridium System, originally conceived of and built by Motorola Corporation. Intended to provide global telecommunications with a series of satellite shells with up to 80 satellites, the system cost greatly exceeded company estimates. The high cost of the ground units and the communication charges soon led to bankruptcy. The U.S. military purchased the system and now operates it at a profit, providing global wide bandwidth telecommunication for military and commercial users. Due to the polar orbit, connectivity is not latitude dependent. (Geostationary systems can communicate easily with the lower latitudes but have problems poleward of 60° latitude.) The system can be adapted to transfer more data from buoys and floats than is possible with the Argos system. For these applications it is critical that the in situ platform be equipped with a GPS receiver for accurate geographic location.

S16.9.13.2. Satellite Navigation

Determining the location of ships has been another important function of satellites since the early 1970s. The earliest system, NAVSTAR, used a single shell of polar-orbiting satellites to determine the ship's location when the satellite passed overhead, based on the Doppler shift of the radio signal from the ship to the satellite. NAVSTAR was supported and operated by the U.S. Navy but was available to ships from all nations. Commercial receiving units quickly developed into low-cost systems for accurate

positioning. Coupled with good estimates of ship's speed and heading, NAVSTAR provided an excellent means for mapping the course of a vessel at sea. Used in conjunction with a shorter range system, such as LORAN (short range radio navigation based on beacons installed in coastal regions), the satellite navigation system provided a very precise check of ship geolocation. At low latitudes, satellite position fixes were possible every couple of hours depending on the number of satellites in operation. At higher latitudes, where the orbits of the polar-orbiting satellites nearly overlap, fixes were much more frequent.

The widely used GPS replaced NAVSTAR beginning in 1993. GPS was developed and is operated by the U.S. Department of Defense (DoD), which provides very precise, accurate geographic and time information. Prior to 2000, GPS was operated in two modes: higher accuracy for military users (Precise Positioning Service, PPS) and a degraded signal (Standard Positioning Service, SPS) for all other users. After 2000, SPS was discontinued and all signals now are of the higher accuracy.

To provide continuous access to users, GPS uses six shells of navigational satellites (Figure S16.56) to at least three satellites simultaneously, and usually uses five to eight (Dana, 1999, accessed 2009). The minimum system has 24 satellites, although often there are more as new ones are launched as replacements. The satellites are in daily-repeating orbits. Accuracy in both the horizontal and vertical directions is ± 100 m for SPS and ± 22 m for PPS. Thus GPS can be used for aircraft navigation to report altitude as well as geographic location. GPS can also be used to accurately determine the time (200 ns for PPS).

GPS signals are processed in a GPS receiver, enabling the receiver to compute position, velocity, and time. Receivers are made for aircraft, ships, vehicles, and for individuals.

"Differential" GPS (DGPS) is a method of greatly improving SPS accuracy to up to $+10$ cm

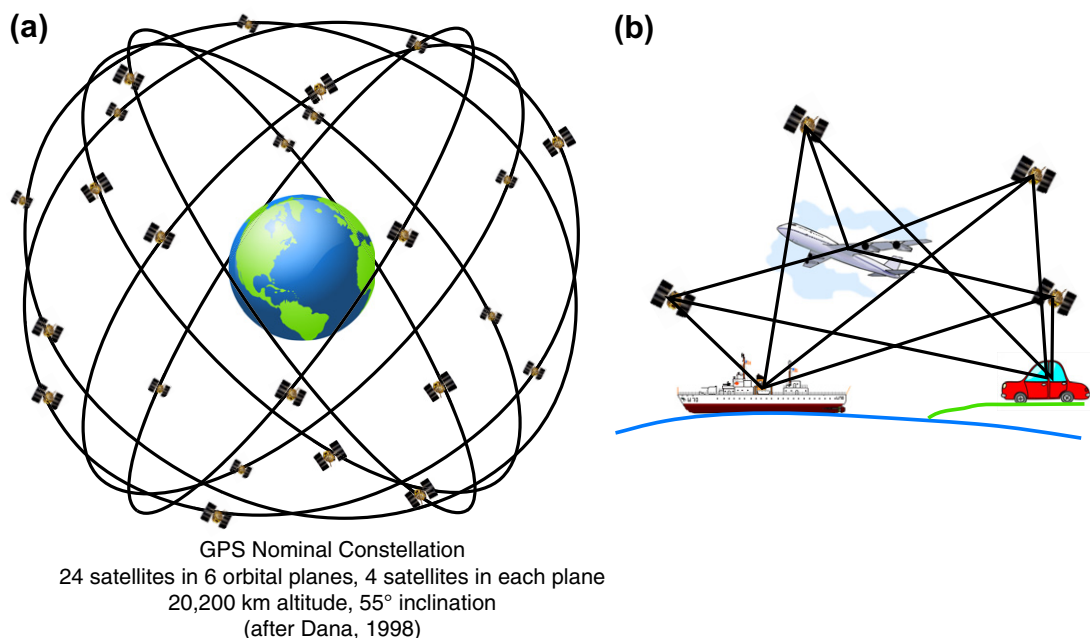


FIGURE S16.56 (a) GPS satellite orbits and (b) GPS contacts with receivers. Source: After Dana (1999).

by using GPS reference stations with precisely known positions. These stations broadcast information on the error of the satellite locations. DGPS was originally introduced to reduce the large errors of the SPS system (prior to 2000), but it improves on even the more precise PPS.

The Russian global navigation system (GLO-NASS) consists of 21 satellites in 3 shells. It became operable in the mid-1990s but then fell into disrepair. ESA plans its own network of global navigation satellites called Galileo. It will include 30 satellites in 3 shells and will be interoperable with GPS, and is intended to be more accurate than GPS. It is planned to be operational in 2013.

S16.10. DATA ARCHIVES AND DATA CENTERS

Oceanographic data are archived in various data centers. Most countries have a central

data archive. The primary international repositories for in situ data are the three World Data Centers for Oceanography located in the United States, Russia, and China, under the umbrella of the International Council for Science (ICSU). The World Data Center in the United States is NOAA's National Oceanographic Data Center (NODC), located in Silver Springs, Maryland. Sea ice information, including satellite information, is archived in the United States at the National Snow and Ice Data Center.

Satellite data are so voluminous that many different data centers have been set up to archive and disseminate these data. NASA's EOS includes Data Active Archive Centers (DAACs). PO.DAAC (<http://podaac.jpl.nasa.gov/>) is located at NASA's Jet Propulsion Laboratory (JPL) in Pasadena, California. In conjunction with the French space agency (CNES), PO.DAAC processes, archives and disseminates all altimetry data and data products. PO.DAAC also handles NASA scatterometer data products

and SST products derived from infrared satellite imagery as well as some other smaller data sets. NOAA provides its satellite data through its NOAA Satellites and Information (NOAASIS) Web site. The final archive of all U.S. weather satellite data as well as for NASA EOS data is NOAA's National Climatic Data Center (NCDC), located in Asheville, North Carolina. The "satellite active archive" at NCDC provides wide access to environmental satellite data. ESA provides access to satellite SST and ocean color data through its Ionia Web site.

The Global Ocean Observing System (GOOS; <http://www.ioc-goos.org/>) is part of the Global Earth Observing System of Systems (GEOSS). GOOS provides a framework for different types of oceanographic data centralization and products. This differs from data archiving, which is mainly covered by the oceanographic data centers such as those listed above.

References

- Aanderaa Instruments, 2000. Recording current meter RCM7 and RMC8. Aanderaa Instruments, <<http://www.aanderaa.com>> (accessed 5.13.04). (Link to RCM7-8 information is no longer active 6.2.09.)
- Argo 3000, 2007. Argo 3000. <http://www-argo.ucsd.edu/FrArgo_3000.html> (accessed 2.18.09).
- Avsic, T., Send, U., Skarsoullis, E., 2005. Six years of tomography observations in the central Labrador Sea. *J. Acoust. Soc. Am.* 107, 28–34.
- Beardsley, R., 1987. A Comparison of the Vector-Averaging Current Meter and New Edgerton. Germeshausen, and Grier, Inc., Vector-Measuring Current Meter on a Surface Mooring in Coastal Ocean Dynamics Experiment 1. *J. Geophys. Res.* 92, 1845–1859.
- Bourlès, B., Lumpkin, R., McPhaden, M.J., Hernandez, F., Nobre, P., Campos, E., Yu, L., Planton, S., Busalacchi, A., Moura, A.D., Servain, J., Trotte, J., 2008. The Pirata Program: History, accomplishments, and future directions. *Bull. Am. Meteor. Soc.* 89, 1111–1125.
- Bowen, M.M., Emery, W.J., Wilkin, J.L., Tildesley, P.L., Barton, I.J., Knewton, R., 2002. Multiyear surface currents from sequential thermal imagery using the maximum cross-correlation technique. *J. Atm. Ocean. Tech.* 19, 1665–1676.
- Carlson, R.E., 2011. The Secchi Disk. Secchi Dip-In. <http://www.secchidipin.org/secchi.htm> (accessed 3.23.11).
- Cartwright, D.E., 1999. *Tides: A Scientific History*. Cambridge University Press, UK, 292 pp.
- Cheney, R.E., Marsh, J.G., Beckley, B.D., 1983. Global mesoscale variability from collinear tracks of SEASAT altimeter data. *J. Geophys. Res.* 88, 4343–4354.
- Collins, M.J., Emery, W.J., 1988. A computational method for estimating sea ice motion in sequential SEASAT synthetic aperture radar imagery by matched filtering. *J. Geophys. Res.* 93, 9241–9251.
- Cornuelle, B., Wunsch, C., Behringer, D., Birdsall, T., Brown, M., Heinmiller, R., Knox, R., Metzger, K., Munk, W., Spiesberger, J., Spindel, R., Webb, D., Worcester, P., 1985. Tomographic maps of the ocean mesoscale. Part 1: Pure acoustics. *J. Phys. Oceanogr.* 15, 133–152.
- Dana, P.H., 1999. The Geographer's Craft Project. Department of Geography, The University of Colorado at Boulder, developed 1994, copyright 1999. <<http://www.colorado.edu/geography/gcraft/notes/gps/gps.html>> (accessed 2.18.09).
- Davis, R.E., Killworth, P.D., Blundell, J.R., 1996. Comparison of autonomous Lagrangian circulation explorer and fine resolution Antarctic model results in the South Atlantic. *J. Geophys. Res.* 101, 855–884.
- Dietrich, G., Kalle, K., Krauss, W., Siedler, G., 1980. *General Oceanography*. Ulrich Roll, S., Ulrich Roll, H.U., (Trans.), second ed. Wiley, New York (Wiley-Interscience), 626 pp.
- Dushaw, B.D., 2002. Acoustic Thermometry of Ocean Climate (ATOC). Applied Physics Laboratory, University of Washington. <<http://staff.washington.edu/dushaw/atoc.html>> (accessed July, 2008).
- Dushaw, B.D., 2003. Acoustic thermometry in the North Pacific. *CLIVAR Exchanges* 26, 5 pp.
- Emery, W., Fowler, C., Maslanik, J., 1995. Satellite remote sensing of ice motion. In: Ikeda, M., Dobson, F.W. (Eds.), *Oceanographic Applications of Remote Sensing*. CRC Press, Boca Raton, Florida, 492 pp.
- Emery, W.J., Cherkauer, K., Shannon, B., Reynolds, R.W., 1997. Hull mounted bulk sea surface temperature measurements from volunteer observing ships. *J. Atm. Ocean. Tech.* 14, 1237–1251.
- Emery, W.J., Thomas, A.C., Collins, M.J., Crawford, W.R., Mackas, D.L., 1986. An objective method for computing advective surface velocities from sequential infrared satellite images. *J. Geophys. Res.* 91, 12, 865–12,878.
- Emery, W.J., Thomson, R.E., 2001. *Data Analysis Methods in Physical Oceanography*, second ed. Elsevier, Amsterdam, 638 pp.
- Esterson, G.L., 1957. The induction conductivity indicator: a new method for conductivity measurement at sea. *Chesapeake Bay Institute Technical Report*, 57-3, 183 pp.
- Faraday, M., 1832. The Bakerian Lecture — Experimental researches in electricity. Second Series. Sec. 5. Terrestrial

- magneto-electric induction. *Philos. T. Roy. Soc. London Part I*, 163–177.
- Flosadottir, A., 2004. Research cables around the world. NOAA/PMEL. <<http://www.pmel.noaa.gov/wbcurrents>> (accessed 5.13.04).
- Folland, C.K., Parker, D.E., 1995. Correction of instrumental biases in historical sea surface temperature data. *Q.J. Roy. Meteor. Soc.* 121, 319–367.
- Fowler, C., Emery, W.J., Maslanik, J.A., 2004. Satellite-derived evolution of Arctic sea ice age: October 1978 to March 2003. *IEEE Geosci. Rem. Sens. Lett.* 1, 71–74.
- Fu, L-L., Holt, B., 1982. SEASAT views oceans and sea ice with synthetic aperture radar. Jet Propulsion Laboratory publication 81–120. Pasadena, CA, 200 pp.
- General Oceanics, 2009. MK3C/WOCE CTD. <<http://www.generaloceanics.com/genocean/mk3c.htm>> (accessed 5.29.09).
- Gloersen, P., Campbell, W.J., Cavalieri, D.J., Comiso, J.C., Parkinson, C.L., Zwally, H.J., 1992. Arctic and Antarctic Sea Ice, 1978–1987: Satellite Passive-Microwave Observations and Analysis, Spec. Publ., 511, 290 pp. NASA, Washington, D. C.
- Guildline, 2009. Guildline8400BDatasheet pdf. Guildline Instruments. <<http://www.guildline.com/Datasheet/Guildline8400BDatasheet.pdf>> (accessed 6.1.09).
- Hamon, B.V., 1955. A temperature-salinity-depth recorder. *Conseil Permanent International pour l'Exploration de la Mer. J. Conseil* 21, 22–73.
- Hamon, B.V., Brown, N.L., 1958. A temperature-chlorinity-depth recorder for use at sea. *J. Sci. Instrum.* 35, 452–458.
- Howe, B., Chereskin, T.K., 2007. Oceanographic Measurements. In: Tropea, C., Yarin, A.L., Foss, J.F. (Eds.), *Springer Handbook of Experimental Fluid Mechanics*. Springer, Berlin, pp. 1179–1271.
- Howe, B., Worcester, P., Spindel, R., 1987. Ocean Acoustic Tomography: Mesoscale Velocity. *J. Geophys. Res.* 92, 3785–3805.
- ICPC, 2007. International Cable Protection Committee. <http://www.ispc.org/cabledb/Scientific_Cable_db.htm> (accessed 6.1.09).
- InterOcean Systems, 2011. S4 current meter family. InterOcean Systems, Inc. <<http://www.interoceansystems.com/s4main.htm>> (accessed 3.21.11).
- Larsen, J.C., Sanford, R.B., 1985. Florida Current volume transports from voltage measurements. *Science* 227, 302–304.
- Ledwell, J.R., Watson, A.J., Law, C.S., 1993. Evidence for slow mixing across the pycnocline from an open-ocean tracer-release experiment. *Nature* 364, 701–703.
- Lewis, E.L., 1980. The Practical Salinity Scale 1978 and its antecedents. *IEEE. J. Oceanic Eng. OE-5*, 3–8.
- Longuet-Higgins, M.S., Stern, M.E., Stommel, H.M., 1954. The electrical field induced by ocean currents and waves, with applications to the method of towed electrodes. *Papers in Phys. Oceanogr. and Met. MIT and Woods Hole Oceanogr. Inst.* 13 (1), 1–37. <<http://hdl.handle.net/1912/1064>>.
- Mariano, A.J., Ryan, E.H., Perkins, B.D., Smithers, S., 1995. The Mariano Global Surface Velocity Analysis 1.0. USCG Report CG-D-34–95, 55 pp. <<http://oceancurrents.rsmas.miami.edu/index.html>>(accessed 3.4.09).
- Marine Physical Lab, SIO, 2009. Floating Instrument Platform- FLIP. Marine Physical Lab, SIO, University of California, San Diego. 2003–2009. <<http://www.mpl.ucsd.edu/resources/flip.intro.html>> (accessed 5.29.09).
- McPhaden, M.J., Meyers, G., Ando, K., Masumoto, Y., Murty, V.S.N., Ravichandran, M., Syamsudin, F., Vialar, J., Yu, L., Yu, 2009. W., RAMA: The research moored array for African-Asian-Australian monsoon analysis and prediction. *Bull. Am. Meteorol. Soc.* 90, 459–480.
- Morawitz, W.M.L., Sutton, P.J., Worcester, P.F., Cornuelle, B.D., Lynch, J.F., Pawlowicz, R., 1996. Three-dimensional observations of a deep convective chimney in the Greenland Sea during winter 1988/1989. *J. Phys. Oceanogr.* 26, 2316–2343.
- Munk, W., Worcester, P., Wunsch, C., 1995. *Ocean Acoustic Tomography*. Cambridge Monographs on Mechanics. Cambridge University Press, Cambridge, UK, 447 pp.
- Munk, W., Wunsch, C., 1979. Ocean acoustic tomography: a scheme for large scale monitoring. *Deep-Sea Res.* 26, 123–161.
- NASA GSFC, 2004. Remote Sensing Tutorial. NASA Goddard Space Flight Center. <<http://rst.gsfc.nasa.gov>> (accessed 04.28.11).
- NASA/JPL-Caltech, 2004a. Ocean surface topography from space — Missions. NASA Jet Propulsion Laboratory. <<http://topex-www.jpl.nasa.gov/mission/mission.html>>; (accessed 5.11.04).
- NASA/JPL-Caltech, 2004b. WINDS home page. NASA Jet Propulsion Laboratory. <<http://winds.jpl.nasa.gov/>> (accessed 5.04).
- NASA/University of Texas, 2004. GRACE gravity model — gravity recovery and climate experiment gravity model. University of Texas at Austin Center for Space Research. <<http://www.csr.utexas.edu/grace/gravity/>> (accessed 5.04).
- National Ice Center, 2004. <<http://www.natice.noaa.gov>> (accessed 5.11.04).
- Nerem, R.S., 2009. Global mean sea level tide gauges. University of Colorado at Boulder. <<http://sealevel.colorado.edu/tidegauges.php>> (accessed 6.1.09).
- Neumann, G., Pierson, W.J., 1966. *Principles of Physical Oceanography*. Prentice-Hall, Englewood Cliffs, N.J. 545 pp.

- Ninnis, R.M., Emery, W.J., Collins, M.J., 1986. Automated extraction of pack ice motion from advanced very high resolution radiometer imagery. *J. Geophys. Res.* 91, 10725–10734.
- NOAA Global Drifter Program, 2009. The Global Drifter Program. NOAA AOML GDP. <http://www.aoml.noaa.gov/phod/dac/gdp_information.html> (accessed 6.1.09).
- NOAA Marine Modeling and Analysis Branch, 2004. MMAB sea ice analysis page. NOAA, Marine Modeling and Analysis Branch. <<http://polar.ncep.noaa.gov/seaice/Analyses.html>> (accessed 5.11.04).
- NOAA NDBC, 2008. Moored buoy program. NOAA National Data Buoy Center. <<http://www.ndbc.noaa.gov/mooredbuoy.shtml>> (accessed 2009).
- NOAA NESDIS, 2009. Geostationary Satellite Server, NOAA Satellite and Information Service. <<http://www.goes.noaa.gov>> (accessed 6.2.09).
- NOAA PMEL, 2009a. Impacts of El Niño and benefits of El Niño prediction. <http://www.pmel.noaa.gov/tao/el_nino/impacts.html> (accessed 3.26.09).
- NOAA PMEL, 2009b. The TAO project. TAO Project Office, NOAA Pacific Marine Environmental Laboratory. <<http://www.pmel.noaa.gov/tao/>> (accessed 6.1.09).
- NOAA UOTC, 2009. The expendable Bathythermograph (XBT). NOAA Upper Ocean Thermal Center. <<http://www.aoml.noaa.gov/goos/uot/xbt-what-is.php>> (accessed 6.1.09).
- Ocean World, 2009. Buoys, tide gauges, Nansen bottles and the like. Ocean World. <<http://oceanworld.tamu.edu/students/satellites/satellite2.htm>>, (accessed 6.1.09).
- Paroscientific, Inc., 2009. Digiquartz High Pressure Sensor Design. <<http://www.paroscientific.com/pdf/DQAdvantage.pdf>>. (accessed 5.29.09).
- Pinkel, R., 1979. Observation of strongly nonlinear motion in the open sea using a range-gated Doppler sonar. *J. Phys. Oceanogr.* 9, 675–686.
- Preisendorfer, R.W., 1986. Secchi disk science: Visual optics of natural waters. *Limn. Oceanogr.* 31, 909–926.
- Reynolds, R.W., 1988. A real-time global sea surface temperature analysis. *J. Clim.* 1, 75–87.
- Reynolds, R.W., Smith, T.M., 1994. Improved global sea surface temperature analyses using optimum interpolation. *J. Clim.* 7, 929–948.
- Reynolds, R.W., Smith, T.M., 1995. A high-resolution global sea surface temperature climatology. *J. Clim.* 8, 1571–1583.
- Richardson, M.J., Gardner, W.D., 1997. Tools of the trade. *Quarterdeck* 5(1), Texas A&M University Department of Oceanography. <<http://oceanography.tamu.edu/Quarterdeck/QD5.1/qdhome.5.1.html>> (accessed 2.19.09).
- Rosby, T., 1969. On monitoring depth variations of the main thermocline acoustically. *J. Geophys. Res.* 74, 5542–5546.
- Rosby, T., 2007. Evolution of Lagrangian methods in oceanography. In: Griffa, A., Kirwan, A.D., Mariano, A.J., Özgökmen, T., Rosby, H.T. (Eds.), *Lagrangian analysis and prediction of coastal and ocean dynamics*. Cambridge University Press, pp. 1–39.
- Rosby, T., Dorson, D., Fontaine, J., 1986. The RAFOS system. *J. Atm. Ocean. Tech.* 3, 672–679.
- Rosby, T., Webb, D., 1970. Observing abyssal motion by tracking Swallow floats in the SOFAR channel. *Deep-Sea Res.* 17, 359–365.
- Rowe, F., Young, J., 1979. An ocean current profiler using Doppler sonar. *IEEE Proc. Oceans* 79, 292–297.
- Scripps Institution of Oceanography, 2009. R/V Melville Photos. Scripps Institution of Oceanography, UCSD. <<http://shipsked.ucsd.edu/Ships/Melville/>> (accessed 6.1.09).
- Sea-Bird Electronics, Inc., 2009a. SEACAT Thermosalinograph. <<http://www.seabird.com/products/ThermoS.htm>> (accessed 5.29.09).
- Sea-Bird Electronics, Inc. 2009b. Profilers. <<http://www.seabird.com/products/profilers.htm>> (accessed 5.29.09).
- Secchi Dip-In, 2011. Secchi disk. Secchi Dip-In, Department of Biological Sciences, Kent State University. <<http://www.secchidipin.org/secchi.htm>> (accessed 3.23.11).
- Send, U., Schott, F., Gaillard, F., Desaubies, Y., 1995. Observation of a deep convection regime with acoustic tomography. *J. Geophys. Res.* 100, 6927–6941.
- Stewart, R.H., 1985. *Methods of Satellite Oceanography*. University of California. Press, Berkeley.
- Strickland, J.D.H., Parsons, T.R., 1972. *A Practical Handbook of Sea-Water Analysis* (second ed.). Fish. Res. Bd. Can. Bull. 167, 311 pp.
- Swallow, J.C., 1955. A neutral-buoyancy float for measuring deep currents. *Deep-Sea Res.* 3 (1), 93–104.
- TAO, 2009. The TAO project. TAO Project Office, NOAA Pacific Marine Environmental Laboratory. <<http://www.pmel.noaa.gov/tao/>> (accessed 6.1.09).
- Teledyne RD Instruments, 2011. Teledyne RDI marine measurements. Teledyne RDI. <<http://www.rdinstruments.com/sen.aspx>> (accessed 3.21.11).
- TriOS, 2009. TriOS optical sensors —Ramses. TriOS GmbH, <<http://www.trios.de>> (accessed 2.19.09).
- Tyler, J.E., 1968. The Secchi disc. *Limnology and Oceanogr.* 13, 1–6.
- UNESCO, 1981. *The Practical Salinity Scale 1978 and the International Equation of State of Seawater 1980*. Tech. Pap. Mar., Sci. 36, 25 pp.
- University of Rhode Island Graduate School of Oceanography, 2009. RAFOS float group home page. <<http://www.po.gso.uri.edu/rafos/>> (accessed 5/29/09).
- U.S. Argo Program, 2009. Argo home page. Scripps Institution of Oceanography. University of California, San Diego. <<http://www-argo.ucsd.edu/>> (accessed 02.18.09).

- USGS, 2005. Instrumentation. U.S. Department of the Interior, U.S. Geological Survey. <<http://pubs.usgs.gov/dds/dds74/WEBPAGES/instrumentation.html>> (accessed 6.1.09).
- Vastano, A.C., Borders, S.E., 1984. Sea surface motion over an anticyclonic eddy on the Oyashio Front. *Rem. Sens. Environ.* 16, 87–90.
- Von Arx, W.S., 1950. An electromagnetic method for measuring the velocities of ocean currents from a ship under way. *Pap. Phys. Oceanogr. Meteor. MIT and Woods Hole Oceanogr. Inst.* 11 (3), 1–62.
- Watts, D.R., Rossby, H.T., 1977. Measuring dynamic heights with inverted echo sounders: Results from MODE. *J. Phys. Oceanogr.* 7, 345–358.
- Weller, R.A., Davis, R.E., 1980. A vector measuring current meter. *Deep-Sea Res.* 27, 565–582.
- Wertheim, G.K., 1954. Studies of the electrical potential between Key West, Florida and Havana, Cuba. *Trans. Am. Geophys. Union* 35, 872–882.
- WHOI Image Galleries, 2009. Image of the Day — October 6, 2006. Woods Hole Oceanographic Institution. <<http://www.whoi.edu/page.do?pid=10897&i=588&x=184>> (accessed 6.1.09).
- Wilkin, J.L., Bowen, M., Emery, W.J., 2002. Mapping mesoscale currents by optimal interpolation of satellite radiometer and altimeter data. *Ocean Dynam.* 52, 95–103.
- WMOJCOMM, 2009. The Global Sea Level Observing System (GLOSS), World Meteorological Organisation, Joint Technical Commission for Oceanography and Marine Meteorology. <<http://www.gloss-sealevel.org/>> (accessed 5.29.09).
- WOCE, 2009. Drifters. World Ocean Circulation Experiment Global Data Resource. <<http://woce.nodc.noaa.gov/wdiu/index.htm>> (accessed 6.1.09).
- Young, F.B., Gerard, H., Jevons, W., 1920. On electrical disturbances due to tides and waves. *Philos. Mag. Series 6* (40), 149–159.
- Zhang, H.-M., Prater, M., Rossby, T., 2001. Isopycnal Lagrangian statistics from the North Atlantic Current RAFOS float observations. *J. Geophys. Res.* 106, 13817–13836.

